Université de Lille

Laboratoire de Mécanique, Multiphysique, Multiéchelle (FRE2016)

Ecole Doctorale Sciences Pour l'Ingénieur (SPI)

THESE

Pour l'obtention du grade de

DOCTEUR DE L'UNIVERSITE DE LILLE

Mention Mécanique

Shakedown of porous materials

Présenté par

Jin ZHANG

Soutenue le 28 septembre 2018

JURY

E. Charkaluk	Directeur de recherches CNRS, Ecole Polytechnique	Rapporteur
I. Doghri	Professeur, Université catholique de Louvain	Rapporteur
C. Bouby	Maître de Conférences, Université de Lorraine	Examinateur
D. Kondo	Professeur, Université Pierre et Marie Curie	Examinateur
E. Rouhaud	Professeur, Université de Technologie de Troyes	Examinateur

ENCADREMENT

G. De Saxcé	Professeur, Université de Lille	Directeur de thèse
A. Oueslati	Maître de Conférences, HDR, Université de Lille	Co-encadrant
W. Q. Shen	Maître de Conférences, HDR, Polytech'Lille	Co-encadrant

Acknowledgment

This research was carried out during my PhD study in Laboratoire de Mécanique, Multiphysique, Multi-échelle.

Firstly, I would like to express my deepest and most sincere gratitude to my supervisor Pr. Géry DE SAXCE for offering me this opportunity to discover the world of mechanics, and for his support, patience, confidence and immense knowledge. I could not have imagined having a better advisor and mentor, and it is such a great honor for me to be his student.

Secondly, I am very grateful to my co-supervisors Mr. Abdelbacet OUESLATI and Mr. Wanqing SHEN. They provided me selflessly with continuous help and advice on every side of my research over last three years, and made a greet contribution of all the publications.

I would like to thank to Professor CHARKALUK and Professor DOGHRI for being the rapporteurs of my thesis, and also to Professor KONDO, Mrs. ROUHAUD, and Mrs. BOUBY who have kindly examined my work.

Additionally, I acknowledge specially Mr. An Danh Nguyen for his kind explanation of the use of the optimizer IPOPT, and of the numerical shakedown method during my stay in Aachen. Equally, my gratitude is towards Mr. Long CHENG for his valuable guidance and advice.

Great thanks also give to all my friends of Lamcube and in Lille. I deeply appreciate their friendship and the common memory with them, especially for Mr. and Mrs. CLEMENT, who treat me as a family member.

Last but not the least, I would like to thank my parents and my wife for accompanying and supporting me spiritually and unconditionally to go through the most difficult moment of my academic career.

Jin ZHANG

September 2018, Villeneuve D'ascq

Abstract

Key words: *Porous material, Shakedown analysis , Homogenization*

This thesis is devoted to the determination of shakedown limit states of porous ductile materials based on Melan's static theorem by considering the hollow sphere model, analytically and numerically. First of all, we determine the analytical macroscopic shakedown criterion of the considered unit cell with von Mises matrix under alternating and pulsating special loading cases. The proposed macroscopic analytical criterion depends on the first and second macroscopic stresses invariants, the sign of the third one and Poisson's ratio. Then, the procedure is extended to the general cyclically repeated loads by the construction of a more appropriate trial residual stress field allowing analytical computations and the improvement of the previous model simultaneously. Moreover, this approach is applied to porous materials with Drucker-Prager matrix.

The idea relies firstly on the exact solution for the pure hydrostatic loading condition. It turns out that the collapse occurs by fatigue. Next, suitable trial stress fields are built with additional terms to capture the shear effects. The safety domain, defined by the intersection of the shakedown limit domain and the limit analysis domain (Shen et al., 2015; Guo et al., 2008) corresponding to the sudden collapse by development of a mechanism at the first cycle, is fully compared with step-by-step incremental elastic-plastic simulations and simplified direct computations.

At last, we provide a direct numerical method to predict the shakedown safety domain of porous materials subjected to multi-varying independent loadings by considering the critical loading path of the load domain instead of the whole history. The shakedown problem is transformed into a large-size optimization problem, which can be solved efficiently by the non-linear optimizer IPOPT to give out not only the limit load factor, but also the corresponding residual stress field for the shakedown state.

Résumé

Key words: *Matériaux poreux, Analyse d'adaptation, Homogénéisation*

Cette thèse est consacrée à la détermination des états limites de l'adaptation des matériaux ductiles poreux sur la base du théorème de Melan et en considérant le modèle de la sphère creuse. Dans un premier temps, nous proposons le critère analytique macroscopique d'adaptation avec la matrice de von Mises sous deux charges particuliers, alterné et pulsé. Le critère analytique dépend des première et seconde invariants des contraintes macroscopiques, du signe du troisième et du coefficient de Poisson. Ensuite, ce critère est étendu aux charges cycliques répétées générales par la construction d'un champ de contraintes résiduelles d'essai plus approprié permettant simultanément des calculs analytiques et l'amélioration du modèle précédent. De plus, il est également utilisé pour les matériaux ductiles poreux avec une matrice de Drucker-Prager.

L'idée repose d'abord sur la solution exacte pour le charge purement hydrostatique. Il s'avère que la ruine se produit par fatigue. Ensuite, des champs de contrainte d'essai appropriés sont construits avec des termes supplémentaires pour capter les effets de cisaillement. Le domaine de sécurité, défini par l'intersection du domaine d'adaptationet celui d'analyse limite (Shen et al., 2015; Guo et al., 2008) (la ruine survenant brusquement par formation d'un mécanisme au premier cycle), est entièrement comparé avec des simulations élasto-plastique incrémentales et des calculs directs simplifiés.

Enfin, nous fournissons une méthode numérique directe pour prédire le domaine de sécurité de l'adaptation des matériaux poreux soumis à des charges variant de manière indépendente en considérant le chemin critique du domaine de chargement au lieu de l'histoire entière. Le problème de l'adaptation est transformé en un problème d'optimisation de grande taille, qui peut être résolu efficacement par l'optimiseur non-linéaire IPOPT pour donner non seulement le facteur de charge limite, mais aussi le champ de contrainte résiduelle correspondant à l'état d'adaptation.

Main notations

E	Young's modulus
ν	Poisson's coefficient
F	yield function
f	porosity
$\boldsymbol{f}$	body force vector
$\boldsymbol{u}$	displacement vector
$\boldsymbol{v}$	velocity field
W	external work of applied force
α	load factor
α_{SD}	shakedown limit load factor
σ_0	yield stress in tension or compression
σ_m	microscopic hydrostatic stress
σ_e	microscopic equivalent stress
$\boldsymbol{\sigma}$	microscopic stress field
$\boldsymbol{\sigma}^E$	elastic stress field in the fictitious elastic body
$\boldsymbol{\sigma}_0^E$	elastic stress field corresponding to reference load
Σ_m	macroscopic hydrostatic stress
Σ_e	macroscopic equivalent stress
$\boldsymbol{\Sigma}$	macroscopic stress field
$\boldsymbol{\varepsilon}$	microscopic strain field
$\dot{\boldsymbol{\varepsilon}}^e$	elastic strain rate field
$\dot{\boldsymbol{\varepsilon}}^p$	plastic strain rate field
$\boldsymbol{E}$	macroscopic strain field
$\boldsymbol{\rho}$	residual stress field
$\bar{\boldsymbol{\rho}}$	time-independent residual stress field
$\mathscr{P}$	load domain
$\mathscr{P}_0$	reference load domain
λ	plastic multiplier

Contents

General introduction

In ductile fracture, the strength and plastic deformations of materials are strongly affected by the presence of heterogeneities (micro-cracks, voids, inclusions, etc.) and depend also on the external applied loads. Indeed, for structures made up with ductile materials, experiments (Kobayashi et al., 1991; Schmidt et al., 1991) have clearly shown that, the limit load at collapse under cyclic mechanical load or temperature fields, is always lower than that the one under monotonic load. Even below the ultimate load, the structure's safety can not be guaranteed if subjected to cyclic repeated loads as shown in Figure 1.

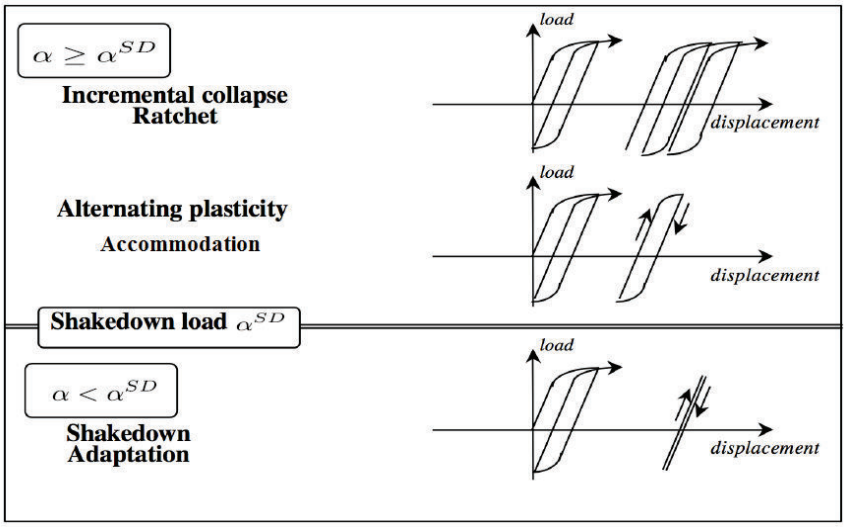

Figure 1: Incremental collapse, alternating plasticity and shakedown.

Let us note a positive real number α as the load factor to govern the size of the load domain. The experimental tests show that continued application of the variable loads in time on a structure made of an elastic perfectly plastic material may result in the following possible situations:

- Above a particular value α^{SD} of the load factor, we can observe that the accumulation of plastic strains gives birth to an incremental collapse mechanism, with monotonically increasing excessive deflections. This kind of structural failure is called incremental collapse or ratcheting.

- Another possibility above the load α_{SD} is that, although the reversal plastic strains remain small and the incremental collapse is prevented, the alternating plastic strain increments occurs, which is likely to lead to fracture by exhaustion of ductility after certain number of cycles(Manson, 1954; Coffin Jr, 1954). This behavior is called alternating plasticity or accommodation.

- On the other hand, below α_{SD}, after possibly some elastic-plastic strains, the structure shakes down to purely elastic behavior: after the transient phase a stabilization of the plastic deformations, the plastic flow ceases completely. Hence, the total work dissipated is bounded in time. We say that the structure shakes down.

Collapse by development of a mechanism, as in limit analysis, can be considered as the particular case of ratcheting where the collapse occurs during the first cycle. The first two failures can be both pointed out by the fact that the total plastic work dissipated is unbounded. As a result, the safety of the structure requires that the power dissipated by the plastic deformation due to variable thermo-mechanical loads should eventually cease. The corresponding load factor α_{SD} is called shakedown load factor. The experimental observations show that α^{SD} is always situated below the limit load α^{L}, sometimes with a significant difference. Above this value, the structure fails by ratcheting or alternating plasticity.

It is worth to remark that a complete step-by-step computation of the overall history up to the limit state (see for instance (Taleb and Hauet, 2009)) can be very time-consuming or even exceed the capacity of the computer. For this reason, the so-called Direct Methods based on shakedown theorems, extended from the classical limit analysis to determine the ultimate load α^{L}, are playing a more and more important role for the prediction of structural failures beyond the elastic range. The shakedown analysis allows a direct access (see (Chinh, 2007; Polizzotto, 2010; Simon, 2013)) to the essential information for engineers, the value of the shakedown factor below which the structural safety is guaranteed in mathematically constructive manners (Save et al., 1997; Maier et al., 2000; Weichert and Maier, 2014), which is potentially more economical than step-by-step inelastic analysis. Besides, sometimes we do not have the full information on the evolution of loads as a time function, for example, the loading path is unknown, then shakedown analysis *must* be used.

There are two dual theoretical theorems as in shakedown analysis. The statical one, with the key-concept of time-independent residual stress field, was introduced historically the first. Papers by Bleich (Bleich, 1932), Melan (Melan, 1936) and Symonds (Symonds, 1951) are considered as the starting point of the method. The kinematical approach and the basic concepts of admissible plastic strain increment were introduced by Koiter (Koiter, 1960) and developed by Neal (Neal, 1956), Gokhfeld (Gokhfeld, 1966)

and Sawczuk (Sawczuk, 1969). An improved formulation including the concept of loading factor was proposed by Martin (Martin, 1975).

The idea to apply shakedown concepts to the fatigue of materials is due to Dang Van (Dang-Van, 1973). Starting with the pioneering Orowan's paper (Orowan, 1939) on grain plasticity, he states that fatigue does not occur if all grains reach an elastic shakedown state. In order to estimate the stress-strain state at the meso scale, a simple homogenization scheme of a plastic inclusion in an elastic matrix is considered by Dang Van (Dang-Van, 1993), Papadopoulos (Papadopoulos, 1994), Charkaluk et al. (Charkaluk et al., 2009).

In the framework of the micromechanics of ductile porous media, Gurson proposed in a famous paper (Gurson et al., 1977) a closed analytical formula for the upper bound limit analysis approach of a hollow sphere having a von Mises solid matrix, with several extensions accounting for void shape effects (Gologanu et al., 1997; Gărăjeu and Suquet, 1997; Monchiet et al., 2007). Based on a relaxed yield criterion,an alternative stress variational approach which provides a quasi-lower bound —slightly more accurate as Gurson model— leading to a macroscopic criterion depending not only on the first and second invariant of the macro-stress but also on the third one, was recently proposed(Cheng et al., 2014; Shen et al., 2015). Combining the limit analysis and conic programming, accurate numerical approximations can be obtained by considering the hollow sphere (Thoré et al. (Thoré et al., 2009)) or the hollow spheroid (Pastor et al. (Pastor et al., 2013)).

On the ground of micromechanical simulation, the problem of porous unit cell subjected to cyclic loading was investigated from a more theoretical point of view by Gilles et al. (Gilles et al., 1992). They concluded that the reduction of ductility under cyclic loadings probably arises from an effect of gradual increase of the mean porosity during one cycle with the number of cycles, effect called ratcheting of the porosity by Lacroix et al. in (Lacroix et al., 2016). These latter authors proposed an improved version of Leblond-Perrin-Devaux model (Leblond et al., 1995) which allows a satisfactory reproduction of the results of the micromechanical simulations.

Unlike these works which are concerned only by the former cycles during the transient phase, our aim in the present work is to determine the limit state of porous ductile materials under cyclically variable repeated loads by considering the hollow sphere model in Gurson's spirit. Unlike the kinematical approach, the statical one, based on Melan's theorem, does not require burdensome calculations of integrals that may lead to heavy expressions. If there exists a time-independent residual stress field such that, added to the elastic stress response in a corresponding fictitious perfectly elastic body, the resulting stress is plastically admissible everywhere at any time, the hollow sphere shakes down and, following Dang Van,

we state the fatigue does not occur. In order to determine the safety domain under cyclic loading, we maximize the size of the load domain, that provides a fatigue criterion for porous ductile materials.

The theorems of limit analysis and shakedown analysis provide a powerful method for determination of the limit loads under which the structure remains stable. However, although exact collapse loads can be determined analytically for various problems, complete solution rarely was obtained for individual problems with complex geometric forms and boundary conditions. For shakedown analysis, the analytical evaluation of α_{SD} is much more difficult because of numerous possible combinations of the loads. Concerning the limit analysis, one can quote the computation of the overall yield stress for soils reinforced by periodic linear inclusions (de Buhan et al. (de Buhan and Hassen, 2013)) and periodically heterogeneous plates (Bleyer et al. (Bleyer et al., 2015)). Concerning the shakedown analysis, Hachemi et al. (Hachemi et al., 2000, 2014) proposed a numerical methodology to investigate the failure of periodic composite materials under thermo-mechanical variable loads in presence of plasticity and damage. In Chen et al. (Chen et al., 2013), it is combined with interior point method for efficient computation. In our research, we aim at also providing a numerical method to determine the shakedown limit of ductile porous materials by transforming the statical theorem to a large-size optimization problem.

This thesis is composed of 4 chapters as follows:

Chapter 1 In the first chapter, the basic concepts of the theory of plasticity are firstly recalled. Secondly, we introduce briefly the classical limit analysis approach (statical and kinematical ones) and then the application to porous materials with Gurson's hollow sphere model. In the third part, the main purpose, the extensions to repeated cyclic loadings, is precisely introduced. Then, the basic shakedown theorems, the statical approach (Melan's theorem), which is the base of this thesis, and the dual kinematical one (Koiter's theorem) are recalled.

Chapter 2 In this chapter, we derive analytically a macroscopic criterion to determine the shakedown domain for ductile porous media with von Mises under cyclic loads by the use of Melan's theorem. The exact solution for the pure hydrostatic loading condition is firstly derived, and then combined with an additional trial terms to capture the shear effects. This new macroscopic shakedown criterion depends on the macroscopic mean stress, equivalent stress, the sign of the third invariant of stress deviator, the porosity and the Poisson's coefficient. The key point relies on the choice of a more appropriate trial residual stress field allowing analytical computations.

Chapter 3 This chapter aims at calculating the shakedown limit of hollow sphere model with Drucker-Prager matrix. Likewise, the key idea is in two steps: (i) the choice of appropriate trial stress and trial resid-

ual stress fields and (ii) then maximizing the size of the load domain in the spirit of the standard lower shakedown theorem. Together with the limit analysis-based yield criterion corresponding to the sudden collapse by development of a mechanism at the first cycle, it defines the safety domain of porous materials subjected to cyclic load processes. The safe domain is little sensitive to variations of the friction angle, however, it is considerably reduced compared to the one under monotonic loads obtained by limit analysis.

Chapter 4 The last chapter is devoted to provide a direct numerical method to predict the shakedown safety domain of porous materials subjected to multi-varying independently loadings. Considering the critical loading path of the load domain instead of the whole history, the statical shakedown condition leads to a large-size optimization problem, of which the objective function is the shakedown limit factor, with the discretization of a three dimensional model with von Mises matrix. By the application of a non-linear optimizer IPOPT using the interior-point method, the proposed optimization is solved efficiently to give not only the limit load factor, but also the corresponding residual stress tensor for the shakedown state. In order to access the reliability of the present method, the obtained results are illustrated and compared to the incremental step-by-step FEM computations with the same load program.

Chapter 1

Limit analysis and shakedown theory : basic concepts and application to porous materials

In this introductory chapter, the fundamental concepts of plasticity theory in small deformations are recalled. First, we present the basic definitions and some classical hypothesis concerning the elastic plastic constitutive laws formulations. Perfect plasticity, hardening and non associated plasticity are briefly outlined. Then, we introduce the statical and kinematical limit analysis approaches to model collapse of rigid plastic solids under monotonic loads. Without being exhaustive, the application of the upper and lower bounds theorems of limit analysis for the ductile rupture of porous materials are presented. The shakedown theorems, the statical approach (Melan's theorem), and the dual kinematical one (Koiter's theorem) are then provided. A particular attention is focused on Melan's theorem since it is the base of this thesis. Finally, although few papers are dealing with the analysis of ductility under cyclic loadings, the bibliography on the shakedown of ductile porous materials is listed.

1.1 An overview of fundamentals of elastoplastic theory in small deformations

1.1.1 Elastic perfectly plastic materials

We consider a deformable body Ω surrounded by the surface $\partial\Omega$, and made of an elastic perfectly plastic material, which behaves elastically below the yield stress σ_0 and begins to yield if it reaches the yield

stress. The surface $\partial\Omega$ is composed of two parts: $\partial\Omega_u$ on which is imposed the displacement $\bar{\boldsymbol{u}}$ and $\partial\Omega_s$ on which is imposed the surface load $\bar{\boldsymbol{p}}$.

The plastic deformation is assumed to occur under a constant flow stress and it can undergo unlimited plastic deformations when it is subjected to a state of stress with $F(\boldsymbol{\sigma}) = 0$, where F represents the yield function of Cauchy's stress tensor $\boldsymbol{\sigma}$. Elasticity and plasticity are combined by the additive decomposition of the strain into its elastic part and its plastic one:

$$\boldsymbol{\varepsilon} = \boldsymbol{\varepsilon}^e + \boldsymbol{\varepsilon}^p \tag{1.1}$$

The elastic strains are related to the stresses through Hookes law:

$$\boldsymbol{\varepsilon}^e = \boldsymbol{S}\boldsymbol{\sigma} \tag{1.2}$$

where $\boldsymbol{S}$ is the compliance tensor for an isotropic homogeneous body given by:

$$S_{ijkl} = \frac{1}{E}\left[(1+\nu)\,\delta_{ij}\delta_{kl} - \nu\delta_{ij}\delta_{kl}\right] \tag{1.3}$$

in which E, ν donate the Young modulus and Poisson's ratio respectively, and δ_{ij} is Kronecker's symbol.

Besides, under the assumption of small deformations, we adopt the internal compatibility equations to relate the strain field $\boldsymbol{\varepsilon}$ and the displacement field $\boldsymbol{u}$:

$$\boldsymbol{\varepsilon}(\boldsymbol{u}) = grad_s\boldsymbol{u} \quad in\,\Omega \tag{1.4}$$

where the displacements $\boldsymbol{u}$ are subjected to the boundary kinematical condition:

$$\boldsymbol{u} = \bar{\boldsymbol{u}} \quad on\,\partial\Omega_u \tag{1.5}$$

Likewise, the stress fields $\boldsymbol{\sigma}$ also need to fulfill internal the equilibrium equations:

$$div\boldsymbol{\sigma} + \boldsymbol{f} = \boldsymbol{0} \quad in\,\Omega \tag{1.6}$$

where $\boldsymbol{f}$ donates the body forces vector, and the stress field is also subjected the boundary condition:

$$\boldsymbol{\sigma}\boldsymbol{n} = \bar{\boldsymbol{p}} \quad on\,\partial\Omega_s \tag{1.7}$$

in which $\boldsymbol{n}$ is the unit vector towards out of the boundary.

The surface with the equation

$$F(\boldsymbol{\sigma}) = 0 \tag{1.8}$$

is called the yield surface, which depends only on the state of stress for elastic perfectly plastic materials. As a result, the stress space is divided by the yield surface into three parts: $F(\boldsymbol{\sigma}) < 0$ corresponds to the elastic behaviors; $F(\boldsymbol{\sigma}) = 0$ means that plastic flow occurs when the stress state is on the yield surface; $F(\boldsymbol{\sigma}) > 0$ corresponds to states of stress that cannot be attained for the perfectly plastic material.

In Drucker's sense, an inelastic material is considered stable at a stress point if deformed by any stress increment $\Delta\boldsymbol{\sigma}$, it absorbs a positive work $\Delta\boldsymbol{\sigma} : \Delta\boldsymbol{\varepsilon} > 0$ (Drucker, 1963).

We may deduce Hill's principle of maximum power principle (Hill, 1948) from Drucker's postulate:

$$(\boldsymbol{\sigma} - \boldsymbol{\sigma}^*)\, \dot{\boldsymbol{\varepsilon}}^p \geq 0 \tag{1.9}$$

$\boldsymbol{\sigma}^*$ is any attainable stress state inside the yield surface.

Drucker's stability postulate (Drucker, 1956, 1963) has the following important consequences:

- **Convexity.** Materials that obey the Drucker's stability postulate always have a convex yield function F in the stress space. The plastic strain rate $\dot{\boldsymbol{\varepsilon}}^p$ associated to $\boldsymbol{\sigma}$ by the plastic yielding rule satisfies Hill's maximum power principle (1.9) (Hill, 1948):

- **Normality.** The plastic strain rate $\dot{\boldsymbol{\varepsilon}}^p$ must be normal to the yield surface and directed toward the exterior of this surface (Mises, 1928; Drucker, 1951; Koiter, 1953):

$$\dot{\boldsymbol{\varepsilon}}^p = \lambda \frac{\partial F}{\partial \boldsymbol{\sigma}} \tag{1.10}$$

  where $\lambda \geq 0$ is the plastic multiplier. The normality law (1.10) is also called the associated plastic flow law.

The quantity $D(\dot{\boldsymbol{\varepsilon}}^p) = \boldsymbol{\sigma} : \dot{\boldsymbol{\varepsilon}}^p$ is called the plastic dissipation, and from (1.9) we can deduce the **principle of maximum plastic dissipation**: *of all possible stress states $\boldsymbol{\sigma}^*$ (within or on the yield surface), the one which arises is that which requires the maximum plastic work*

$$D(\dot{\boldsymbol{\varepsilon}}^p) \geq \boldsymbol{\sigma}^* : \dot{\boldsymbol{\varepsilon}}^p \tag{1.11}$$

1.1.2 Hardening plasticity

The model of perfect plasticity can not be always applied since for most common materials, in the hardening case, the yield limit can be modified with the deformation history (Nguyen, 2000).

The initial yield surface is expressed by (1.8). For the elastic perfectly plastic model, the yield surface remains unchanged, but in the hardening case, the yield surface may change size, shape and position:

$$F(\boldsymbol{\sigma}, K_i) = 0 \tag{1.12}$$

where K_i represents the hardening parameters, which change during plastic deformation and determine the evolution of the yield surface. At first yield, the hardening parameters are zero, and $F(\boldsymbol{\sigma}, 0) = F_0(\boldsymbol{\sigma})$.

In the following part, we introduce some classical hardening models.

- **Isotropic hardening**. The yield surface is homothetic in the stress space and expands with increasing stress (Eterovic and Bathe, 1990; Atluri, 1984). The yield function takes the expression:

$$F(\boldsymbol{\sigma}, K_i) = F_0(\boldsymbol{\sigma}) - K = 0 \tag{1.13}$$

  The shape of the yield function is specified by the initial yield function and its size is determined by the hardening parameter K.

- **Kinematic Hardening**. In this case, the yield surface remains the same shape and size but merely translates in stress space (Chaboche, 1991; Dafalias, 1983; Abdel-Karim and Ohno, 2000). Then the yield function takes the following form:

$$F(\boldsymbol{\sigma}, K_i) = F_0(\boldsymbol{\sigma}, \boldsymbol{\alpha}) = 0 \tag{1.14}$$

  Here the hardening parameter $\boldsymbol{\alpha}$ is called the back-stress, and the yield surface is shifted relative in the stress space by $\boldsymbol{\alpha}$.

- **Mixed hardening**. In this more complex hardening case, the position, shape and size of the yield surface are changed (Schwer and Murray, 1994; Axelsson and Samuelsson, 1979). The hardening parameters are now the scalar K and the tensor α, then the yield function is given:

$$F(\boldsymbol{\sigma}, K_i) = F_0(\boldsymbol{\sigma}, \boldsymbol{\alpha}) - K = 0 \tag{1.15}$$

However, the effects of hardening is not considered in this research.

1.1.3 Non-associated plasticity

Materials like soil and rocks have often non-associated plastic behaviors, where the the plastic strain rate is not normal to yield surface (Stoughton, 2002; Stoughton and Yoon, 2004). We introduce the plastic potential G to describe the plastic flow rule (Vermeer and De Borst, 1984):

$$d\boldsymbol{\varepsilon}^p = d\lambda \frac{\partial G}{\partial \boldsymbol{\sigma}} \tag{1.16}$$

Here let us take Drucker-Prager's model for example (Cheng et al., 2015a), the plastic strain rate $\dot{\boldsymbol{\varepsilon}}^p$ is given:

$$\dot{\boldsymbol{\varepsilon}}^p = d_{eq} \frac{\partial G}{\partial \boldsymbol{\sigma}} \tag{1.17}$$

where $d_{eq} = \sqrt{2/3\boldsymbol{d}' : \boldsymbol{d}'}$ with $\boldsymbol{d}'$ being the deviatoric part of the plastic strain rate $\dot{\boldsymbol{\varepsilon}}^p$.

The yield function F and the plastic potential G are in the form:

$$\begin{aligned} F(\boldsymbol{\sigma}) &= \sigma_e - 3\alpha\sigma_m - \sigma_0 \leq 0 \\ G(\boldsymbol{\sigma}) &= \sigma_e - 3\beta\sigma_m - \sigma_0 \end{aligned} \tag{1.18}$$

in which σ_m and σ_e represent the mean stress and effective stress, respectively; α is the pressure sensitivity factor related to the friction angle ϕ, and β related to the dilatancy angle Ψ:

$$tan\phi = 3\alpha \qquad tan\Psi = 3\beta \tag{1.19}$$

If the friction angle is equal to the dilatancy angle $\phi = \Psi$, the plastic potential G is the yield function F, and we recover the associated flow rule.

For the study of the limit load of non-associated material, the bipotential approach has been developed since last decades (De Saxcé, 1995; De Saxcé and Feng, 1998; Hjiaj et al., 2003; Magnier et al., 2014; Cheng et al., 2015a). *Noticing that, in the shakedown problem of pressure sensitive material in Chapter 3, we focus our attention only on the associated material.*

1.2 Plastic Limit analysis

Limit analysis is the oldest and most developed approach which allows rapid access to the requested information to determine the limit loads for materials and structures (Gvozdev, 1960; Hill, 1951; Prager et al., 1958; Drucker et al., 1952). Before talking about the theorems of limit analysis, we shall introduce firstly the principle of virtual work (Cook et al., 1974).

Principle of virtual work: *For a considered body in equilibrium under a virtual displacement $\delta\boldsymbol{u}$, the virtual work of external forces on this virtual displacement field $\delta\boldsymbol{u}$ satisfying the kinematical boundary condition (1.5) is equal to the virtual work of the internal forces on the virtual strains $\delta\boldsymbol{\varepsilon}$ corresponding to the considered virtual displacements.*

$$\int_{\Omega} \boldsymbol{\sigma} : \delta\boldsymbol{\varepsilon}\, dV = \int_{\Omega} \bar{\boldsymbol{f}} \cdot \delta\boldsymbol{\varepsilon}\, dV + \int_{\partial\Omega_s} \bar{\boldsymbol{p}} \cdot \delta\boldsymbol{\varepsilon}\, dS \tag{1.20}$$

Note that the Principle of virtual work can represent the compatibility equations (1.4) and internal equilibrium conditions (1.6) in the form of energy.

1.2.1 Basic concepts

We define the set of kinematical admissible displacement fields:

$$\mathscr{K}_a = \{\mathbf{u} \quad s.t. \quad \mathbf{u}(\mathbf{x}) = \mathbf{u}^d \quad on \quad \partial\Omega_u\}\,. \tag{1.21}$$

and the strain field, symmetric part of the displacement gradient, is $\boldsymbol{\varepsilon}(\mathbf{u}) = grad_s\mathbf{u}$.

The set of statically admissible stress fields is such as:

$$\mathscr{S}_a = \{\boldsymbol{\sigma} \quad s.t. \quad div\,\boldsymbol{\sigma} = \mathbf{0} \quad in\Omega, \quad \boldsymbol{\sigma}\cdot\boldsymbol{n} = \bar{\boldsymbol{p}} \quad on \quad \partial\omega_s\} \tag{1.22}$$

where $\boldsymbol{n}$ is the unit outward normal vector of the matrix and the body force is not considered.

A stress field $\boldsymbol{\sigma}$, belong to the set of set of statically admissible stress fields $\mathscr{S}_a$, is called licit if it is plastically admissible:

$$F(\boldsymbol{\sigma}) \leq 0 \tag{1.23}$$

where F is the convex yield function of the stress tensor.

Likewise, a kinematically admissible strain field $\boldsymbol{\varepsilon} \in \mathscr{K}_a$ is called licit if the external power of the load is positive $P_{ext}(\boldsymbol{u}) > 0$.

Besides, if the stress tensor $\boldsymbol{\sigma}$ and the plastic strain rate tensor $\dot{\boldsymbol{\varepsilon}}^p$ can be associated by the normality law (1.10), the total power $P(\boldsymbol{\sigma})$ of the applied loads is equal to the total dissipation $D(\dot{\boldsymbol{\varepsilon}}^p)$.

From Hill's maximum power principle (1.9), for a plastic strain rate field $\dot{\boldsymbol{\varepsilon}}^p$ and the corresponding stress field $\boldsymbol{\sigma}$ associated by the normality law, the power of $\boldsymbol{\sigma}$ on $\dot{\boldsymbol{\varepsilon}}$ noted $P(\boldsymbol{\sigma},\dot{\boldsymbol{\varepsilon}})$ is larger or equal to the one of any attainable stress field $\boldsymbol{\sigma}^*$:

$$P(\boldsymbol{\sigma},\dot{\boldsymbol{\varepsilon}}) \geq P(\boldsymbol{\sigma}^*,\dot{\boldsymbol{\varepsilon}}) \tag{1.24}$$

Due to the Maximum dissipation principle (1.11), the left side of the previous inequality is the power of dissipation $\int_\Omega D(\dot{\boldsymbol{\varepsilon}})dV$ of the plastic strain rate, so:

$$\int_\Omega D(\dot{\boldsymbol{\varepsilon}})dV \geq P(\boldsymbol{\sigma}^*,\dot{\boldsymbol{\varepsilon}}) \tag{1.25}$$

We note the limit load of the structure under monotone load as α_l. For a given licit stress field, there is a corresponding limit load which can be denoted by α_-. Similarly, for a given licit plastic strain rate $\dot{\boldsymbol{\varepsilon}}$, an intensity of loading α_+ is defined as the power of the given load α_+ equals the power of dissipation of $\dot{\boldsymbol{\varepsilon}}$. As a result, the dual theorems of limit analysis can then be expressed in the following way:

- **Statical theorem**: *Any load α_- corresponding to a licit stress field is smaller than or equal to the limit load: $\alpha_- \leq \alpha_l$.*
- **Kinematical theorem**: *Any load α_+ corresponding to a licit plastic strain rate field is larger than or equal to the limit load: $\alpha_+ \geq \alpha_l$.*

The method of limit analysis started and has been developed in several researches (Hodge, 1959; Onat, 1960; Lance and Onat, 1963; Hill, 1950). *The descriptions of these two fundamental theorem of limit analysis are inspired from (Save et al., 1997; Hodge, 1959)*

1.2.2 Ductile rupture of porous media

To apply the limit analysis methods to ductile porous media, Gurson (Gurson et al., 1977) has proposed a kinematical limit analysis approach of a hollow sphere having a von Mises solid matrix which delivered an upper bound of the searched macroscopic criterion. Based on this pioneering work, a number of micromechanical-based extensions have been further proposed in the literature by using kinematical approach which requires the choice of a suitable trial velocity field (Garajeu, 1995; Gărăjeu and Suquet, 1997; Monchiet et al., 2007). Tvergaard at al. (Tvergaard, 1981; Tvergaard and Needleman, 1984) have extended it to the GTN (Gurson-Tvergaard-Needelman) model which has been widely used by many

researchers for various structural applications. Over the applications of ductile materials, one the most important development is to take into consideration of void shape effects allowing the computational investigation of the effects of penny shaped cracks on ductile behavior (Gologanu et al., 1997; Madou and Leblond, 2012a,b). Besides, a more complex case for anisotropic plastic matrix with spherical voids was studied in (Benzerga and Besson, 2001) and extended to spheroidal cavities latterly in (Monchiet et al., 2006, 2008; Keralavarma and Benzerga, 2010). The influences of void size and void distribution are considered by (Fritzen et al., 2012; Shen et al., 2017)

On the other hand, few applications of the statical theorem have been devoted to porous media. A semi-analytical approach to deliver a lower bound criterion for ductile porous media by some fitting procedure based on numerical computations is firstly provided by (Yi and Duo, 1989; Sun and Wang, 1995). In a recent work, Cheng et al. (Cheng et al., 2014) proposed a new Stress Variational Homogenization (SVM) of ductile porous materials having a von Mises matrix providing a quasi-lower bound depending on the first, second and third invariants of the macro-stress, and extend to arbitrary 3D stress loadings case accounting for Lode angle effect (Cheng et al., 2015b). Shen et al. has improved this model by the construction of a strictly statically admissible stress field under pure deviatoric loads (Shen et al., 2015).

For Gurson's model, we consider a reference unit cell or macro-element Ω composed of a void ω and matrix $\Omega_M = \Omega - \omega$. The macro-element Ω is bounded by surface $\partial\Omega$ and the void ω by $\partial\omega$. The porosity is denoted $f = \frac{\omega}{\Omega} = (a/b)^3$ with a and b the inner and outer rayons of the sphere, respectively.

The homogenization problem consists in determining the macroscopic stress for which there exist at least an admissible couple $(\boldsymbol{v}, \boldsymbol{\sigma}) \in \mathscr{K}_a \times \mathscr{S}_a$ satisfying anywhere in the matrix the yield criterion and the normality rule. [1] From Hill's classical principle (Hill, 1950), we adopt the homogeneous deformation boundary condition $\boldsymbol{v}(\boldsymbol{x}) = \boldsymbol{D} \cdot \boldsymbol{x}$. The overall stress $\boldsymbol{\Sigma}$ and strain rate $\boldsymbol{D}$ are defined as volume averages of their microscopic counterparts $\boldsymbol{\sigma}$ and $\boldsymbol{d}$:

$$\boldsymbol{\Sigma} = \frac{1}{|\Omega|}\int_{\Omega_M} \boldsymbol{\sigma}\, dV\,, \qquad \mathbf{D} = \frac{1}{|\Omega|}\int_{\Omega} \boldsymbol{d}\, dV\,. \tag{1.26}$$

and Hill-Mandel's lemma (Hill, 1967):

$$\boldsymbol{\Sigma} : \boldsymbol{D} = \frac{1}{|\Omega|}\int_{\Omega_M} (\boldsymbol{\sigma} : \boldsymbol{d})\, dV \tag{1.27}$$

[1] *For more details about the homogenization and application of kinematical limit analysis method to hollow sphere, the reader can refer to (Leblond and Germain, 2003).*

The function of maximum local plastic dissipation $\pi(\boldsymbol{d})$ of a admissible stress field $\boldsymbol{\sigma}^*$ is defined by:

$$\pi(\boldsymbol{d}) = \max_{\boldsymbol{\sigma}^* \in \mathscr{S}_a} (\boldsymbol{\sigma}^* : \boldsymbol{d}) \tag{1.28}$$

and the macroscopic plastic dissipation $\Pi(\boldsymbol{D})$:

$$\Pi(\boldsymbol{D}) = \min_{\boldsymbol{v} \in \mathscr{K}_a} \frac{1}{|\Omega|} \int_{\Omega_M} (\boldsymbol{\sigma} : \boldsymbol{d})\, dV \tag{1.29}$$

Thus, for any $\boldsymbol{\Sigma}$ and $\boldsymbol{D}$ such that there exist a stress field $\boldsymbol{\sigma} \in \mathscr{S}_a$ with $F(\boldsymbol{\Sigma}) \leq 0$, it is seen:

$$\boldsymbol{\Sigma} : \boldsymbol{D} \leq \Pi(\boldsymbol{D}) \tag{1.30}$$

For the macroscopic stress tensor $\boldsymbol{\Sigma}$ associated with $\boldsymbol{D}$ at limit states, we have $\boldsymbol{\Sigma} : \boldsymbol{D} = \Pi(\boldsymbol{D})$, the yield surface at macroscopic scale can be defined by the equation $F(\boldsymbol{\Sigma}, \boldsymbol{D}) = \boldsymbol{\Sigma} : \boldsymbol{D} - \Pi(\boldsymbol{D})$:

$$\begin{cases} F(\boldsymbol{\Sigma}, \boldsymbol{D}) = \boldsymbol{\Sigma} : \boldsymbol{D} - \Pi(\boldsymbol{D}) = 0 \\ \dfrac{\partial F}{\partial \boldsymbol{D}}(\boldsymbol{\Sigma}, \boldsymbol{D}) = \boldsymbol{\Sigma} - \dfrac{\partial \Pi}{\partial \boldsymbol{D}}(\boldsymbol{D}) = 0 \end{cases} \tag{1.31}$$

So the macroscopic limit stress of the hollow sphere can be obtained by:

$$\boldsymbol{\Sigma} = \frac{\partial \Pi}{\partial \boldsymbol{D}}(\boldsymbol{D}) \tag{1.32}$$

In order to apply the kinematical limit analysis methods to ductile porous materials with von Mises matrix, Gurson (Gurson et al., 1977) has proposed a particular microscopic velocity field in the spherical coordinates which is totally determined by the macroscopic strain rate $\boldsymbol{D}$:

$$\boldsymbol{v}(\boldsymbol{x}) = \frac{D_m}{f} \frac{a^3}{r^2} \boldsymbol{e}_r + \boldsymbol{D}' \boldsymbol{x} \tag{1.33}$$

where $\boldsymbol{D}'$ is the deviatoric part of $\boldsymbol{D}$. By adopting an inequality:

$$\Pi(\boldsymbol{D}) \leq \Pi^+(\boldsymbol{D}) = \frac{1}{|\Omega|} \int_a^b dr \left(\int_{S(r)} (\pi(\boldsymbol{d}))^2\, dS \right)^{1/2} \tag{1.34}$$

with

$$\pi(\boldsymbol{d}) = \sigma_0 d_{eq} = \sigma_0 (\boldsymbol{d} : \boldsymbol{d})^{1/2} \tag{1.35}$$

The upper bound of the macroscopic dissipation Π_{hom} can be expressed only by $\boldsymbol{D}$, and the limit stress at the macroscopic scale takes the form $\boldsymbol{\Sigma} = \partial\Pi^+/\partial\boldsymbol{D}$. More precisely, if we consider the spheric and deviatoric part, then the admissible states can be expressed by:

$$\boldsymbol{\Sigma} = \frac{\partial\Pi^+}{\partial D_m}\frac{\partial D_m}{\partial \boldsymbol{D}} + \frac{\partial\Pi^+}{\partial D_e}\frac{\partial D_e}{\partial \boldsymbol{D}} \tag{1.36}$$

with the macroscopic mean stress $\Sigma_m = \partial\Pi^{hom}/\partial D_m$ and equivalent stress $\Sigma_e = \partial\Pi^{hom}/\partial D_e$, which leads finally to the famous Gurson's criterion:

$$\left(\frac{\Sigma_e}{\sigma_0}\right)^2 + 2f\,cosh\left(\frac{3\Sigma_m}{2\sigma_0}\right) - 1 - f^2 = 0 \tag{1.37}$$

Noticing that Gurson's criterion depends only on the first and second invariant of the macroscopic stress tensor, but not on the third one. Recently, based on a relaxed yield criterion with the same hollow sphere model, Cheng et al. (Cheng et al., 2014) proposed an alternative stress variational approach which provides a quasi-lower bound more accurate depending also on the sign of the third stress invariant.

It has been shown in (Cheng et al., 2014) that the statical variational principal (Hill, 1948) for the RVE is equivalent to the following minimization problem:

$$\min_{\boldsymbol{\sigma}\in\mathscr{S}_a}(-\boldsymbol{D}:\boldsymbol{\Sigma}) \tag{1.38}$$

under the yield condition $F(\sigma) = 0$, and if $\boldsymbol{\sigma}$ is statically admissible, $\boldsymbol{\Sigma}$ depends on it through:

$$\boldsymbol{\Sigma} = \frac{1}{|\,\Omega\,|}\int_{\partial\Omega}(\boldsymbol{\sigma}\cdot\mathbf{n})\otimes\boldsymbol{x}\;dS \tag{1.39}$$

An approximation is then proposed to satisfy the condition $F(\sigma) = 0$ in an average sense:

$$F(\sigma) = \frac{1}{|\,\Omega\,|}\int_{\Omega_M} F(\boldsymbol{\sigma})\;dV = 0 \tag{1.40}$$

Inspired from (Guo et al., 2008), the minimization problem (1.38) is transformed into an equivalent saddle-point problem:

$$\max_{\dot\Lambda\geq 0}\min_{\boldsymbol{\sigma}\in\mathscr{S}_a}\left(\mathscr{L}(\boldsymbol{\sigma},\dot\Lambda) = \dot\Lambda\frac{1}{|\,\Omega\,|}\int_{\Omega_M} F(\boldsymbol{\sigma})\;dV - \boldsymbol{D}:\boldsymbol{\Sigma}\right) \tag{1.41}$$

by imposing Lagrange's multiplier field $\dot\Lambda$ to be uniform in Ω_M.

Finally, by the choice of a trial stress field σ and expressing it with respect to the invariants of the

macroscopic one, the macroscopic yield condition takes the following form by performing the variation with respect to $\dot{\Lambda}$:

$$\mathscr{F}(\boldsymbol{\Sigma}) = \frac{1}{|\,\Omega\,|}\int_{\Omega_M} F(\boldsymbol{\sigma}(\boldsymbol{\Sigma}))\, dV \leq 0 \tag{1.42}$$

Similar to the normality law (1.10), with respect to $\boldsymbol{\Sigma}$ the macroscopic plastic flow rule reads:

$$\boldsymbol{D} = \dot{\Lambda}\frac{\partial \mathscr{F}(\boldsymbol{\Sigma})}{\partial \boldsymbol{\Sigma}} \tag{1.43}$$

It is interestingly seen that, in the spirit of Gurson's paper, almost all the the kinematical and statical limit analysis of porous materials with an associated matrix requires the choice of a trial velocity field or stress field which is generally built by adding deviatoric terms to the exact one for hydrostatic loading.

1.3 Extension to repeated cyclic loadings

1.3.1 Asymptotic responses and shakedown theorems

In the case of variable repeated loads, the magnitude of the ultimate load α_l is not the only factor characterizing the structural safety. Experiments have shown that although below α_l, the asymptotic behaviors (when time tends to infinity) for the limit state, characterized by evolution inelastic deformation and hardening, can be ratcheting, accommodation or adaptation (shakedown) [2].

- **Ratcheting**: In this case, we can observe the accumulation of plastic strains gives birth to an incremental collapse mechanism, with monotonically increasing excessive deflections (see Figure 1.1) (Hassan and Kyriakides, 1992). The ruin of the structure then occurs very quickly either by excessive deformation, either by cracking. This kind of failure is called ratcheting due to progressive accumulation of plastic deformation.

- **Accommodation**: The behavior observed on Figure 1.2 is called alternating plasticity or accommodation. although the reversal plastic strains remain small and the incremental collapse is prevented, the alternating plastic strain increments also leads to fracture by exhaustion of ductility after after the transient phase (Laitusis et al., 2007). At each point, the plastic deformation changes during the cycle, but recovers its initial values at the end of the cycle:

$$\lim_{\tau\to+\infty}\int_{\tau}^{\tau+Te} \dot{\boldsymbol{\varepsilon}}^p(\boldsymbol{x},t)\,dt = 0 \tag{1.44}$$

[2] The Asymptotic responses are inspired from (Maitournam, 2013)

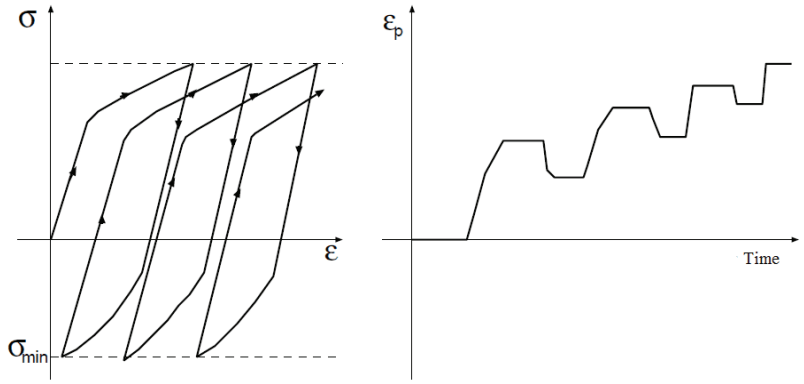

Figure 1.1: Ratcheting

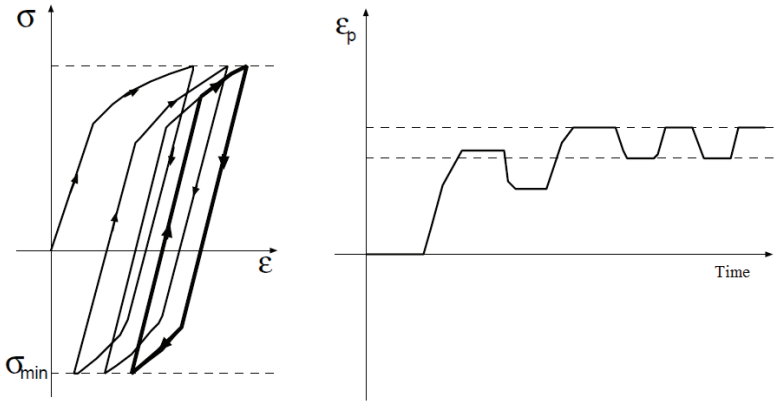

Figure 1.2: Accommodation

- **Shakedown**: As shown on Figure 1.3, the structure endures a finite number of cycles with a stabilization of the plastic strains, and the structure shakes down to purely elastic behavior (Druyanov and Roman, 1998). In this case, at any point of the structure, when the time variable t becomes sufficiently large, the plastic strain $\boldsymbol{\varepsilon}^p(\boldsymbol{x}, t)$ tends towards a fixed value $\boldsymbol{\varepsilon}^p_\infty(\boldsymbol{x})$:

$$\lim_{t\to+\infty} \boldsymbol{\varepsilon}^p(\boldsymbol{x}, t) = \boldsymbol{\varepsilon}^p_\infty(\boldsymbol{x}) \tag{1.45}$$

At the point of view of energy, the shakedown occurs if the total dissipated energy remains bounded when t goes to infinity, permanent plastic deformation tending then to a fixed value at every point:

$$\lim_{\tau\to+\infty} \int_0^\tau \int_\Omega D(\boldsymbol{\varepsilon}^p)\, dV\, dt < +\infty \quad or \quad \lim_{\tau\to+\infty} \int_\tau^{\tau+Te} D(\boldsymbol{\varepsilon}^p)\, dt = 0 \tag{1.46}$$

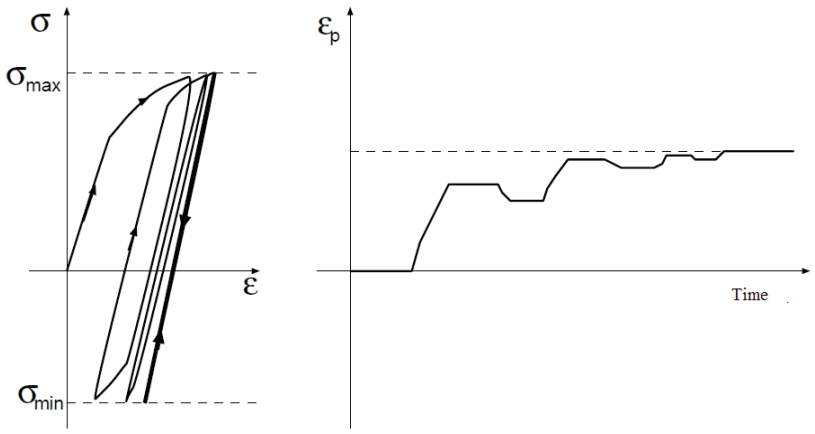

Figure 1.3: Shakedown

The first two failures (accommodation and ratcheting) can be both pointed out by the fact that the total dissipation is unbounded (Maitournam, 2013; Weichert and Maier, 2014). The corresponding safety load factor is noted as α_{SD}, below which the shakedown occurs.

On the other hand, the study of Wöhler's curves (Fritzen et al., 2012) defines two different types of fatigue of the structure under cyclic loadings: high-cycle fatigue and low-cycle fatigue. The low-cycle fatigue appears in the case of accommodation. The law of low-cycle fatigue (or plastic fatigue) (Manson, 1954; Coffin Jr, 1954) gives the number of cycles N_F leading to the fracture which depends on the local plastic strain amplitude $\Delta\varepsilon^p$ according to laws of which the most simple has the following form :

$$\Delta\varepsilon^p = \varepsilon_F \left(N_F\right)^{-\gamma} , \tag{1.47}$$

where the exponent γ and the fatigue-ductility coefficient ε_F are material dependent positive constants. In the case of high-cycle fatigue, the structure subjected to cyclic loadings is in an elastic or shakedown state. In reality, the macroscopic stress of mechanics continuous media are an average of mesoscopic stress in the different constituents of the REV. Macroscopic adaptation is therefore an adaptation based on on average values, witch does not guarantee the shakedown state at the constituent level. On the ground of the pioneering Orowan's work (Orowan, 1939) on grain plasticity, Dang Van (Dang-Van, 1973) developed his shakedown-based approach for the high-cycle fatigue, assuming that the damage occurs at the mesoscopic scale and stating that *fatigue does not occur if all grains reach a shakedown state.*

Now to analyse directly the shakedown states, we denote $\boldsymbol{\sigma}^E$ and $\boldsymbol{\varepsilon}^E$ the instantaneous values of the stresses and strains in the corresponding fictitious elastic body. The residual stresses $\boldsymbol{\rho}$ and strains $\boldsymbol{\eta}$ are

defined by

$$\boldsymbol{\rho} = \boldsymbol{\sigma} - \boldsymbol{\sigma}^E, \qquad \boldsymbol{\eta} = \boldsymbol{\varepsilon} - \boldsymbol{\varepsilon}^E \tag{1.48}$$

In general, the residual stress field $\boldsymbol{\rho}$ can be taken as any solution of the homogeneous equilibrium equations and in equilibrium with vanishing loads and belongs to the set of *residual stress fields*:

$$\mathcal{N} = \{\boldsymbol{\rho} \quad | \quad div\,\boldsymbol{\rho} = \mathbf{0} \quad in\Omega, \quad \boldsymbol{\rho}\cdot\boldsymbol{n} = \mathbf{0} \quad on\partial\Omega_s\} \tag{1.49}$$

Likewise, the residual strain field $\boldsymbol{\eta}$ belongs to the set $\mathcal{N}^*$:

$$\mathcal{N}^* = \{\boldsymbol{\eta} \quad | \quad \boldsymbol{\eta} = grad_s\boldsymbol{u} \quad in\Omega, \quad \boldsymbol{u} = \mathbf{0} \quad on\partial\Omega_u\} \tag{1.50}$$

The key idea of the statical approach is to define the *admissible residual stress fields* (in Melan's sense) $\bar{\boldsymbol{\rho}}(\boldsymbol{x})$, corresponding to the load domain $\mathcal{S}$, such that (Melan, 1936):

- $\bar{\boldsymbol{\rho}}$ is time-independent,
- $\bar{\boldsymbol{\rho}}$ is a residual stress field : $\bar{\boldsymbol{\rho}} \in \mathcal{N}$,
- $\bar{\boldsymbol{\rho}}$ is *plastically admissible* in the sense that:

$$\forall \boldsymbol{\sigma}^E \in \mathcal{S}, \quad F(\boldsymbol{\sigma}^E + \bar{\boldsymbol{\rho}}) \leq 0 \quad in \quad \Omega \quad at \quad any \quad time \tag{1.51}$$

Moreover, if $F(\boldsymbol{\sigma}^E + \bar{\boldsymbol{\rho}}) < 0$ in Ω at any time, $\bar{\boldsymbol{\rho}}(\boldsymbol{x})$ is said to be a *strictly admissible residual stress field.* Hence, the following theorem was proved by Melan (Melan, 1936):

Melan's theorem (Statical theorem): *If a strictly admissible residual stress field $\bar{\boldsymbol{\rho}}$ can be found, the body shakes down regardless of its initial state.*

[3] To prove Melan's theorem, we suppose that an admissible residual stress field $\bar{\boldsymbol{\rho}}$ exists. The fictitious residual elastic energy of the stress difference $(\boldsymbol{\rho} - \bar{\boldsymbol{\rho}})$ notes:

$$\mathcal{R} = \int_\Omega (\boldsymbol{\rho} - \bar{\boldsymbol{\rho}}) : \boldsymbol{S}(\boldsymbol{\rho} - \bar{\boldsymbol{\rho}})\, dV \geq 0 \tag{1.52}$$

By Hooke's law (1.2)

$$\boldsymbol{\eta} = (\boldsymbol{S}\boldsymbol{\sigma}^E + \boldsymbol{\varepsilon}^p) - \boldsymbol{S}\boldsymbol{\sigma} = \boldsymbol{S}(\boldsymbol{\sigma} - \boldsymbol{\sigma}^E) + \boldsymbol{\varepsilon}^p \tag{1.53}$$

[3] *The proof of this statical theorem is inspired from (Weichert and Maier, 2014).*

It can be remarked that:

$$\boldsymbol{\eta}^E = \boldsymbol{S}\boldsymbol{\rho}, \quad \boldsymbol{\eta}^p = \boldsymbol{\varepsilon}^p \tag{1.54}$$

And because of the time-independent strain field $\bar{\boldsymbol{\eta}}^E$, the time derivative of (1.52) is reduced to:

$$\dot{\mathscr{R}} = \int_\Omega (\boldsymbol{\rho} - \bar{\boldsymbol{\rho}}) : \dot{\boldsymbol{\eta}}^E \, dV \tag{1.55}$$

Owing to (1.54), (1.55) can be rewritten as:

$$\dot{\mathscr{R}} = \int_\Omega (\boldsymbol{\rho} - \bar{\boldsymbol{\rho}}) : \dot{\boldsymbol{\eta}} \, dV - \int_\Omega (\boldsymbol{\rho} - \bar{\boldsymbol{\rho}}) : \dot{\boldsymbol{\varepsilon}}^p \, dV \tag{1.56}$$

As $\bar{\boldsymbol{\rho}} \in \mathscr{N}$ and $\dot{\boldsymbol{\eta}} \in \mathscr{N}^*$, because of virtual power principle (1.20), the first term of the right hand side vanishes. According to the definition of the residual stress fields:

$$\boldsymbol{\rho} - \bar{\boldsymbol{\rho}} = (\boldsymbol{\sigma} - \boldsymbol{\sigma}^E) - (\bar{\boldsymbol{\sigma}} - \boldsymbol{\sigma}^E) = \boldsymbol{\sigma} - \bar{\boldsymbol{\sigma}} \tag{1.57}$$

one has:

$$\dot{\mathscr{R}} = -\int_\Omega (\boldsymbol{\sigma} - \bar{\boldsymbol{\sigma}}) : \dot{\boldsymbol{\varepsilon}}^p \, dV \tag{1.58}$$

And from the definition of the dissipation,

$$\dot{\mathscr{R}} = -\int_\Omega D(\dot{\boldsymbol{\varepsilon}}^p) - \bar{\boldsymbol{\sigma}} : \dot{\boldsymbol{\varepsilon}}^p \, dV \tag{1.59}$$

Because of the maximum dissipation principle (1.11), then $\dot{\mathscr{R}} \leq 0$.

Now from the shakedown behavior, we need to prove that the total dissipation is bounded . As $\boldsymbol{\sigma}$ and $\bar{\boldsymbol{\sigma}}$ belong to the interior of the elastic domain, there exists a scalar $m > 1$ such that $m\bar{\boldsymbol{\sigma}}$ is plastically admissible. Because of Hill's maximum power principle (1.11), one has:

$$m(\bar{\boldsymbol{\sigma}} - \boldsymbol{\sigma}) : \dot{\boldsymbol{\varepsilon}}^p + (m-1)\boldsymbol{\sigma} : \dot{\boldsymbol{\varepsilon}}^p = (m\bar{\boldsymbol{\sigma}} - \boldsymbol{\sigma}) : \dot{\boldsymbol{\varepsilon}}^p \leq 0 \tag{1.60}$$

Consequently, we can deduce from the previous equation:

$$\int_0^t \int_\Omega \boldsymbol{\sigma} : \dot{\boldsymbol{\varepsilon}}^p \, dV \, dt \leq \frac{m}{m-1} \int_0^t \int_\Omega (\boldsymbol{\sigma} - \bar{\boldsymbol{\sigma}}) : \dot{\boldsymbol{\varepsilon}}^p \, dV \, dt = -\frac{m}{m-1} \int_0^t \dot{\mathscr{R}} \, dt = \frac{m}{m-1} (\mathscr{R}(0) - \mathscr{R}(t)) \tag{1.61}$$

Because $\mathscr{R}(t)$ is non negative and one has :

$$\mathscr{R}(0) - \mathscr{R}(t) \leq \mathscr{R}(0) \tag{1.62}$$

that leads to the expression of total dissipation:

$$\forall t \geq 0, \int_0^t \int_\Omega \boldsymbol{\sigma} : \dot{\boldsymbol{\varepsilon}}^p \, dV \, dt \leq \frac{m}{m-1} \mathscr{R}(0) \tag{1.63}$$

$\frac{m}{m-1}\mathscr{R}(0)$ is time independent and has finite value, so Melan's theorem has been proved.

For the practical use of Melan's theorem, let us introduce the notion of the loading domain. The load $\boldsymbol{\Sigma}$ is supposed to belong to a convex load domain $\mathscr{P}$ which, for instance, can be described by convex combination of elementary loads $\boldsymbol{\Sigma}_1, \cdots, \boldsymbol{\Sigma}_n$:

$$\boldsymbol{\Sigma}(t) = \sum_{k=1}^{n} \mu_k(t) \boldsymbol{\Sigma}_k, \qquad \sum_{k=1}^{n} \mu_k(t) = 1, \qquad \mu_1(t) \geq 0, \cdots, \mu_n(t) \geq 0 \tag{1.64}$$

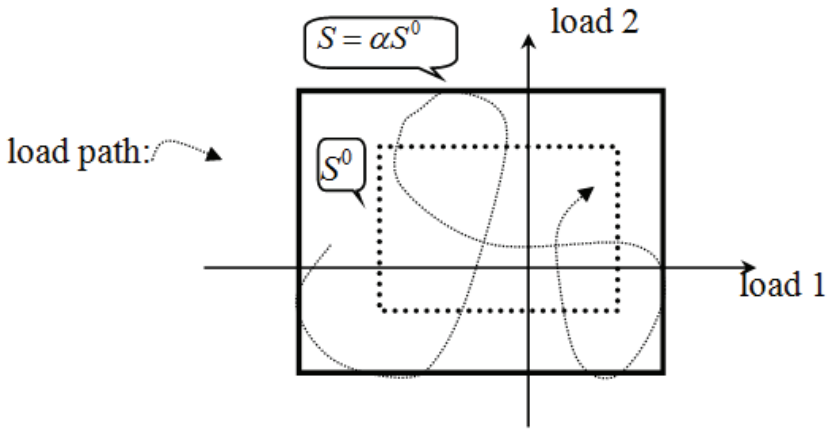

Figure 1.4: Load domain

For the previous actions, the elastic responses in displacement $\boldsymbol{u}^E$, in strain $\boldsymbol{\varepsilon}^E$ and in stress $\boldsymbol{\sigma}^E$, in a corresponding fictitious perfectly elastic body, satisfy Hooke's law. Because of the linearity of the elastic response, the stress field $\boldsymbol{\sigma}^E$ belongs to a convex polyhedral load domain $\mathscr{S} = \alpha \mathscr{S}^0$, homothetic to the reference load domain $\mathscr{S}^0$ corresponding to the load domain $\mathscr{P}^0$ (Figure 1.4). We note the stress field $\boldsymbol{\sigma}^E$ by:

$$\boldsymbol{\sigma}^E = \alpha \boldsymbol{\sigma}_0^E \tag{1.65}$$

where α is the load factor and the reference elastic stress field $\boldsymbol{\sigma}_0^E$ corresponding to the reference load.

Thus, the problem of the shakedown consists in searching the maximum value of the coefficient α which is noted α^{SD} such that the Melan's condition remains fulfilled. The occurrence of shakedown is guaranteed due to **König's statement**(König and Siemaszko, 1988): *If a given structure shakes down over a cyclic load path containing all the vertices of the hyper-polyhedral load domain $\mathscr{P}$ then it shakes down over any load path contained within the $\mathscr{P}$.*

Similar to the analysis limit in the previous subsection, we can prove that: *any load factor α_- corresponding to admissible residual stress fields* (1.51) *is smaller than or equal to the limit load $\alpha_- \leq \alpha_{SD}$.*

In a similar manner to what has been established in limit analysis, there exist a dual shakedown approach to the statical one. Likewise, for the kinematical approach, we consider the plastic strain rate field $\dot{\boldsymbol{\varepsilon}}^p$„ for which the increment plastic strain field over a loading cycle is $\Delta\boldsymbol{\varepsilon}^p = \oint \dot{\boldsymbol{\varepsilon}}^p dt \in \mathscr{N}^*$. Koiter's theorem can be stated as follows (Koiter, 1960):

Koiter's theorem (Kinematical theorem): *If there exists a plastic deformation rate $\dot{\boldsymbol{\varepsilon}}^p$ over the whole history on the interval $[0,+\infty]$, we have*:

$$\int_0^{+\infty}\int_\Omega \boldsymbol{\sigma}^E : \dot{\boldsymbol{\varepsilon}}^p dV\, dt \leq \int_0^{+\infty}\int_\Omega D(\dot{\boldsymbol{\varepsilon}}^p) dV\, dt \tag{1.66}$$

then the shakedown will occur.

Or if we define the admissible plastic strain rates over a loading cycle in Koiter's sense:

- $\Delta\boldsymbol{\varepsilon}^p = \oint \dot{\boldsymbol{\varepsilon}}^p dt \in \mathscr{N}^*$
- $\dot{\boldsymbol{\varepsilon}}^p$ is plastically admissible: $\oint \int_\Omega \boldsymbol{\sigma}_0^E : \dot{\boldsymbol{\varepsilon}}^p dV\, dt > 0$

Hence, the Kinematical theorem (Halphen, 1980) can be stated by Halphen in the following way: *if the body does not shake down, the admissible plastic strain rate can be found.*

For more detailed proofs of these theorems, please refer to (Save et al., 1997; Weichert and Maier, 2014; Leblond and Germain, 2003)

1.3.2 Shakedown analysis of porous composites.

Although the bibliography on the ductile failure of porous materials under monotonic loads is abundant and renewed, there are few papers dealing with the modeling of ductility under cyclic loadings and most of them concern micromechanics-based numerical approaches.

Available experiments regarding structures made up with ductile metals (Kobayashi et al., 1991; Schmidt et al., 1991) have revealed that fracture strains under cyclic loads are significantly lower than the ones reached under monotonic load conditions. Basing upon incremental finite element simulations of the elastic plastic response of a hollow cylinder subjected to repeated loads, Gilles al Gilles et al. (1992) have suggested that this strength reduction under cyclic conditions is due to a gradual increase void growth during each cycle, an occurrence called 'ratcheting of porosity'. Later, this ratcheting of porosity has been confirmed by Devaux et al Devaux et al. (1997) through numerical computations similar to those of Gilles et al, but with a better control of the triaxiality. Also, the authors have demonstrated that classical Gurson's model is unable to predict this phenomenon. Besson et al Besson and Guillemer-Neel (2003) have included isotropic and linear kinematic hardening in a Gurson-like model. A more satisfactory reproduction of numerical results, particularly the void ratcheting, has been derived by Lacroix et al Lacroix et al. (2016) by the use of an improved variant of the so-called LPD model due to Leblond et al Leblond et al. (1995) with a more refined description of strain hardening. In the same context, numerical investigation of the response of cubic elementary cell containing a single spherical or ellipsoidal pore have been carried out by Mbiakop et al. Mbiakop et al. (2015) and have shown that he microstructure evolves toward a void shape ratcheting. Recently, Cheng et al Cheng et al. (2017) adopted a semi-analytical method for the elastic plastic response of porous solids comprising ellipsoidal voids with isotropic and linear kinematic hardening under cyclic loads within the framework of nonlinear homogenization. Based on a mixed variational principle, an other shakedown analysis is developed to obtain the yield function from the specific strain energy by (Ruiz and Silveira, 2018).

In the following chapters, we apply Melan's theorem to porous materials by adopting the hollow sphere model with von Mises (Chapter 2) and associated Drucker-Prager's matrix (Chapter 3) analytically and numerically.

Chapter 2

A macroscopic criterion of shakedown limit for von Mises ductile porous materials subjected to general cyclic loadings

This chapter is devoted to the determination of shakedown limit states of porous ductile materials under cyclically repeated loads by considering the hollow sphere model with von Mises matrix. We adopt Melan's statical approach based on time-independent residual stress fields. First, we determine the exact solution for the pure hydrostatic loading for two limit cyclic loading cases: (i) the alternating and (ii) the pulsating loads. It turns out that the collapse occurs by fatigue. Next, all possible intermediate cyclic loading cases ranging between the two limit cyclic loading cases and involving shear effect are treated. The key idea relies on the choice of an appropriate and rich trial residual stress field allowing analytical computations. The new analytical safe criterion depends on the first and second macroscopic stresses invariants and the sign of the third one. Finally, the obtained results are fully discussed and compared to numerical results derived by both shakedown direct method and incremental elastic plastic simulations.

2.1 Introduction

To determine limit loads for materials and structures operating beyond the elastic limit is since ever one of the most important tasks of engineers. For this purpose, the so-called Direct Methods play an increasing role due to the fact that they allow rapid access to the requested information in mathematically constructive manners. They embrace limit analysis, the oldest and most developed approach, and shake-

down analysis, a powerful extension to the variable repeated loads potentially more economical than step-by-step inelastic analysis (Maier et al., 2000; Save et al., 1997).

The limit analysis allows to predict the ultimate load α^L, called the limit load. This theory, developed intuitively in the 1930's, theoretically and experimentally based in the 1950's, is now widely used and has become recommended by design Codes on pressure vessels (ASME) and on reinforced concrete slabs (European Committee for Concrete).

However, in the case of variable repeated loads, the magnitude of the ultimate load is not the only factor characterizing the structural safety. Even below α^L, three limit states (ratcheting, accommodation and shakedown) may take place, of which the first two are unstable as described in the previous chapter. The corresponding limit, under which the structure shakes down, is noted as α^{SD}.

Concerning shakedown analysis of ductile porous medias, few works have been devoted to the subject and most of them concern numerical micromechanical approaches (Gilles et al., 1992; Devaux et al., 1997; Mbiakop et al., 2015; Lacroix et al., 2016; Leblond et al., 1995).

Intriguingly, all the studies cited above utilize Gurson-like approach within the framework of limit analysis for the study of voided ductile media subjected to cyclic loads. It is our belief that the natural context for such studies should be the static or kinematic shakedown framework. Accordingly, in this chapter, on shakedown analysis of ductile porous materials with a von Mises matrix under cyclically repeated load, we propose a homogenized analytical macroscopic shakedown criterion by considering Gurson's hollow sphere model. Based on a microscopic trial stress field, we adopt Melan's statical approach to determine the safe limit domain by maximizing the size of the load domain for general repeated loadings with the definition of the macroscopic stress ratio:

$$-1 \leq R = \Sigma_- / \Sigma_+ < 1 \tag{2.1}$$

Σ_- and Σ_+ being the minimum and maximum load amplitude during the cyclic loading process, respectively. Thus, alternating load and pulsating one can be considered as two particular loading cases described by $R = -1$ and $R = 0$, respectively. Besides, the load case corresponding to $R = 1$ represents the monotonic load process for which the collapse occurs by development of a mechanism which agreed with numerical simulations.

This chapter is organized as follows: In Section 2.2, a brief review of the classical Hill-Mandel lemma for the average-field theory and Melan's shakedown theorem are presented as the starting point for the following derivation. In section 2.3, we study the steady-state behavior of the hollow sphere under re-

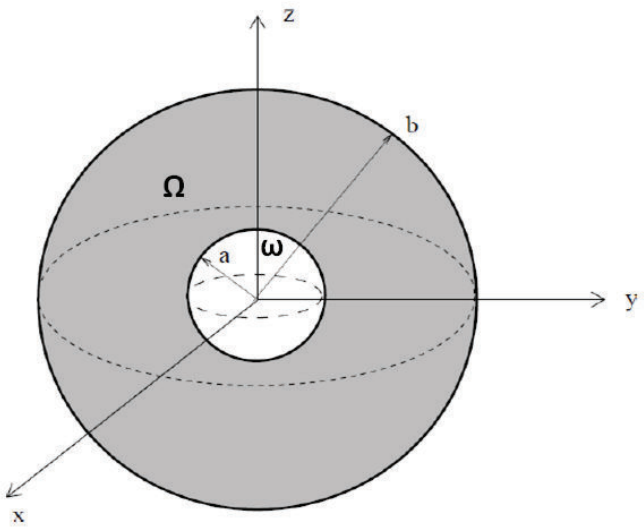

Figure 2.1: Hollow sphere model

peated pure hydrostatic loading. Owing to the spherical symmetry of this problem, analytical computations giving the collapse by fatigue or by development of mechanism are exact. Section 2.4 is devoted to the derivation of a macroscopic shakedown of the unit cell under general repeated loads involving shear. To this end, suitable admissible stress fields are built by adding an additional deviatoric trial field to exact stress field under pure hydrostatic loading in order to capture the shear effects. Once the trial stress fields are built, we maximize the size of the load domain, in the spirit of Melan's theorem, that provides the macroscopic shakedown safety domain. Moreover, Subsection 2.4.3 is concerned with the derivation of the relationship between the elastic limit and the amplitude of cyclic shakedown limit load. In Section 2.5, direct and step-by-step numerical simulations are both performed to access the established criterion. Finally, concluding remarks and perspectives are finally summarized in the last section.

2.2 Basic relations

Let us consider a reference unit cell or macro-element Ω composed of a void ω and matrix $\Omega_M = \Omega - \omega$ (Figure 2.1). The macro-element Ω is bounded by surface $\partial\Omega$ and the void ω by $\partial\omega$. The matrix is made of an elasto-plastic material (hardening is not considered) with a yield criterion:

$$F(\boldsymbol{\sigma}) \leq 0\,, \tag{2.2}$$

where F is a convex function of Cauchy's stress tensor $\boldsymbol{\sigma}$.

From the classical Hill's lemma (Hill, 1950), the macroscopic stress $\boldsymbol{\Sigma}$ and macroscopic strain $\mathbf{E}$ are obtained as volume averages of their microscopic counterparts $\boldsymbol{\sigma}$ and $\boldsymbol{\varepsilon}$:

$$\boldsymbol{\Sigma} = \frac{1}{|\,\Omega\,|}\int_{\Omega} \boldsymbol{\sigma}\, dV\,, \qquad \mathbf{E} = \frac{1}{|\,\Omega\,|}\int_{\Omega} \boldsymbol{\varepsilon}\, dV\,. \tag{2.3}$$

The set of statically admissible stress fields is such as:

$$\mathscr{S}_a = \{\boldsymbol{\sigma} \quad s.t. \quad div\,\boldsymbol{\sigma} = \mathbf{0} \quad in\Omega, \quad \boldsymbol{\sigma}\cdot\boldsymbol{n} = \mathbf{0} \quad on\partial\omega, \quad \boldsymbol{\sigma} = \mathbf{0} \quad in\omega\} \tag{2.4}$$

where $\boldsymbol{n}$ is the unit outward normal vector of the matrix. If $\boldsymbol{\sigma}$ is statically admissible, it is worth to remark that $\boldsymbol{\Sigma}$ depends on it through:

$$\boldsymbol{\Sigma} = \frac{1}{|\,\Omega\,|}\int_{\partial\Omega} (\boldsymbol{\sigma}\cdot\boldsymbol{n})\otimes\boldsymbol{x}\, dS \tag{2.5}$$

where $\boldsymbol{x}$ is the position vector in the cartesian coordinate system, and dS is an infinitesimal element of the surface area at the external boundary $\partial\Omega$.

Then, the field defined by :

$$\boldsymbol{\rho} = \boldsymbol{\sigma} - \boldsymbol{\sigma}^E \tag{2.6}$$

belongs to the set of *residual stress fields*:

$$\mathscr{N} = \{\boldsymbol{\rho} \quad | \quad div\,\boldsymbol{\rho} = \mathbf{0} \quad in\Omega, \quad \boldsymbol{\rho}\cdot\boldsymbol{n} = \mathbf{0} \quad on\partial\omega, \quad \boldsymbol{\rho} = \mathbf{0} \quad in\omega\} \tag{2.7}$$

We describe a varying load as

$$\boldsymbol{\Sigma}(t) = \sum_{k=1}^{n} \mu_k(t)\boldsymbol{\Sigma}_k, \qquad \sum_{k=1}^{n} \mu_k(t) = 1, \qquad \mu_k^- \le \mu_k(t) \le \mu_k^+ \tag{2.8}$$

where $\boldsymbol{\Sigma}(t)$ stands for a total instantaneous load and the reference load $\boldsymbol{\Sigma}$ can be described by convex combination of elementary loads $\boldsymbol{\Sigma}_n$. Let us denote p_0 and q_0 as two reference loads, for instance, the two independent variable loads can be described by $p(t) = \mu_1(t)p_0$ and $q(t) = \mu_2(t)q_0$. The rectangular reference load domain $\mathscr{P}_0$ is indicated in Figure 2.2(a), where $\bar{\mu}_n^-$ and $\bar{\mu}_n^+$ are constant lower and upper bounds.

Then, because of the linearity of the elastic response in the fictitious body when shakedown occurs, the total stress field can be assumed as:

$$\boldsymbol{\sigma} = \alpha\boldsymbol{\sigma}^E + \boldsymbol{\rho} \tag{2.9}$$

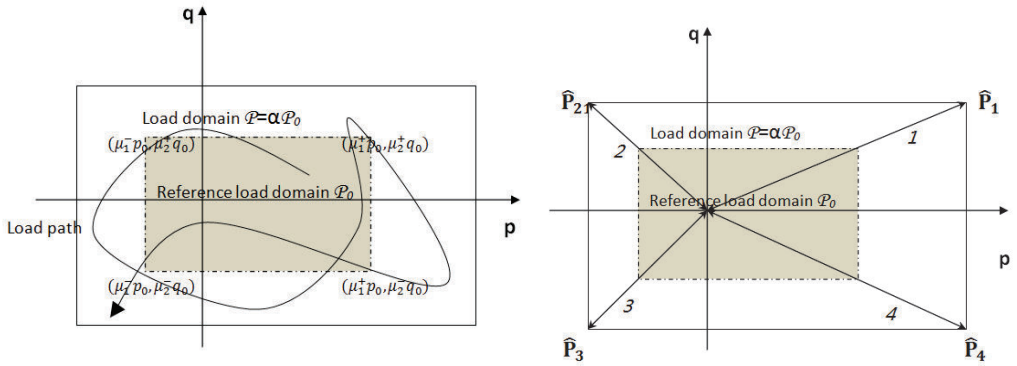

(a) Load domain for shakedown analysis

(b) Critical cycles of load

Figure 2.2: Determination of shakedown domain

where $\alpha > 1$ is the load factor. Hence, Melan's lower bound theorem of shakedown (Melan, 1936) can be expressed as follows:

If a time-independent residual stress field $\bar{\boldsymbol{\rho}} \in \mathcal{N}$, and a load factor α can be found, such that for all loads in the domain $\mathcal{P}$, the yield criterion holds everywhere in Ω at anytime:

$$F(\alpha \boldsymbol{\sigma}^E + \bar{\boldsymbol{\rho}}) < 0 \tag{2.10}$$

then the body shakes down within the given domain $\mathcal{P}$. The greatest value of admissible α is called shakedown factor, noted α_{SD}.

2.3 Pure hydrostatic loading

2.3.1 Problem formulation

We consider a hollow sphere, of which the macro-element V is enclosed by surface S, made up of a spherical cavity embedded in a homothetic cell of a rigid-plastic isotropic and homogeneous material with von Mises model. The inner and outer radii are respectively denoted a and b, giving the void volume fraction $f = (a/b)^3 < 1$. The matrix material obeys the associated von Mises criterion represented by the yield function:

$$F(\boldsymbol{\sigma}) = \sigma_e(\boldsymbol{\sigma}) - \sigma_0 \leq 0 \tag{2.11}$$

where $\sigma_e = \sqrt{\frac{3}{2}\mathbf{s} : \mathbf{s}}$ is the von Mises equivalent stress and $\sigma_0 > 0$ represents the yield stress in tension.

The hollow sphere is subjected to a uniform hydrostatic stress q upon its external boundary. Owing

to (2.5), the average mean stress is:

$$\Sigma_m = \frac{1}{3} Tr\left(\boldsymbol{\Sigma}\right) = q \tag{2.12}$$

Taking into account the central symmetry of the problem, the spherical coordinate (r,θ,φ) are used, r being the radius, θ the inclination angle, φ the azimuth one, with orthonormal frame $\{\mathbf{e}_r,\mathbf{e}_\theta,\mathbf{e}_\phi\}$, and all the fields are depending only on r. Owing to (2.12), the stress field in the fictitious elastic body is:

$$\boldsymbol{\sigma}^E = \frac{\Sigma_m}{1-f}\left(\mathbf{1} + \frac{1}{2}\left(\frac{a}{r}\right)^3 \left(\mathbf{e}_\theta \otimes \mathbf{e}_\theta + \mathbf{e}_\phi \otimes \mathbf{e}_\phi - 2\,\boldsymbol{e}_r \otimes \boldsymbol{e}_r\right)\right) \tag{2.13}$$

where $\mathbf{1}$ is the second order unit tensor. For von Mises model, the yield function is:

$$\max_{a\le r\le b} \sigma_e = \max_{a\le r\le b} \frac{3}{2}\frac{\Sigma_m}{1-f}\left(\frac{a}{r}\right)^3 \le \sigma_0 \tag{2.14}$$

Hence, the first yielding occurs on the void boundary and the *elastic limit average mean stress* is:

$$\Sigma_m^e = \frac{2}{3}\left(1-f\right)\sigma_0 \tag{2.15}$$

2.3.2 Collapse by fatigue

Beyond this limit, plastic strains appear and our aim is to determine when the macro-element shakes down using Melan's theorem if the load Σ_m belongs to the domain:

$$\Sigma_{m-} \le \Sigma_m \le \Sigma_{m+} = \Sigma_{m-} + \Delta\Sigma_m \tag{2.16}$$

where Σ_{m-} and Σ_{m+} are the minimum and maximum macroscopic hydrostatic loads during the cyclic loading precess, respectively.

Because of the central symmetry, the residual stress field is:

$$\bar{\boldsymbol{\rho}} = \bar{\rho}_{rr}\boldsymbol{e}_r \otimes \boldsymbol{e}_r + \bar{\rho}_{\theta\theta}(\boldsymbol{e}_\theta \otimes \boldsymbol{e}_\theta + \boldsymbol{e}_\phi \otimes \boldsymbol{e}_\phi) \tag{2.17}$$

and must satisfy the only internal equilibrium equation:

$$\frac{r}{2}\frac{d\bar{\rho}_{rr}}{dr} = \bar{\rho}_{\theta\theta} - \bar{\rho}_{rr} \tag{2.18}$$

Although it is not strictly imposed by the equilibrium conditions stated in (2.4), it is shrewd to build an

admissible residual stress field such that:

$$\bar{\rho}_{rr}(b) = 0 \tag{2.19}$$

Indeed, according to (2.5), the average mean residual stress:

$$\boldsymbol{\Sigma}_r = \frac{1}{|\,\Omega\,|}\int_{\partial\Omega} (\bar{\boldsymbol{\rho}}\cdot\mathbf{n})\otimes\boldsymbol{x}\, dS \tag{2.20}$$

vanishes and the average mean stress is equal to the corresponding value in the fictitious elastic body:

$$\boldsymbol{\Sigma} = \boldsymbol{\Sigma}_r + \boldsymbol{\Sigma}^E = \boldsymbol{\Sigma}^E \tag{2.21}$$

To build the residual stress field, we are inspired by Hodge's solution for the shakedown of thick tube (Hodge Jr, 1954). Combining with the latter equation, the condition enforces (1.51) that for $a \le r \le b$ and for Σ_m such that (2.16), one has:

$$|\,\frac{r}{2}\frac{d\bar{\rho}_{rr}}{dr} + \frac{3}{2}\frac{\Sigma_m}{1-f}\left(\frac{a}{r}\right)^3\,| \le \sigma_0 \tag{2.22}$$

For the given load domain, the previous inequality is fulfilled, provided that:

$$-\sigma_0 \le \frac{r}{2}\frac{d\bar{\rho}_{rr}}{dr} + \frac{3}{2}\frac{\Sigma_{m-}}{1-f}\left(\frac{a}{r}\right)^3 \le \sigma_0, \qquad -\sigma_0 \le \frac{r}{2}\frac{d\bar{\rho}_{rr}}{dr} + \frac{3}{2}\frac{\Sigma_{m+}}{1-f}\left(\frac{a}{r}\right)^3 \le \sigma_0 \tag{2.23}$$

Considering the superior and inferior envelopes, we retain only the strongest inequalities :

$$-\sigma_0 - \frac{3}{2}\frac{\Sigma_{m-}}{1-f}\left(\frac{a}{r}\right)^3 \le \frac{r}{2}\frac{d\bar{\rho}_{rr}}{dr} \le \sigma_0 - \frac{3}{2}\frac{\Sigma_{m+}}{1-f}\left(\frac{a}{r}\right)^3 \tag{2.24}$$

Hence, there exists a time-independent residual stress field only if for $a \le r \le b$:

$$-\sigma_0 - \frac{3}{2}\frac{\Sigma_{m-}}{1-f}\left(\frac{a}{r}\right)^3 \le \sigma_0 - \frac{3}{2}\frac{\Sigma_{m+}}{1-f}\left(\frac{a}{r}\right)^3 \tag{2.25}$$

or, owing to $1-f>0$ and (2.16):

$$\Delta\Sigma_m\left(\frac{a}{r}\right)^3 \le \frac{4}{3}(1-f)\,\sigma_0 \tag{2.26}$$

Because $\Delta\Sigma_m$ is positive, the previous condition is satisfied anywhere in the body if it is fulfilled at $r=a$, hence the shakedown condition:

$$\Delta\Sigma_m \le \frac{4}{3}(1-f)\,\sigma_0 \tag{2.27}$$

It is worth to observe that the shakedown limit on the cycle amplitude is the double of the elastic limit

(2.15):

$$\Delta\Sigma_m \leq \Delta\Sigma_m^{SD} = 2\,\Sigma_m^e = \frac{4}{3}(1-f)\,\sigma_0 \tag{2.28}$$

Now, we have to prove the existence of an admissible residual stress field under this condition. Considering the equality is satisfied in the right hand part of condition (2.16) and (2.24) in the inner part $a \leq r \leq c$ of the body:

$$\frac{r}{2}\frac{d\bar{\rho}_{rr}}{dr} = \sigma_0 - \frac{3}{2}\frac{\Sigma_{m+}}{1-f}\left(\frac{a}{r}\right)^3 \tag{2.29}$$

integrating and taking into account $\bar{\rho}_{rr}(a) = 0$ and (2.19), one has :

$$\begin{aligned}\bar{\boldsymbol{\rho}} = -2\sigma_0 &\left(\ln\left(\frac{a}{r}\right)\mathbf{1} - \frac{1}{2}\left(\boldsymbol{e}_\theta\otimes\boldsymbol{e}_\theta + \boldsymbol{e}_\phi\otimes\boldsymbol{e}_\phi\right)\right)\\ &- \frac{\Sigma_{m+}}{1-f}\left(\mathbf{1} + \frac{1}{2}\left(\frac{a}{r}\right)^3\left(\boldsymbol{e}_\theta\otimes\boldsymbol{e}_\theta + \boldsymbol{e}_\phi\otimes\boldsymbol{e}_\phi - 2\,\boldsymbol{e}_r\otimes\boldsymbol{e}_r\right)\right)\end{aligned} \tag{2.30}$$

which is an admissible residual stress field for $a \leq r \leq c$ as shown on Figure 2.3. We prolongate it in the outer region $c \leq r \leq b$ by the elastic solution of the problem of a hollow sphere of inner radius c and outer one b with hydrostatic loading $\bar{\rho}_{rr}(c) = \rho_0$ and (2.19):

$$\bar{\boldsymbol{\rho}} = -\frac{\rho_0}{1-f_e}\left(f_e\mathbf{1} + \frac{1}{2}\left(\frac{c}{r}\right)^3\left(\boldsymbol{e}_\theta\otimes\boldsymbol{e}_\theta + \boldsymbol{e}_\phi\otimes\boldsymbol{e}_\phi - 2\,\boldsymbol{e}_r\otimes\boldsymbol{e}_r\right)\right) \tag{2.31}$$

where $f_e = (c/b)^3 < 1$. Let $f_p = (a/c)^3 < 1$ such that $f = f_p f_e$. Then the stress continuity entails:

$$\rho_0 = -\frac{2}{3}\sigma_0 \ln f_p - \frac{1-f_p}{1-f}\Sigma_{m+} \tag{2.32}$$

2.3.3 Collapse by development of a mechanism

Moreover, because the equality has been chosen in (2.24), it is worth to remark that all the macro-element is plastified when $\Sigma_m = \Sigma_{m+}$ if $c = b$ hence the *limit load* Σ_m^L is reached. As $\rho_0 = 0$ and $f_p = f$, the limit load is:

$$\Sigma_m^L = -\frac{2}{3}\sigma_0 \ln f \tag{2.33}$$

which is a particular case of Gurson model (Gurson et al., 1977). It is clear that the collapse by fatigue occurs only if:

$$\Sigma_{m+} = \Sigma_{m-} + \Delta\Sigma_m^{SD} \leq \Sigma_m^L \tag{2.34}$$

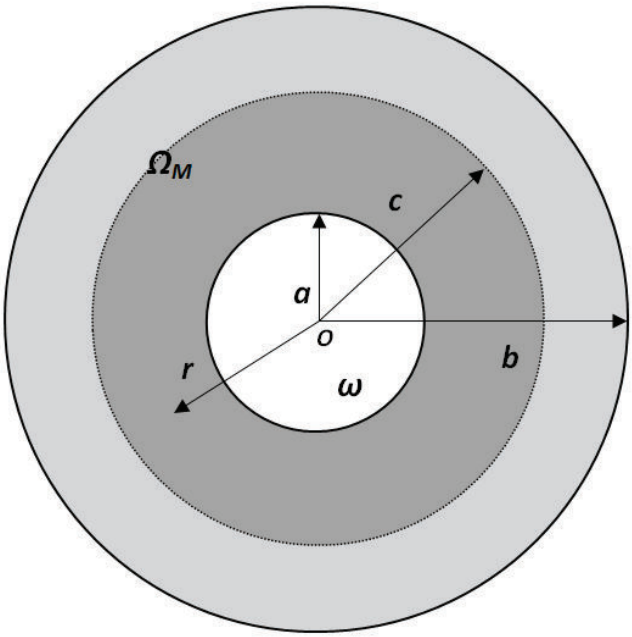

Figure 2.3: The hollow sphere under pure hydrostatic load.

If $\Sigma_{m-} = 0$, owing to (2.28) and (2.33), the fatigue collapse occurs under the condition:

$$2(1-f)+\ln f \leq 0 \tag{2.35}$$

which is satisfied if:

$$f \leq 0.203 \tag{2.36}$$

if $\Sigma_{m-} = -\Sigma_{m+}$, the fatigue collapse occurs provided:

$$1-f+\ln f \leq 0 \tag{2.37}$$

which is satisfied anyway.

It is worth noting, that the analysis of the effective asymptotic response of the hollow sphere undergoing combined and cyclic hydrostatic and shear loads has been worked out and are provided in (Zhang et al., 2017b). To shorten this chapter this study is not reported here.

2.4 Shakedown under general loadings

2.4.1 Constructing of a new trial stress field

In this section, we consider the hollow sphere under general cyclic loads involving shear effects. The trial stress field is considered as the sum of the two following fields:

1. A heterogeneous stress tensor inspired from the exact solution under pure hydrostatic loadings which is expressed as follows in the spherical coordinates $\{\mathbf{e}_r, \mathbf{e}_\theta, \mathbf{e}_\phi\}$:

$$\boldsymbol{\sigma}^{(1)} = \boldsymbol{\sigma}^{E(1)} + \bar{\boldsymbol{\rho}}^{(1)} \tag{2.38}$$

   where $\boldsymbol{\sigma}^{E(1)}$ is the stress field in the fictitious elastic body:

$$\boldsymbol{\sigma}^{E(1)} = \frac{\Sigma_m}{1-f}\left(\mathbf{1} + \frac{1}{2}\left(\frac{a}{r}\right)^3 (\mathbf{e}_\theta \otimes \mathbf{e}_\theta + \mathbf{e}_\phi \otimes \mathbf{e}_\phi - 2\,\boldsymbol{e}_r \otimes \boldsymbol{e}_r)\right) \tag{2.39}$$

   where $\Sigma_m = \frac{1}{3} tr(\Sigma)$ is the macroscopic hydrostatic stress, and $\bar{\boldsymbol{\rho}}^{(1)}$, the corresponding residual stress field in the inner region $a \le r \le c$, is inspired from the exact solution:

$$\begin{aligned}\bar{\boldsymbol{\rho}}^{(1)} = &-A_0\left(\ln\left(\frac{a}{r}\right)\mathbf{1} - \frac{1}{2}(\boldsymbol{e}_\theta \otimes \boldsymbol{e}_\theta + \boldsymbol{e}_\phi \otimes \boldsymbol{e}_\phi)\right) \\ &- \frac{\Sigma_{m+}}{1-f}\left(\mathbf{1} + \frac{1}{2}\left(\frac{a}{r}\right)^3 (\boldsymbol{e}_\theta \otimes \boldsymbol{e}_\theta + \boldsymbol{e}_\phi \otimes \boldsymbol{e}_\phi - 2\,\boldsymbol{e}_r \otimes \boldsymbol{e}_r)\right)\end{aligned} \tag{2.40}$$

   A_0 being a constant to be determined.

2. A deviatoric part to capture the shear effects, is taking in the following form, in spherical coordinates $\{\mathbf{e}_r, \mathbf{e}_\theta, \mathbf{e}_\phi\}$:

$$\boldsymbol{\sigma}^{(2)} = \boldsymbol{\sigma}^{E(2)} + \bar{\boldsymbol{\rho}}^{(2)} \tag{2.41}$$

   where a statically admissible stress field in the fictitious unit cell, inspired from the exact elastic solution of an elastic hollow sphere subjected to axisymmetric and deviatoric loads (Zhang et al.,

2018), is taken in the following form in the spherical frame:

$$\begin{aligned}\boldsymbol{\sigma}^{E(2)} = &\left[\frac{a^3\left(18a^2+5r^2\left(-5+\nu\right)\right)\left(1+3\cos(2\theta)\right)}{2\,r^5\left(-7+5\nu\right)}-\frac{1+3\cos(2\theta)}{2}\right]A_1\left(\mathbf{e}_r\otimes\mathbf{e}_r\right)\\ &+\left[\frac{a^3\left(27a^2+5r^2\left(1-2\nu\right)-3\left(21a^2+5r^2\left(-1+2\nu\right)\right)\cos^2\left(\theta\right)\right)}{2\,r^5\left(-7+5\nu\right)}+\frac{-1+3\cos(2\theta)}{2}\right]A_1\left(\mathbf{e}_\theta\otimes\mathbf{e}_\theta\right)\\ &+\left[\frac{a^3\left(9a^2+25r^2\left(-1+2\nu\right)-45\left(a^2+r^2\left(-1+2\nu\right)\right)\cos^2\left(\theta\right)\right)}{2\,r^5\left(-7+5\nu\right)}+1\right]A_1\left(\mathbf{e}_\phi\otimes\mathbf{e}_\phi\right)\\ &+\left[\frac{3a^3\left(12a^2-5r^2\left(1+\nu\right)\right)\sin(2\theta)}{2\,r^5\left(-7+5\nu\right)}+\frac{3\sin(2\theta)}{2}\right]A_1\left(\mathbf{e}_r\otimes\mathbf{e}_\theta+\mathbf{e}_\theta\otimes\mathbf{e}_r\right)\end{aligned} \tag{2.42}$$

where A_1 is a constant parameter.

Certainly, the expression of the trial residual stress field $\boldsymbol{\sigma}^{E(2)}$ given by (2.42) is rather lengthy but was chosen after unsatisfactory trial with shortest expressions. Of course, adding extra terms should improve the accuracy.

Now, attention is focused on the derivation of a new admissible deviatoric residual stress tensor $\tilde{\boldsymbol{\rho}}^{(2)}$ alloying the analytical derivation of a macroscopic shakedown criterion for intermediate loads ($-1 \leq R < 1$). To this end, the key point is inspired from the method of solution for the pure hydrostatic loading carried out in (Zhang et al., 2017b). More precisely, the key idea consists in assuming that the average residual stress $\boldsymbol{\Sigma}_r$ vanishes so that the average mean stress is equal to the corresponding value in the fictitious elastic body:

$$\boldsymbol{\Sigma} = \boldsymbol{\Sigma}_r + \boldsymbol{\Sigma}^E = \boldsymbol{\Sigma}^E \tag{2.43}$$

Then the axisymmetric macroscopic stress tensor, resulting from (2.39) and (2.42), takes the form:

$$\boldsymbol{\Sigma} = \Sigma_m \mathbf{1} + (1-f)\, A_1(\mathbf{e}_r\otimes\mathbf{e}_r + \mathbf{e}_\theta\otimes\mathbf{e}_\theta - 2\mathbf{e}_\phi\otimes\mathbf{e}_\phi)\,, \tag{2.44}$$

The macroscopic equivalent stress Σ_e and the third invariant of the macroscopic stress deviator J_3 can be obtain easily from (2.44):

$$\Sigma_e = 3(1-f)\mid A_1\mid, \qquad J_3 = -2\,(1-f)^3 A_1^3\,. \tag{2.45}$$

in which J_3 is the determinant of the deviatoric part of $\boldsymbol{\Sigma}$. Due to the relation of sign between parameter A_1 and J_3:

$$sign(A_1) = -sign(J_3) \tag{2.46}$$

we deduce:

$$A_1 = -sign(J_3)\,\frac{\Sigma_e}{3(1-f)} \tag{2.47}$$

For a variable hydrostatic loading combined with a constant shear loading, we consider the load domain defined by two elementary loads $\boldsymbol{\Sigma}_+$ and $\boldsymbol{\Sigma}_-$:

$$\boldsymbol{\Sigma}_\pm = \Sigma_{m\pm}\mathbf{1} - sign(J_{3\pm})\,\frac{\Sigma_{e\pm}}{3}\left(\mathbf{e}_r\otimes\mathbf{e}_r + \mathbf{e}_\theta\otimes\mathbf{e}_\theta - 2\mathbf{e}_\phi\otimes\mathbf{e}_\phi\right) \tag{2.48}$$

Consequently, $\boldsymbol{\sigma}^{E(2)}$ (2.42) can be rewritten in the following form by replacing A_1:

$$\begin{aligned}
\boldsymbol{\sigma}^{E(2)} = -\frac{sign(J_3)\Sigma_e}{3(1-f)}\Bigg\{ &\left[\frac{a^3\left(18a^2+5r^2\left(-5+\nu\right)\right)\left(1+3\cos(2\theta)\right)}{2\,r^5\left(-7+5\nu\right)} - \frac{1+3\cos(2\theta)}{2}\right](\mathbf{e}_r\otimes\mathbf{e}_r)\\
+ &\left[\frac{a^3\left(27a^2+5r^2\left(1-2\nu\right)-3\left(21a^2+5r^2\left(-1+2\nu\right)\right)\cos^2(\theta)\right)}{2\,r^5\left(-7+5\nu\right)} + \frac{-1+3\cos(2\theta)}{2}\right](\mathbf{e}_\theta\otimes\mathbf{e}_\theta)\\
+ &\left[\frac{a^3\left(9a^2+25r^2\left(-1+2\nu\right)-45\left(a^2+r^2\left(-1+2\nu\right)\right)\cos^2(\theta)\right)}{2\,r^5\left(-7+5\nu\right)} + 1\right](\mathbf{e}_\phi\otimes\mathbf{e}_\phi)\\
+ &\left[\frac{3a^3\left(12a^2-5r^2\left(1+\nu\right)\right)\sin(2\theta)}{2\,r^5\left(-7+5\nu\right)} + \frac{3\sin(2\theta)}{2}\right](\mathbf{e}_r\otimes\mathbf{e}_\theta+\mathbf{e}_\theta\otimes\mathbf{e}_r)\Bigg\}
\end{aligned} \tag{2.49}$$

Referring to the derivation of the shakedown limit for the hydrostatic load in (Zhang et al., 2017b), it is shrewd to build a deviatoric residual stress field so that its equivalent stress has the same form as the hydrostatic residual field $\bar{\boldsymbol{\rho}}^{(1)}$, in order to avoid the approximation during the shakedown analysis. To this end, the new deviatoric residual stress field is split in two parts as follows:

$$\bar{\boldsymbol{\rho}}^{(2)} = \bar{\boldsymbol{\rho}}^{(2a)} + \bar{\boldsymbol{\rho}}^{(2b)}\,, \tag{2.50}$$

where $\bar{\boldsymbol{\rho}}^{(2a)}$ is taking the following form in spherical coordinates:

$$\begin{aligned}
\bar{\boldsymbol{\rho}}^{(2a)} = \frac{sign(J_{3+})\Sigma_{e+}}{3(1-f)}\Bigg\{ &\left[\frac{a^3\left(18a^2+5r^2\left(-5+\nu\right)\right)\left(1+3\cos(2\theta)\right)}{2\,r^5\left(-7+5\nu\right)} - \frac{1+3\cos(2\theta)}{2}\right](\mathbf{e}_r\otimes\mathbf{e}_r)\\
+ &\left[\frac{a^3\left(27a^2+5r^2\left(1-2\nu\right)-3\left(21a^2+5r^2\left(-1+2\nu\right)\right)\cos^2(\theta)\right)}{2\,r^5\left(-7+5\nu\right)} + \frac{-1+3\cos(2\theta)}{2}\right](\mathbf{e}_\theta\otimes\mathbf{e}_\theta)\\
+ &\left[\frac{a^3\left(9a^2+25r^2\left(-1+2\nu\right)-45\left(a^2+r^2\left(-1+2\nu\right)\right)\cos^2(\theta)\right)}{2\,r^5\left(-7+5\nu\right)} + 1\right](\mathbf{e}_\phi\otimes\mathbf{e}_\phi)\\
+ &\left[\frac{3a^3\left(12a^2-5r^2\left(1+\nu\right)\right)\sin(2\theta)}{2\,r^5\left(-7+5\nu\right)} + \frac{3\sin(2\theta)}{2}\right](\mathbf{e}_r\otimes\mathbf{e}_\theta+\mathbf{e}_\theta\otimes\mathbf{e}_r)\Bigg\}
\end{aligned} \tag{2.51}$$

and the second part $\bar{\boldsymbol{\rho}}^{(2b)}$ writes as follows in spherical coordinates:

$$\bar{\boldsymbol{\rho}}^{(2b)} = \rho_{rr}^{(2b)} \mathbf{e}_r \otimes \mathbf{e}_r + \rho_{\theta\theta}^{(2b)} \mathbf{e}_\theta \otimes \mathbf{e}_\theta + \rho_{\phi\phi}^{(2b)} \mathbf{e}_\phi \otimes \mathbf{e}_\phi + \rho_{r\theta}^{(2b)} \left(\mathbf{e}_r \otimes \mathbf{e}_\theta + \mathbf{e}_\theta \otimes \mathbf{e}_r\right) \tag{2.52}$$

$\rho_{rr}^{(2b)}$, $\rho_{\theta\theta}^{(2b)}$, $\rho_{\phi\phi}^{(2b)}$ and $\rho_{r\theta}^{(2b)}$ being the functions of r and θ.

We suppose the deviatoric parts $\boldsymbol{s}^{E(2)}$, $\boldsymbol{s}^{(2b)}$ of $\boldsymbol{\sigma}^{E(2)}$, $\bar{\boldsymbol{\rho}}^{(2b)}$ have the following relation:

$$\boldsymbol{s}^{(2b)} = A_3 \, K(r) \, \boldsymbol{s}^{E(2)} \tag{2.53}$$

where $K(r)$ is a function of r and A_3 the constant to be determined. In practice, the expressions of $\bar{\boldsymbol{\rho}}^{(2b)}$ and $K(r)$ are given in Appendix 2.6.

Consequently, the new trial stress field in the matrix:

$$\boldsymbol{\sigma} = \boldsymbol{\sigma}^{(1)} + \boldsymbol{\sigma}^{(2)} \, , \tag{2.54}$$

and a vanishing stress field is considered in the void ω.

Finally, in the spherical frame, together with (2.39), (2.40), (2.49), (2.51) and (2.52), the complete stress field (2.54) reads for $a \le r \le c$:

$$\begin{aligned}
\boldsymbol{\sigma} = & \left[\left(\frac{a^3\left(18a^2+5r^2\left(-5+\nu\right)\right)\left(1+3\cos(2\theta)\right)}{2\,r^5\left(-7+5\nu\right)} - \frac{1+3\cos(2\theta)}{2} \right) \frac{sign(J_{3+})\Sigma_{e+} - sign(J_3)\Sigma_e}{3(1-f)} \right. \\
& \left. + \rho_{rr}^{(2b)} - \ln\left(\frac{a}{r}\right) A_0 - \frac{\Sigma_{m+}-\Sigma_m}{1-f}\left(1-\left(\frac{a}{r}\right)^3\right) \right] \left(\mathbf{e}_r \otimes \mathbf{e}_r\right) \\
& + \left[\rho_{\theta\theta}^{(2b)} + \frac{a^3\left(27a^2+5r^2\left(1-2\nu\right)-3\left(21a^2+5r^2\left(-1+2\nu\right)\right)\cos^2(\theta)\right)}{2\,r^5\left(-7+5\nu\right)} \frac{sign(J_{3+})\Sigma_{e+} - sign(J_3)\Sigma_e}{3(1-f)} \right. \\
& \frac{\left(3\cos(2\theta)-1\right)}{2} \frac{sign(J_{3+})\Sigma_{e+} - sign(J_3)\Sigma_e}{3(1-f)} - \ln\left(\frac{a}{r}\right) A_0 + \frac{A_0}{2} - \frac{\Sigma_{m+}-\Sigma_m}{1-f}\left(1+\frac{1}{2}\left(\frac{a}{r}\right)^3\right) \left. \right] \left(\mathbf{e}_\theta \otimes \mathbf{e}_\theta\right) \\
& + \left[\left(\frac{a^3\left(9a^2+25r^2\left(-1+2\nu\right)-45\left(a^2+r^2\left(-1+2\nu\right)\right)\cos^2(\theta)\right)}{2\,r^5\left(-7+5\nu\right)} + 1 \right) \frac{sign(J_{3+})\Sigma_{e+} - sign(J_3)\Sigma_e}{3(1-f)} \right. \\
& \left. + \rho_{\phi\phi}^{(2b)} - \ln\left(\frac{a}{r}\right) A_0 + \frac{A_0}{2} - \frac{\Sigma_{m+}-\Sigma_m}{1-f}\left(1+\frac{1}{2}\left(\frac{a}{r}\right)^3\right) \right] \left(\mathbf{e}_\phi \otimes \mathbf{e}_\phi\right) \\
& + \left[\left(\frac{3\sin(2\theta)}{2} + \frac{3a^3\left(12a^2-5r^2\left(1+\nu\right)\right)\sin(2\theta)}{2\,r^5\left(-7+5\nu\right)} \right) \frac{sign(J_{3+})\Sigma_{e+} - sign(J_3)\Sigma_e}{3(1-f)} \right. \\
& \left. + \rho_{r\theta}^{(2b)} \right] \left(\mathbf{e}_r \otimes \mathbf{e}_\theta + \mathbf{e}_\theta \otimes \mathbf{e}_r\right)
\end{aligned} \tag{2.55}$$

in which $\rho_{rr}^{(2b)}$, $\rho_{\theta\theta}^{(2b)}$, $\rho_{\phi\phi}^{(2b)}$ and $\rho_{r\theta}^{(2b)}$ are given in Appendix 1.

2.4.2 Macroscopic shakedown criterion under general loading condition

From the new stress field (2.55) and the imposed condition (2.53), the equivalent stress σ_e for $a \le r \le c$ reads:

$$\begin{aligned}\sigma_e^2 = &\left(\frac{A_0}{2} - \frac{3}{2}\frac{\Sigma_{m+}-\Sigma_m}{1-f}\left(\frac{a}{r}\right)^3\right)^2 + \left(\frac{sign(J_{3+})\Sigma_{e+} - sign(J_3)\Sigma_e}{(1-f)} + 3K(r)\,A_3\right)^2 P_2(r,\theta) \\ &+\left(A_0 - 3\,\frac{\Sigma_{m+}-\Sigma_m}{1-f}\left(\frac{a}{r}\right)^3\right) P_1(r,\theta)\left(\frac{sign(J_{3+})\Sigma_{e+} - sign(J_3)\Sigma_e}{(1-f)} + 3K(r)\,A_3\right)\end{aligned} \tag{2.56}$$

where

$$P_1(r,\theta) = \frac{(-5\nu + 10\nu(\frac{a}{r})^3 + 18(\frac{a}{r})^5 - 20(\frac{a}{r})^3 + 7)}{7-5\nu}\,\frac{(3\cos^2(\theta)-1)}{2} \tag{2.57}$$

$$\begin{aligned}P_2(r,\theta) = \Bigg\{\Bigg[&(\frac{1125}{2}\nu - \frac{1175}{2})(\frac{a}{r})^3 + (-\frac{1175}{2}\nu - \frac{2205}{2})(\frac{a}{r})^5 + (225\nu^2 - 1125\nu + \frac{3375}{4})(\frac{a}{r})^6 \\ &+(1125\nu - \frac{2475}{2})(\frac{a}{r})^8 + \frac{1215}{4}(\frac{a}{r})^{10}\Bigg]\cos^4(\theta) + \Bigg[(-150\nu^2 - 165\nu + 525)(\frac{a}{r})^3 \\ &+(675\nu - 945)(\frac{a}{r})^5 + (-225\nu^2 + 900\nu - \frac{1125}{2})(\frac{a}{r})^6 + (-810\nu + 675)(\frac{a}{r})^8 \\ &-\frac{135}{2}(\frac{a}{r})^{10}\Bigg]\cos^2(\theta) + \Bigg[(25\nu^2 - 70\nu + 49) + (50\nu^2 - \frac{115}{2}\nu - \frac{35}{2})(\frac{a}{r})^3 + (-\frac{135}{2}\nu + \frac{189}{2})(\frac{a}{r})^5 \\ &+(100\nu^2 - 175\nu - \frac{475}{4})(\frac{a}{r})^6 + (45\nu - \frac{615}{2})(\frac{a}{r})^8 + \frac{351}{4}(\frac{a}{r})^{10}\Bigg]\Bigg\}\frac{1}{(5\nu-7)^2}\end{aligned} \tag{2.58}$$

Considering the yield condition of von Mises model (2.11), one has:

$$\sigma_e^2 \le \sigma_0^2 \tag{2.59}$$

We suppose that the collapse occurs by fatigue similar to the pure hydrostatic loading case (see (Zhang et al., 2017b)). Resulting from (2.56) and (2.59), the shakedown limit is reached at the point of coordinates (r,θ,ϕ) when the yield function is satisfied simultaneously for the extreme values of the loading:

$$\left(\frac{A_0}{2}\right)^2 + A_0\,3K(r)A_3\,P_1(r,\theta) + P_2(r,\theta)\,(3K(r)A_3)^2 = \sigma_0^2 \tag{2.60}$$

$$\left(\frac{A_0}{2}-\frac{3}{2}\frac{\Delta\Sigma_m}{1-f}\left(\frac{a}{r}\right)^3\right)^2+\left(A_0-3\frac{\Delta\Sigma_m}{1-f}\right)\left(\frac{\Delta\left(sign(J_3)\Sigma_e\right)}{(1-f)}+3K(r)\,A_3\right)P_1(r,\theta)$$
$$+P_2(r,\theta)\left(\frac{\Delta\left(sign(J_3)\Sigma_e\right)}{(1-f)}+3K(r)\,A_3\right)^2=\sigma_0^2 \tag{2.61}$$

where $\Delta\Sigma_m=\Sigma_{m+}-\Sigma_{m-}$. Σ_{m+} and Σ_{m-} are the maximum and minimum average mean stress during the cyclic loading precess.

Because of the central symmetry of the von Mises yield surface, (2.60) and (2.61) must define the same shakedown domain and A_0, A_3 depend only on $\Delta\Sigma_m$, $\Delta(sign(J_3)\Sigma_e)$, respectively.

It is readily seen that when

$$A_0=\frac{3}{2}\frac{\Delta\Sigma_m}{1-f}\left(\frac{a}{r}\right)^3 \qquad and \qquad 3K(r)A_3=-\frac{1}{2}\frac{\Delta\left(sign(J_3)\Sigma_e\right)}{(1-f)} \tag{2.62}$$

the previous condition is fulfilled.

By replacing A_0 and A_2, the shakedown condition (2.60) and (2.61) are reduced to:

$$\left(\frac{3}{4}\frac{\Delta\Sigma_m}{1-f}\right)^2\left(\frac{a}{r}\right)^6-\frac{3}{2}\frac{\Delta\Sigma_m}{1-f}\left(\frac{a}{r}\right)^3\frac{\Delta(sign(J_3)\,\Sigma_e)}{2\left(1-f\right)}P_1(r,\theta)+P_2(r,\theta)\left(\frac{\Delta(sign(J_3)\,\Sigma_e)}{2\left(1-f\right)}\right)^2\leq\sigma_0^2 \tag{2.63}$$

Since $(a/r)^n$ decreases quickly when r increases, it is reasonable to assume that the previous condition is satisfied anywhere in the body if it is fulfilled at $r=a$:

$$\left(\frac{3}{4}\frac{\Delta\Sigma_m}{1-f}\right)^2-\frac{3}{2}\frac{\Delta\Sigma_m}{1-f}\frac{\Delta(sign(J_3)\,\Sigma_e)}{2\left(1-f\right)}P_1(a,\theta)+P_2(a,\theta)\left(\frac{\Delta(sign(J_3)\,\Sigma_e)}{2\left(1-f\right)}\right)^2\leq\sigma_0^2 \tag{2.64}$$

The macroscopic shakedown criterion takes the final form by respecting the sign of J_{3+}:

- When $J_{3+}>0$, the condition is satisfied anywhere if it is fulfilled at the equator $\theta=\pi/2$ where the left part of the previous condition takes its maximum value, hence the shakedown condition reads:

$$\left(\frac{3}{4}\frac{\Delta\Sigma_m}{1-f}\right)^2-\frac{3}{2}\frac{\Delta\Sigma_m}{1-f}\frac{\Delta(sign(J_3)\,\Sigma_e)}{2\left(1-f\right)}P_1(a,\frac{\pi}{2})+P_2(a,\frac{\pi}{2})\left(\frac{\Delta(sign(J_3)\,\Sigma_e)}{2\left(1-f\right)}\right)^2\leq\sigma_0^2 \tag{2.65}$$

  where

$$P_1(a,\frac{\pi}{2})=\frac{5\nu+5}{2(5\nu-7)} \qquad P_2(a,\frac{\pi}{2})=\frac{25(7\nu^2-13\nu+7)}{(5\nu-7)^2}$$

- When $J_{3+}<0$, the condition is satisfied anywhere if it is fulfilled at the poles $\theta=0$ or $\theta=\pi$ where the left part of the previous condition takes its maximum value, hence the shakedown condition

reads:

$$\left(\frac{3}{4}\frac{\Delta\Sigma_m}{1-f}\right)^2-\frac{3}{2}\frac{\Delta\Sigma_m}{1-f}\frac{\Delta(sign(J_3)\Sigma_e)}{2(1-f)}P_1(a,0)+P_2(a,0)\left(\frac{\Delta(sign(J_3)\Sigma_e)}{2(1-f)}\right)^2\leq\sigma_0^2 \tag{2.66}$$

where

$$P_1(a,0)=\frac{5\nu+5}{-5\nu+7}\qquad P_2(a,0)=\frac{25(\nu^2+2\nu+1)}{(5\nu-7)^2}$$

Equation (2.65) and (2.66) constitute the main result of the present paper which generalize the one, proposed by Zhang et al. (Zhang et al., 2017b), to all the intermediate loading cases for the macroscopic stress ratios $-1\leq R<1$, by constructing a more suitable residual stress field $\bar{\boldsymbol{\rho}}^{(2)}$ (2.50) under pure deviatoric load. Moreover, it is worth to notice that, unlike the previous one, the new shakedown criterion does not depends on the residual stress field, and has a consistent expression for different stress ratios $R=\Sigma_-/\Sigma_+$, expressed by the amplitude of the cyclic load $\Delta\Sigma_m$ and $\Delta\Sigma_e$.

2.4.3 Nature of the collapse mechanism

In Zhang et al. (2017b), we have interestingly remarked that the shakedown limit on the cycle amplitude under pure hydrostatic load is the double of the elastic limit:

$$\Delta\Sigma_m^{SD}=2\Sigma_m^E=\frac{4}{3}(1-f)\sigma_0 \tag{2.67}$$

This relationship characterizes the collapse by alternating plasticity responsible of the low-cycle fatigue.

Firstly, we determine the macroscopic elastic limit under general loading. Resulting from the von Mises yield function (2.11) and the elastic stress field (2.39) and (2.49), one has:

$$\left(\frac{3}{2}\frac{\Sigma_m^E}{1-f}\left(\frac{a}{r}\right)^3\right)^2-3\frac{\Sigma_m^E}{1-f}\left(\frac{a}{r}\right)^3\frac{sign(J_3)\Sigma_e^E}{1-f}P_1(r,\theta)+P_2(r,\theta)\left(\frac{sign(J_3)\Sigma_e^E}{1-f}\right)^2\leq\sigma_0^2 \tag{2.68}$$

where $P_1(r,\theta)$ and $P_2(r,\theta)$ have same expressions of (2.57) and (2.58).

Simular to the derivation in Section 2.4.2, the body plasticizes firstly at inner boundary $r=a$, and the macroscopic the elastic criterion reads:

- When $J_3>0$, the body stays elastic if it is fulfilled at the equator $\theta=\pi/2$ and the elastic condition reads:

$$\left(\frac{3}{2}\frac{\Sigma_m^E}{1-f}\right)^2-3\frac{\Sigma_m^E}{1-f}\frac{sign(J_3)\Sigma_e^E}{1-f}P_1(a,\frac{\pi}{2})+P_2(a,\frac{\pi}{2})\left(\frac{sign(J_3)\Sigma_e^E}{1-f}\right)^2\leq\sigma_0^2 \tag{2.69}$$

where

$$P_1(a,\frac{\pi}{2}) = \frac{5\nu+5}{2(5\nu-7)} \qquad P_2(a,\frac{\pi}{2}) = \frac{25(7\nu^2-13\nu+7)}{(5\nu-7)^2}$$

- When $J_3 < 0$, the body stays elastic if it is fulfilled at the poles $\theta = 0$ or $\theta = \pi$ and the elastic condition reads:

$$\left(\frac{3}{2}\frac{\Sigma_m^E}{1-f}\right)^2 - 3\frac{\Sigma_m^E}{1-f}\frac{sign(J_3)\Sigma_e^E}{1-f}P_1(a,0) + P_2(a,0)\left(\frac{sign(J_3)\Sigma_e^E}{1-f}\right)^2 \leq \sigma_0^2 \tag{2.70}$$

where

$$P_1(a,0) = \frac{5\nu+5}{-5\nu+7} \qquad P_2(a,0) = \frac{25(\nu^2+2\nu+1)}{(5\nu-7)^2}$$

It is readily seen that the macroscopic elastic limit for the von Mises matrix is central symmetric, and for a given macroscopic triaxiality T, one has:

$$\Sigma_{m+}^E = -\Sigma_{m-}^E, \qquad sign(J_{3+})\Sigma_{e+}^E = -sign(J_{3-})\Sigma_{e-}^E \tag{2.71}$$

where Σ_{m+}^E and Σ_{m-}^E (resp. Σ_{e+}^E and Σ_{e-}^E) are the macroscopic mean stress (resp. equivalent stress) of the macroscopic elastic limit under compressive and tensile load, respectively.

Comparing (2.69) (2.70) with the shakedown condition (2.65) and (2.66), it is easy to obtain:

$$\begin{aligned} &\Delta\Sigma_m^{SD} = 2\Sigma_{m+}^E = -2\Sigma_{m-}^E \\ &\Delta(sign(J_3)\Sigma_e^{SD}) = 2sign(J_{3+})\Sigma_{e+}^E = -2sign(J_{3-})\Sigma_{e-}^E \end{aligned} \tag{2.72}$$

Consequently, we deduce the relationship between the shakedown limit on the cycle amplitude and the elastic limit under general loading:

$$\Delta\Sigma^{SD} = \Sigma_+^E - \Sigma_-^E = 2\Sigma_+^E \tag{2.73}$$

The relationship (2.67) is therefore always fulfilled for general loading cases. Then the macroscopic shakedown limit depends only on the elastic stress field and, since the hydrostatic elastic field $\boldsymbol{\sigma}^{E(1)}$ is the exact solution, a more suitable deviatoric stress field will surely improve the accuracy of the shakedown criterion.

Therefore, the accuracy of the prediction is not significantly affected by the trial residual field but strongly depends on the choice of elastic stress field approximation.

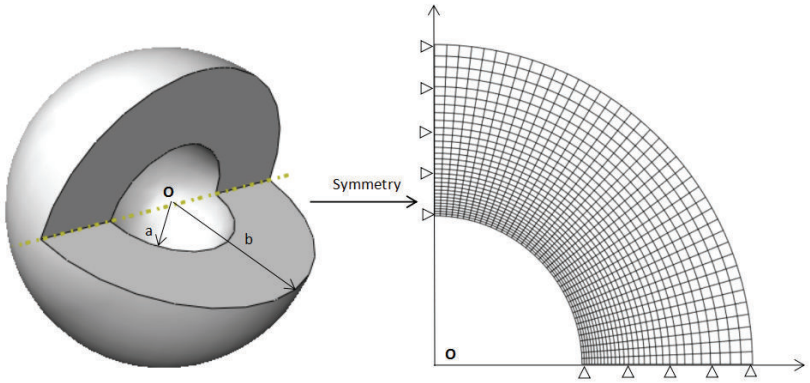

Figure 2.4: Hollow sphere model and initial mesh

2.5 Assessment of the new macroscopic shakedown criterion

In this section, we aim at assessing the predictive capability of the new shakedown criterion. Both shakedown direct method and step-by-step elastic plastic numerical computations are performed to validate the obtained theoretical solution for the intermediate loading cases (the macroscopic stress ratio $R = -1, -1/5, 0$ and $1/5$). Also the new criterion is compared to the one obtained in the previous work Zhang et al. (2017b) for the limit loading cases, namely the alternating and pulsating loads. Finally, the elastic limit and shakedown limit on cyclic amplitude are also illustrated and compared in Subsection 2.5.3.

2.5.1 Comparison with numerical results for intermediate loading cases

In this subsection, the new criterion (2.65) and (2.66) will be compared with numerical results carried out by direct and step-by-step methods for different stress ratio $R = -1, -1/5, 0$ and $1/5$.

Owing to the symmetry of the problem under consideration, we consider only a quarter of the axisymmetric model, containing a spherical void, by adopting 20000 quadratic axisymmetric elements (Figure 2.4). The homogenous velocity field $\boldsymbol{v} = \boldsymbol{D} \cdot \boldsymbol{x}$ is imposed on the external boundary of the model to fulfill the constraint of constant macroscopic stress triaxiality $T = \Sigma_m / \Sigma_e$, which is carried out by a user subroutine MPC (Multi-Points Constraints) implemented in Abaqus/Standard software (Hibbett et al., 1998). This numerical procedure is already described in (Chen et al., 2013; Cheng and Guo, 2007).

Direct numerical computations to determine the fatigue limit and step-by-step simulations to analyze the transient phase before shakedown or collapse are both performed to validate the new analytical criterion for stress ratio $R = -1, -1/5, 0$ and $1/5$ with respecting the different porosities $f = 0.001$, $f = 0.01$

T	Σ_{m+}/σ_0	Σ_{e+}/σ_0	ρ_{11}	ρ_{22}	ρ_{33}	ρ_{12}	Position	
							r	θ
$+\infty$	0.9998	0.0000	89.25	19.44	-105.65	156.15	a	$[0,\pi]$
4.3333	0.8999	0.2077	208.57	-143.10	-65.48	-0.0005	a	$\pi/2$
1.0	0.5859	0.5859	171.81	-195.42	23.60	0.0005	a	$\pi/2$
0.0	0.0	0.9269	74.12	-210.30	136.18	-0.0056	a	$\pi/2$
-1.0	0.5717	0.5717	-106.66	213.34	-106.67	0.0004	a	0
-0.3333	0.3079	0.9236	106.66	-213.34	106.67	0.005	a	0
-0.1026	0.0979	0.9547	55.40	-206.15	150.67	-0.0001	a	$\pi/2$

Table 2.1: Some numerical values of fatigue limit, the corresponding residual stress and the first point where the fatigue occurs under cyclic loading $R=-1/5$ for porosity $f=0.1$

and $f=0.1$ respectively (Figures 2.8, 2.9, 2.10). Poison's coefficient is equal to $\nu=0.3$. In practice, $\Delta\Sigma_m$ and $\Delta\Sigma_e$ are expressed by Σ_{m+} and Σ_{e+}.

In direct method, for each Gauss point $\boldsymbol{x}_g$, let $\boldsymbol{\sigma}_{\pm}^{E0}(\boldsymbol{x}_g)$ be the corresponding elastic stress response and α_g the solution of the local problem:

$$\max_{\bar{\boldsymbol{\rho}},\alpha},\{\alpha \quad | \quad F(\alpha\,\boldsymbol{\sigma}_{\pm}^{E0}(\boldsymbol{x}_g)+\bar{\boldsymbol{\rho}})\le 0\} \tag{2.74}$$

For the alternating loading case, $\boldsymbol{\sigma}_{+}^{E0}(\boldsymbol{x}_g)=-\boldsymbol{\sigma}_{-}^{E0}(\boldsymbol{x}_g)$, and $\boldsymbol{\sigma}_{-}^{E0}(\boldsymbol{x}_g)=0$ for the pulsating one. So the simulation has been reduced to the solution of a big number of problems of optimizations of small dimension. The fatigue limit α is obtained as the minimum value of α_g for all Gauss points $\boldsymbol{x}_g$. Noticing that this is only a simplified method, because we do not consider the equilibrium condition of the produced residual stress tensor at each Gauss point. For the complete numerical shakedown analysis, reads can refer to Chapter 4

From the direct shakedown method, we obtain not only the fatigue limit but also the corresponding residual stress and the location of the first point of the model where the fatigue first occurs as shown on Table 2.1. However, this direct shakedown computation can not distinguish the collapse by fatigue or by development of a mechanism, as in limit analysis. Taking $T=0$ in Table 2.1 for example, the collapse occurs by mechanism at the first cycle (see Figure 2.10) instead of by fatigue.

For the step-by-step incremental method, if the maximum load $\Delta\Sigma_{m+}$ is less than the shakedown limit, the strain-stress curve tends to a linear response and the value of PEEQ (Accumulated Equivalent Plastic Strain) does not increase any more (Figure 2.6) after a certain number of cycles, hence the body shakes down. In practice, the computation is stopped when the variation of PEEQ reaches a given tolerance and, as expected, the width of the cycle for strain tends to zero after certain cycles on the internal

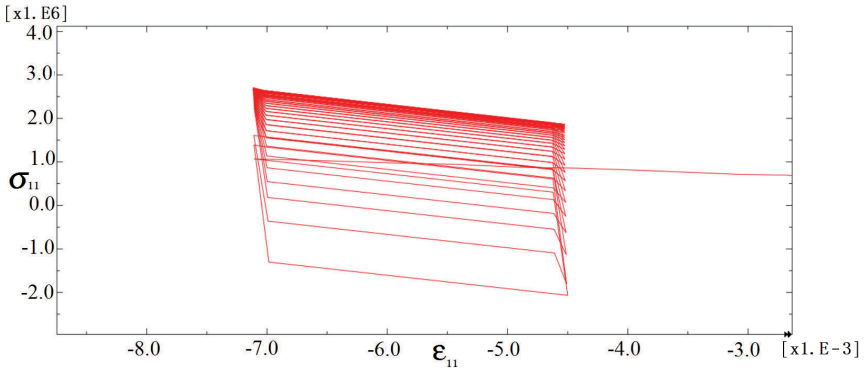

Figure 2.5: ε_{11} under pulsating load ($R = 0$) on the internal boundary at $\theta = \pi/2$ when shakedown occurs for $T = 1.8333$

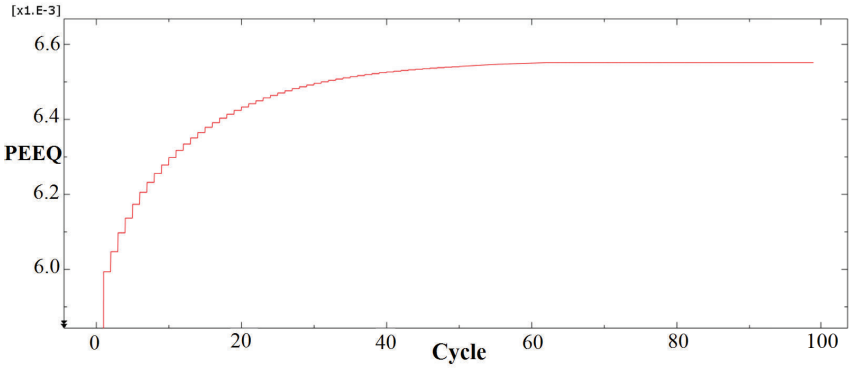

Figure 2.6: Accumulated Equivalent Plastic Strain (PEEQ) under pulsating load ($R = 0$) when shakedown occurs for $T = 1.8333$

boundary as shown on Figure 2.5. On the contrary, when the maximum load Σ_{m+} exceeds the fatigue limit (alternating loading case, for example), plastic shakedown (accommodation) occurs immediately at the first cycle. The equivalent plastic strain continues to accumulate as shown on Figure 2.7 and the dissipation remains increasing in each cycle.

The safety domain is defined by the new shakedown criterion and the yield surface proposed by Shen et al.Shen et al. (2015), corresponding to the collapse by development of a mechanism at the first cycle. With the increase of the stress ration R, the surface of collapse by mechanism becomes larger and, until the extreme case $R = 1$, in which the cyclic load turns into monotonic one, the shakedown criterion is identical to the plastic limit derived from the limit analysis.

It is readily seen that the new criterion is strictly inside the numerical results, which delivers a quasi-lower bound, because of the statical approach based on Melan's theorem. The first point where the fatigue occurs is located on the internal boundary $r = a$ at the equator $\theta = \pi/2$ for $J_{3+} > 0$ and at the poles $\theta = 0$ or π for $J_{3+} < 0$, in accord with the analytical solution.

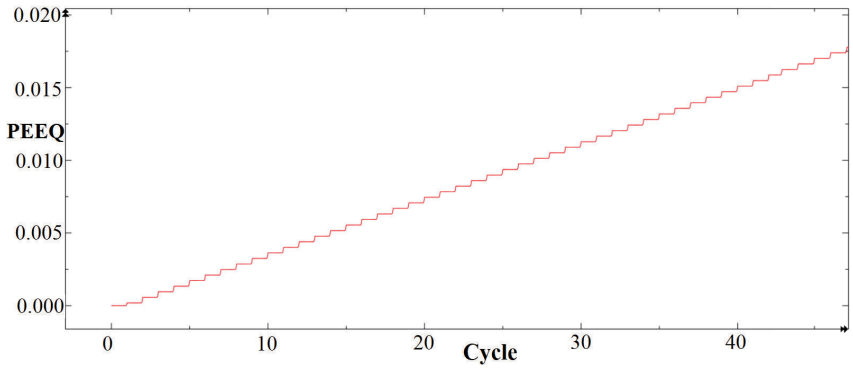

Figure 2.7: Accumulated Equivalent Plastic Strain (PEEQ) when shakedown does not occur for $T = 1.8333$

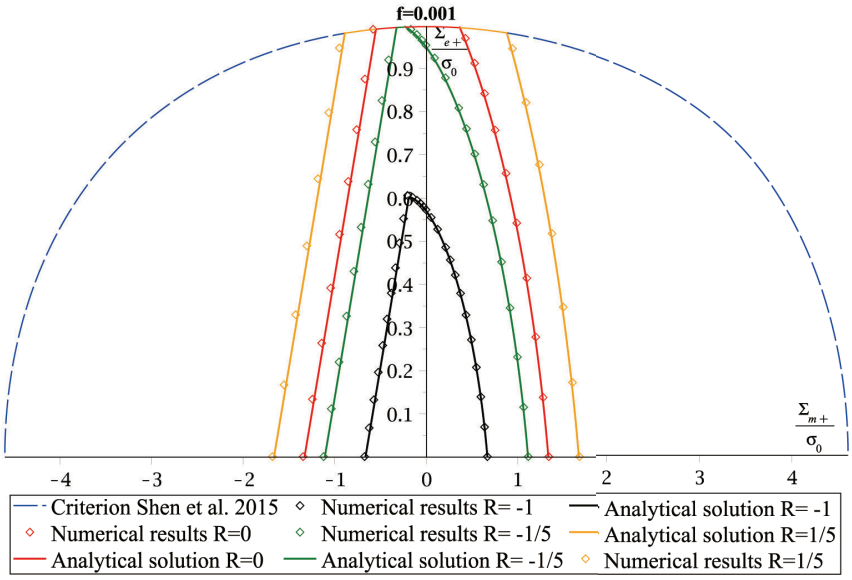

Figure 2.8: Interaction curve for porosity $f = 0.001$

For small porosities $f = 0.001$ (Figure 2.8) and $f = 0.01$ (Figure 2.9), a very good agreement between the analytical and numerical results is observed. But for a larger porosity $f = 0.1$ (Figure 2.10), the differences become noticeable around the deviatoric part is observed. Considering the exclusion of the influence of the residual stress field in the new shakedown criterion, this is due to the chosen elastic stress field under deviatoric load (2.49). Obviously, a suitable elastic stress field in the fictive elastic body is essential to analyze the shakedown limit, and the chosen elastic field (2.49) is appropriate to predict the shakedown domain for small porosities.

For completeness, the numerical results for $R = -1, -1/5, 0$ and $1/5$ with a porosity $f = 0.01$ are reported in Appendix 2.

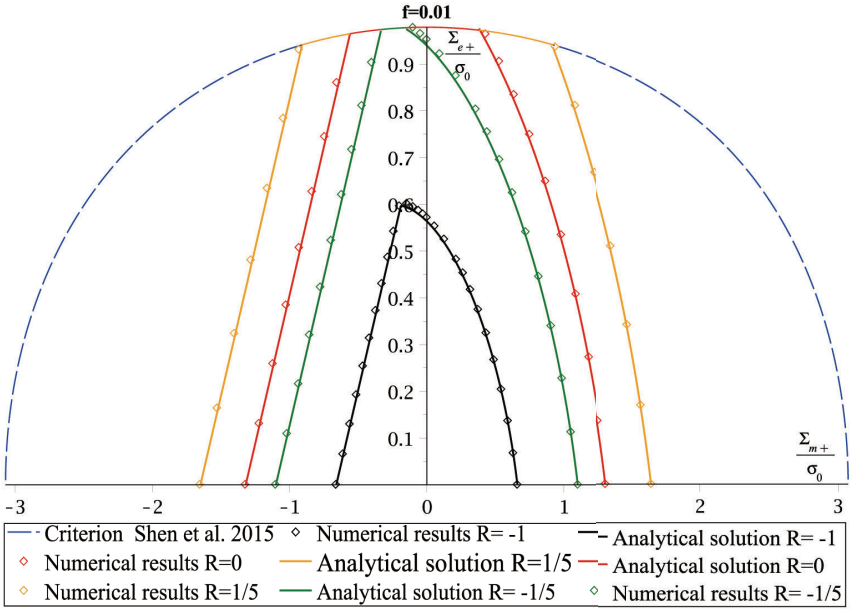

Figure 2.9: Interaction curve for porosity $f = 0.01$

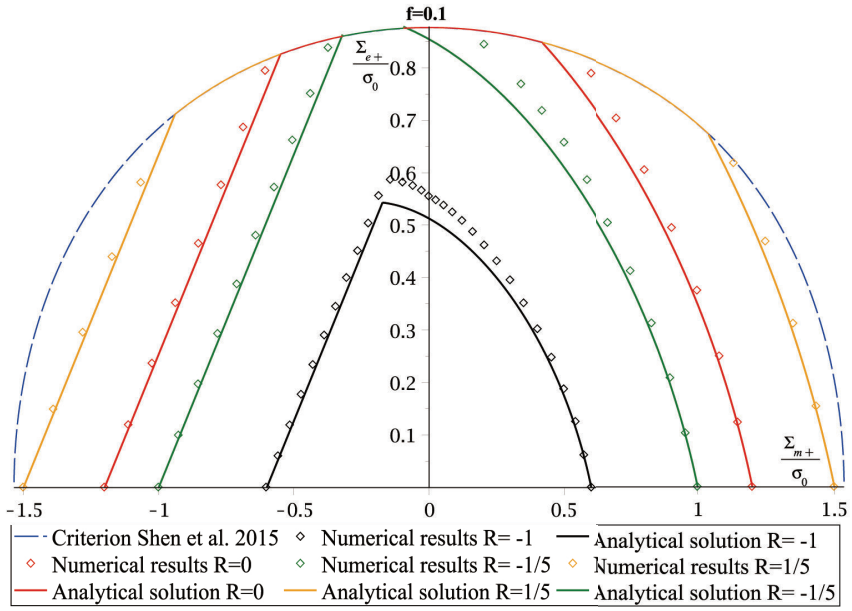

Figure 2.10: Interaction curve for porosity $f = 0.1$

2.5.2 Comparison with the previous criterion in (Zhang et al., 2017b) for alternating and pulsating loading cases

In this subsection, the new shakedown criteria (2.65) and (2.66) are compared with the one proposed in (Zhang et al., 2017b) for alternating and pulsating cyclic loads.

Figure 2.12 illustrate the comparison of the new shakedown criterion, the previous one and the numerical results for the alternating ($R=-1$) and pulsating ($R=0$) loading cases with the porosities $f=0.01$ and $f=0.1$, respectively.

In the particular case of pulsating loading ($R=0$), the curves of the new criterion is always between the old ones and the numerical results. For the pure hydrostatic loading case, the two criteria both fit the exact value $\Delta\Sigma_m^{SD}=\frac{4}{3}(1-f)\sigma_0$. However, the difference between them increases with the decrease of the stress triaxialities $T=\Sigma_m/\Sigma_e$. Obviously, the new one is more accurate. The errors, originating from the trial residual field in the previous research, has been avoided because the new residual field $\bar{\boldsymbol{\rho}}^{(2)}$ (2.50) has no influence in the improved analytical solution (2.65) and (2.66).

In the other particular case of alternating loading ($R=-1$), the curves of the two criteria coincide totally with each other. This is because, for the hollow sphere of von Mises matrix under alternating load, the corresponding microscopic residual stress is vanishing when shakedown occurs. Consequently, the choice of the residual stress field does not affect the shakedown criterion.

It is worth noting that the decreasing of the the macroscopic stress ratio $R=\Sigma_-/\Sigma_+$ causes a reduction of the shakedown domain of the voided cell.

2.5.3 Comparison between the cyclic amplitude of the shakedown limit and the elastic limit

In section 2.4.3, we obtain a special relationship (2.73) under general loading condition. Figure 2.13 illustrates the amplitude of the shakedown limit cyclic load and the elastic limit for porosity $f=0.01$. The same axisymmetric model applied in subsection 2.5.1 is adopted for the determination of the elastic limit by the finite element method. We increase the monotonic load until the plastic strain firstly appears to obtain the macroscopic elastic limit.

As shown on Figure 2.13, the analytical elastic limit is validated by the numerical results for porosity $f=0.01$. Moreover, if we magnify the elastic limit two times, it coincides totally with the shakedown limit on cyclic amplitude. This can also explain why the elastic limit is in accord with the shakedown limit under alternating load ($R=-1$), observed in (Zhang et al., 2017b). Note that the labels of the axis on this figure are Σ_{m+}^E/σ_0, Σ_{e+}^E/σ_0 for elastic limit (green), and $\Delta\Sigma_{m+}^{SD}/\sigma_0$, $\Delta\Sigma_{e+}^{SD}/\sigma_0$ for the amplitude for

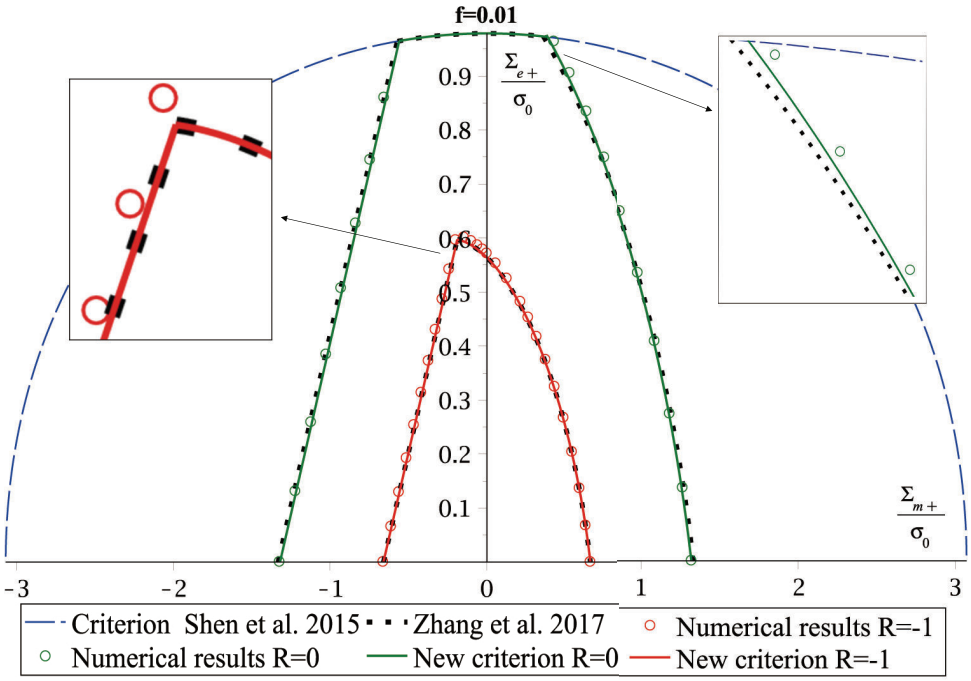

Figure 2.11: Comparison between the new criterion and the previous one in in (Zhang et al., 2017b) for $f = 0.01$

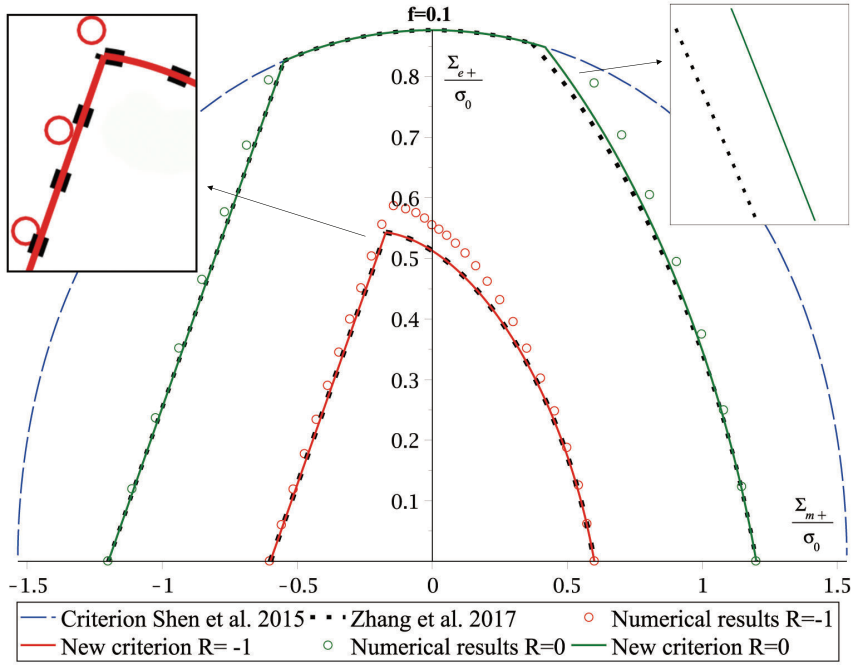

Figure 2.12: Comparison between the new criterion and the old one for $f = 0.1$

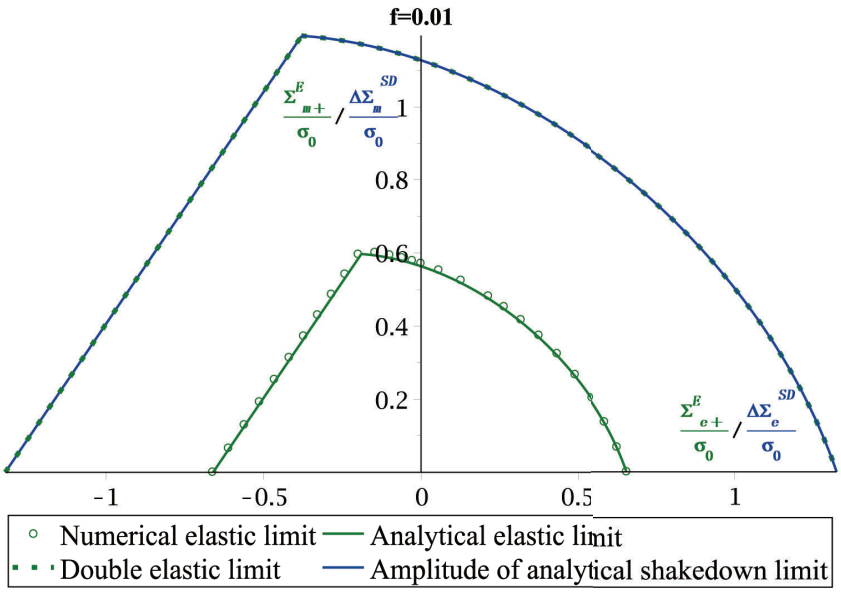

Figure 2.13: Comparison between the amplitude of the shakedown limit cyclic load and the elastic limit for $f = 0.1$

shakedown limit (blue).

2.6 Conclusion

In this chapter, a new macroscopic fatigue criterion of ductile porous materials bas been established based on Melan's static theorem. It allows to determine the shakedown safety domain and the maximum amplitude of cyclic load considering the hollow sphere unit cell with von Mises type matrix. The established results clearly provide a closed form criterion depending the two stress invariant Σ_m and Σ_e, the sign of the third invariant of the stress deviator J_3 and Poisson's coefficient ν. By considering a new residual stress field for the pure deviatoric load, the new criterion improves the one proposed by (Zhang et al., 2017b) in the deviatoric part for stress ratio $-1 \leq R < 1$, while the old one only discussed the alternating ($R = -1$) and the pulsating ($R = 0$) loading cases.

The proposed model has been assessed by comparing to the numerical simulations derived by both shakedown direct method and step-by-step incremental method for $R = -1, -1/5, 0$ and $1/5$, respectively. The new criterion is strictly conservative to predict the shakedown safety domain combining with the one proposed by (Shen et al., 2015), which corresponds to the collapse by development of a mechanism at the first cycle. Moreover, the double relation, between the amplitude of the cyclic shakedown limit load its elastic limit under monotonic load, is proved.

In the perspective, the interest of the present study lies in finding a more appropriate deviatoric stress field in the fictive elastic body and the extension of the proposed model to porous materials with pressure sensitive matrix such as the Drucker-Prager model. Another interesting extension will concern the shakedown of ductile porous materials involving the kinematical hardening. This issue is in progress.

Appendix 1: Determination of $\bar{\boldsymbol{\rho}}^{(2b)}$ and $K(r)$

In section 2.4.1, we hope to construct a residual stress field $\bar{\boldsymbol{\rho}}^{(2b)}$ (2.50) satisfying the imposed condition (2.53), which provides:

$$\rho_{rr}^{2b}-\frac{1}{3}\left(\rho_{rr}^{2b}+\rho_{\theta\theta}^{2b}+\rho_{\phi\phi}^{2b}\right)= A_3K(r)\left(-\frac{\cos(2\theta)+1}{2}\frac{2a^3\left(\left(15\nu r^2+27a^2-30r^2\right)\cos^2(\theta)-5\nu r^2-9a^2+10r^2\right)}{r^5\left(-7+5\nu\right)}\right) \tag{75}$$

$$\rho_{\theta\theta}^{2b}-\frac{1}{3}\left(\rho_{rr}^{2b}+\rho_{\theta\theta}^{2b}+\rho_{\phi\phi}^{2b}\right)= A_3K(r)\left(\frac{\cos(2\theta)-1}{2}-\frac{a^3\left(\left(63a^2-45r^2\right)\cos^2(\theta)+20\nu r^2-27a^2+5r^2\right)}{2r^5\left(-7+5\nu\right)}\right) \tag{76}$$

$$\rho_{\phi\phi}^{2b}-\frac{1}{3}\left(\rho_{rr}^{2b}+\rho_{\theta\theta}^{2b}+\rho_{\phi\phi}^{2b}\right)= A_3K(r)\left(1-\frac{a^3\left(\left(60\nu r^2+45a^2-75r^2\right)\cos^2(\theta)-40\nu r^2-9a^2+35r^2\right)}{2r^5\left(-7+5\nu\right)}\right) \tag{77}$$

$$\rho_{r\theta}^{2b}=A_3K(r)\left(\frac{3a^3\left(12a^2-5r^2\left(1+\nu\right)\right)\sin(2\theta)}{2\,r^5\left(-7+5\nu\right)}+\frac{3\sin(2\theta)}{2}\right) \tag{78}$$

where $K(r)$ is a function of r and A_3 is the constant to be determined.

Due to (2.7), we need to prove the existence of $\bar{\boldsymbol{\rho}}^{(2b)}$ satisfying two following conditions:

- $div\,\bar{\boldsymbol{\rho}}^{(2b)}=\mathbf{0}\quad in\Omega$
- $\bar{\boldsymbol{\rho}}^{(2b)}\cdot\boldsymbol{n}=\mathbf{0}\quad on\partial\omega$

Let us start from the internal equilibrium equation in spherical coordinates:

$$\frac{\partial\sigma_{rr}}{\partial r}+\frac{1}{r}\frac{\partial\sigma_{r\theta}}{\partial\theta}+\frac{1}{r\sin\theta}\frac{\partial\sigma_{r\phi}}{\partial\phi}+\frac{1}{r}\left(2\sigma_{rr}-\sigma_{\theta\theta}-\sigma_{\phi\phi}+\sigma_{r\theta}\cot\theta\right)=0 \tag{79}$$

$$\frac{\partial\sigma_{r\theta}}{\partial r}+\frac{1}{r}\frac{\partial\sigma_{\theta\theta}}{\partial\theta}+\frac{1}{r\sin\theta}\frac{\partial\sigma_{\theta\phi}}{\partial\phi}+\frac{1}{r}\left(\left(\sigma_{\theta\theta}-\sigma_{\phi\phi}\right)\cot\theta+3\sigma_{r\theta}\right)=0 \tag{80}$$

$$\frac{\partial \sigma_{\phi r}}{\partial r}+\frac{1}{r}\frac{\partial \sigma_{\phi\theta}}{\partial \theta}+\frac{1}{r\sin\theta}\frac{\partial \sigma_{\phi\phi}}{\partial \phi}+\frac{1}{r}\left(3\sigma_{r\theta}+2\sigma_{\theta\phi}\right)=0 \tag{81}$$

Due to the axisymmetric loading on the hollow sphere model, the stress components do not depend on ϕ and one has:

$$\sigma_{\phi r}=\sigma_{\phi\theta}=0 \tag{82}$$

Then (81) is automatically satisfied, and (79), (80) are reduced to:

$$\frac{\partial \sigma_{rr}}{\partial r}+\frac{1}{r}\frac{\partial \sigma_{r\theta}}{\partial \theta}+\frac{1}{r}\left(2\sigma_{rr}-\sigma_{\theta\theta}-\sigma_{\phi\phi}+\sigma_{r\theta}\cot\theta\right)=0 \tag{83}$$

$$\frac{\partial \sigma_{r\theta}}{\partial r}+\frac{1}{r}\frac{\partial \sigma_{\theta\theta}}{\partial \theta}+\frac{1}{r}\left(\left(\sigma_{\theta\theta}-\sigma_{\phi\phi}\right)\cot\theta+3\sigma_{r\theta}\right)=0 \tag{84}$$

Therefore, from (75), (76) and (77), we obtain:

$$\rho^{2b}_{\theta\theta}-\rho^{2b}_{\phi\phi}=A_3K(r)\left(\frac{3\left(\cos(2\theta)-1\right)}{2}-\frac{3a^3\left(\left(-20\nu r^2+6a^2+10r^2\right)\cos^2(\theta)+20\nu r^2-6a^2-10r^2\right)}{2r^5\left(-7+5\nu\right)}\right) \tag{85}$$

Taking (78) (85) into (84), the general solution of $\rho_{\theta\theta}$ is:

$$\begin{aligned}\rho^{2b}_{\theta\theta}=-\frac{3A_3\cos^2(\theta)}{2r^5\left(-7+5\nu\right)}\Big[&\left(5a^3\nu r^3-5\nu r^6-12a^5r+5a^3r^3+7r^6\right)\frac{dK(r)}{dr}\\&K(r)\left(10a^3\nu r^2-10\nu r^5+21a^5-5a^3r^2+14r^5\right)\Big]+C_1(r)\end{aligned} \tag{86}$$

where $C_1(r)$ is a function of r.

Then the expression of ρ_{rr} and $\rho_{\phi\phi}$ are given by:

$$\rho^{2b}_{\phi\phi}=\rho^{2b}_{\theta\theta}+\frac{3A_3K(r)}{2}\left(\frac{a^3\left(\left(-20\nu r^2+6a^2+10r^2\right)\cos^2(\theta)+20\nu r^2-6a^2-10r^2\right)}{r^5\left(-7+5\nu\right)}+1-\cos(2\theta)\right) \tag{87}$$

$$\rho^{2b}_{rr}=\rho^{2b}_{\phi\phi}+\frac{3A_3K(r)}{2}\left(\frac{a^3\left(\left(40\nu r^2+51a^2-65r^2\right)\cos^2(\theta)-20\nu r^2-15a^2+25r^2\right)}{2r^5\left(-7+5\nu\right)}-1-\cos(2\theta)\right) \tag{88}$$

substitution in (83) yields:

$$\begin{aligned}\frac{dC_1(r)}{dr} = \frac{A_3}{2r^6(7-5\nu)}\Big[&cos^2(\theta)\left(-60a^3\nu r^3+15r^6\nu+36a^5r+120a^3r^3-21r^6\right)\frac{dK(r)}{dr}\\&+cos^2(\theta)\left(15a^3\nu r^4-15r^7\nu-36a^5r^2+15a^3r^4+21r^7\right)\frac{d^2K(r)}{dr^2}\\&\left(-30r^6\nu+63a^5r-45a^3r^3+43r^6\right)\frac{dK(r)}{dr}+\left(30a^3\nu r^2-135a^5-15a^3r^2\right)K(r)\Big]\end{aligned} \tag{89}$$

Elimination of terms involving $\cos(\theta)$ leads to:

$$\begin{aligned}&\left(-60a^3\nu r^3+15r^6\nu+36a^5r+120a^3r^3-21r^6\right)\frac{dK(r)}{dr}\\&+\left(15a^3\nu r^4-15r^7\nu-36a^5r^2+15a^3r^4+21r^7\right)\frac{d^2K(r)}{dr^2}=0\end{aligned} \tag{90}$$

Therefore, the general solutions of $K(r)$ and $C_1(r)$ are:

$$K(r) = C_2\int e^{\int \frac{-a^3\nu r^2+15\nu r^5+36a^5+120a^3r^2-21r^5}{3r(-5a^3\nu r^2+5\nu r^5+12a^5-5a^3r^2-7r^5)}\,dr}\,dr + C_3 \tag{91}$$

$$\begin{aligned}C_1(r) = \int [&A_3C_2\left(30a^3\nu r^2-135a^5-15a^3r^2\right)\int e^{\int \frac{-a^3\nu r^2+15\nu r^5+36a^5+120a^3r^2-21r^5}{3r(-5a^3\nu r^2+5\nu r^5+12a^5-5a^3r^2-7r^5)}\,dr}\,dr\\&+A_3C_2\left(-30\nu r^6+63a^5r-45a^3r^3+42r^6\right)e^{\int \frac{-a^3\nu r^2+15\nu r^5+36a^5+120a^3r^2-21r^5}{3r(-5a^3\nu r^2+5\nu r^5+12a^5-5a^3r^2-7r^5)}\,dr}\\&+A_3C_3\left(30a^3\nu r^2-135a^5-15a^3r^2\right)]dr+C_4\end{aligned} \tag{92}$$

where C_2 C_3 and C_4 are constants.

By now, all the expressions of $\bar{\boldsymbol{\rho}}^{(2b)}$ are already obtained. It is very important to underline that, we do not need to determine C_2, C_3 and C_4, because these parameters of the residual stress field have no influence in the derivation of the shakedown criterion (2.63). That is to say, C_2, C_3 and C_4 can take any real values except for $C_2 = 0$ (if $C_2 = 0$, $\bar{\boldsymbol{\rho}}^{(2)}$ is same to the corresponding elastic stress field $\boldsymbol{\sigma}^{E(2)}$).

Two remarks can be made for the boundary condition:

1. The choice of the above residual stress field, defined by (2.52), together with (86), (87), (88) and (78), implies that:

$$\Sigma_m^{void} = \frac{1}{|\,\Omega\,|}\int_\omega \sigma_m\,dV = \frac{1}{3\,|\,\Omega\,|}\int_{\partial\omega}\mathbf{x}\cdot(\boldsymbol{\sigma}\,\mathbf{n})\,dS = 0\,. \tag{93}$$

   which then appears as a relaxed form of the void boundary condition for $\bar{\boldsymbol{\rho}}^{(2b)}$, similar to the case of studied in (Zhang et al., 2017b).

2. Due to the corresponding residual mean macroscopic stress tensor in the matrix:

$$Tr(\boldsymbol{\Sigma}_r(\bar{\boldsymbol{\rho}}^{(2)})) = 0 \tag{94}$$

and applying the relaxed inner boundary condition (93) to the outer boundary, the average mean residual stress:

$$\boldsymbol{\Sigma}_r(\bar{\boldsymbol{\rho}}^{(2)}) = \frac{1}{|\,\Omega\,|}\int_{\partial\Omega}(\bar{\boldsymbol{\rho}}^{(2)}\cdot\mathbf{n})\otimes\boldsymbol{x}\,dS = 0 \tag{95}$$

vanishes and the average mean stress is equal to the corresponding value in the fictitious elastic body, which validate the imposed condition (2.21).

Appendix 2: Numerical values of shakedown limit with respect to different values of T for porosity $f = 0.1$

The values of numerical shakedown limit, related to the asterisk points on Figure 2.10 are reported in Table 2. Note that − means the collapse occurs by development of a mechanism instead of fatigue.

R	-1 (alternating)		-1/5		0 (pulsating)		1/5	
T	Σ_{m+}/σ_0	Σ_{e+}/σ_0	Σ_{m+}/σ_0	Σ_{e+}/σ_0	Σ_{m+}/σ_0	Σ_{e+}/σ_0	Σ_{m+}/σ_0	Σ_{e+}/σ_0
$+\infty$	0.6610	0.0000	1.1017	0.0000	1.3220	0.0000	1.6526	0.0000
9.3333	0.6307	0.0676	1.0511	0.1126	1.2655	0.1356	1.5766	0.0000
4.3333	0.5913	0.1365	0.9855	0.2274	1.1827	0.2729	1.4783	0.3411
2.6667	0.5436	0.2039	0.9061	0.3398	1.0870	0.4076	1.3591	0.5097
1.8333	0.4897	0.2671	0.8162	0.4452	0.9800	0.5345	1.2244	0.6678
1.3333	0.4327	0.3245	0.7211	0.5409	0.8654	0.6490	1.0817	0.8113
1.0	0.3746	0.3746	0.6244	0.6244	0.7492	0.7492	0.9366	0.9366
0.7619	0.3179	0.4172	0.5298	0.6954	0.6358	0.8345	–	–
0.5833	0.2642	0.4529	0.4403	0.7548	0.5283	0.9057	–	–
0.4444	0.2142	0.4820	0.3570	0.8033	0.4284	0.9640	–	–
0.2424	0.1273	0.5250	0.2121	0.8750	–	–	–	–
0.1026	0.0567	0.5531	0.0945	0.9218	–	–	–	–
0.0	0.0000	0.5715	0.0000	0.9524	–	–	–	–
$-\infty$	0.6611	0.0000	1.1017	0.0000	1.3220	0.0000	1.6526	0.0000
-9.3333	0.6106	0.0654	1.0177	0.1090	1.2213	0.1309	1.5266	0.1636
-4.3333	0.5606	0.1294	0.9344	0.2156	1.1213	0.2588	1.4016	0.3234
-2.6667	0.5125	0.1922	0.8541	0.3203	1.0249	0.3843	1.2812	0.4804
-1.8333	0.4648	0.2535	0.7747	0.4226	0.9297	0.5071	1.1621	0.6339
-1.3333	0.4180	0.3135	0.6967	0.5226	0.8361	0.6271	1.0451	0.7838
-1.0	0.3724	0.3724	0.6206	0.6206	0.7447	0.7447	0.9309	0.9309
-0.7619	0.3277	0.4301	0.5461	0.7168	0.6553	0.8601	–	–
-0.5833	0.2838	0.4865	0.4730	0.8109	–	–	–	–
-0.4444	0.2408	0.5419	0.4014	0.9032	–	–	–	–
-0.3333	0.1987	0.5962	–	–	–	–	–	–
-0.2424	0.1458	0.6012	–	–	–	–	–	–
-0.1667	0.0991	0.5945	–	–	–	–	–	–
-0.1026	0.0602	0.5868	0.1003	0.9779	–	–	–	–
-0.0476	0.0286	0.5790	0.0459	0.9650	–	–	–	–

Table 2: Numerical values of shakedown limit with respect to different values and the first point where fatigue occurs of T for porosity $f = 0.01$

Chapter 3

Shakedown of porous material with Drucker-Prager dilatant matrix under general cyclic loadings

This chapter is concerned with the shakedown limit states of porous ductile materials with Drucker-Prager matrix under cyclically repeated loads. Following the previous chapter and using the hollow sphere model, a macroscopic fatigue criterion is derived for the general conditions of cyclic loads. The obtained criterion depends on the three invariants of the macroscopic stress tensor, the porosity, the friction angle and Poisson's ratio. Together with the limit analysis-based yield criterion corresponding to the sudden collapse by development of a mechanism at the first cycle, it defines the safety domain of porous materials subjected to cyclic load processes. Interestingly, it is found that the safe domain is little sensitive to variations of the friction angle, however, it is considerably reduced compared to the one under monotonic loads obtained by limit analysis. Further, some particular cases are recovered by the established criterion. Finally, a comparative study between the analytical results and numerical predictions performed by micromechanics-based finite element simulations is conducted for different porosities and friction angles.

3.1 Effective behavior under cyclic pure hydrostatic loading

As in Chapter 2, the representative volume element (RVE) is a thick hollow sphere comprising a concentric and free-traction boundary spherical cavity. The inner and the outer radii are respectively denoted

by a and b that is the porosity is defined by $f = (a/b)^3 < 1$. The matrix material obeys to the associated elastic-perfectly plastic Drucker-Prager model for which the yield function writes:

$$F(\boldsymbol{\sigma}) = \sigma_e(\boldsymbol{\sigma}) + 3\alpha\sigma_m - \sigma_0 \leq 0 \tag{3.1}$$

where $\sigma_e = \sqrt{\frac{3}{2}\mathbf{s}:\mathbf{s}}$ is the equivalent stress defined from the deviatoric part $\mathbf{s}$ of the stress tensor $\boldsymbol{\sigma}$, σ_m is the mean stress, σ_0 represents the yield stress, and α is the pressure sensitivity factor related to the friction angle ϕ by:

$$tan\phi = 3\alpha$$

.

It is worth noting that the Drucker-Prager criterion reduces to the incompressible von Mises model for a vanishing friction angle ($\alpha = 0$). The pressure-dependent Drucker-Prager constitutive law is often used for modeling of rock and soils, concrete and polymeric and some metallic materials.

The hollow sphere undergoes a uniform hydrostatic stress q exerted upon its external boundary $\partial\Omega$. Owing to (1.39), the average mean stress is:

$$\Sigma_m = \frac{1}{3} Tr\,(\boldsymbol{\Sigma}) = q \tag{3.2}$$

Taking into account the central symmetry of the problem, the spherical coordinate (r,θ,φ) are used, r being the radius, θ the inclination angle, φ the azimuth one, with orthonormal frame $\{\mathbf{e}_r,\mathbf{e}_\theta,\mathbf{e}_\phi\}$, and all the fields are depending only on r. Simple computations allow the derivation of the stress field in the fictitious elastic body is:

$$\boldsymbol{\sigma}^E = \frac{\Sigma_m}{1-f}\left(\mathbf{1} + \frac{1}{2}\left(\frac{a}{r}\right)^3 (\mathbf{e}_\theta\otimes\mathbf{e}_\theta + \mathbf{e}_\phi\otimes\mathbf{e}_\phi - 2\,\boldsymbol{e}_r\otimes\boldsymbol{e}_r)\right) \tag{3.3}$$

where $\mathbf{1}$ is the second order unit tensor.

The behaviour of the body remains elastic provided:

$$\max_{a\leq r\leq b}\sigma_e = \max_{a\leq r\leq b}\left(|\,\frac{3}{2}\frac{\Sigma_m}{1-f}\left(\frac{a}{r}\right)^3\,| + 3\alpha\,\frac{\Sigma_m}{1-f}\right) \leq \sigma_0 \tag{3.4}$$

Hence, the first yielding occurs on the void boundary and the *elastic limit average mean stress* is:

$$\Sigma^E_{m\pm} = \frac{(1-f)}{\pm 3/2 + 3\alpha}\,\sigma_0 \tag{3.5}$$

for $\Sigma_m \gtrless 0$.

3.1.1 Collapse by fatigue

Beyond this limit, plastic strains appear and our aim is to determine when the macro-element shakes down using Melan's theorem if the load Σ_m belongs to the domain:

$$\Sigma_{m-} \leq \Sigma_m \leq \Sigma_{m+} = \Sigma_{m-} + \Delta\Sigma_m \tag{3.6}$$

where Σ_{m-} and Σ_{m+} are the minimum and maximum macroscopic hydrostatic loads during the cyclic loading precess, respectively.

Inspired from the previous work of limit analysis of porous materials with Druker-Prager matrix (Cheng et al., 2012), the exact stress field of hollow sphere under pure hydrostatic load beyond the elastic limit is taking the following form:

$$\boldsymbol{\sigma}^* = \frac{A_0}{3\alpha}\left(\left(1-\left(\frac{a}{r}\right)^{3\gamma}\right)\mathbf{1} + \frac{3}{2}\gamma\left(\frac{a}{r}\right)^{3\gamma}(\boldsymbol{e}_\theta \otimes \boldsymbol{e}_\theta + \boldsymbol{e}_\phi \otimes \boldsymbol{e}_\phi)\right) \tag{3.7}$$

where $\gamma = 2\alpha/(2\alpha+\epsilon)$ and $\epsilon = \pm 1$ for $A_0 \gtrless 0$.

We denote $\boldsymbol{\sigma}^E$ the stress field in the corresponding fictitious elastic body, and the residual stress field is defined by:

$$\bar{\boldsymbol{\rho}} = \boldsymbol{\sigma}^* - \boldsymbol{\sigma}^E \tag{3.8}$$

where Σ_m^E takes its extreme values in the inner part $a \leq c \leq b$ of the body when shakedown occurs:

$$\begin{aligned}\bar{\boldsymbol{\rho}} = A_0\left(\left(1-\left(\frac{a}{r}\right)^{3\gamma}\right)\mathbf{1} + \frac{3}{2}\gamma\left(\frac{a}{r}\right)^{3\gamma}(\boldsymbol{e}_\theta \otimes \boldsymbol{e}_\theta + \boldsymbol{e}_\phi \otimes \boldsymbol{e}_\phi)\right)\\ -\frac{\Sigma_{m\pm}}{1-f}\left(\mathbf{1} + \frac{1}{2}\left(\frac{a}{r}\right)^3(\mathbf{e}_\theta \otimes \mathbf{e}_\theta + \mathbf{e}_\phi \otimes \mathbf{e}_\phi - 2\,\boldsymbol{e}_r \otimes \boldsymbol{e}_r)\right)\end{aligned} \tag{3.9}$$

where A_0 is a constant parameter. It can be verified that γ, A_0 and Σ_m have the same sign ϵ.

Taking the positive sign $\epsilon = 1$ for example, the total stress field under the pure hydrostatic load for $a \leq c \leq b$ is taking the following form:

$$\begin{aligned}\boldsymbol{\sigma} = A_0\left(\left(1-\left(\frac{a}{r}\right)^{3\gamma}\right)\mathbf{1} + \frac{3}{2}\gamma\left(\frac{a}{r}\right)^{3\gamma}(\boldsymbol{e}_\theta \otimes \boldsymbol{e}_\theta + \boldsymbol{e}_\phi \otimes \boldsymbol{e}_\phi)\right)\\ -\frac{\Sigma_{m+}-\Sigma_m}{1-f}\left(\mathbf{1} + \frac{1}{2}\left(\frac{a}{r}\right)^3(\mathbf{e}_\theta \otimes \mathbf{e}_\theta + \mathbf{e}_\phi \otimes \mathbf{e}_\phi - 2\,\boldsymbol{e}_r \otimes \boldsymbol{e}_r)\right)\end{aligned} \tag{3.10}$$

Combining with the yield function (3.1), one has:

$$\left|\frac{3\gamma A_0}{2}\left(\frac{a}{r}\right)^{3\gamma}-\frac{3}{2}\frac{\Sigma_{m+}-\Sigma_m}{1-f}\left(\frac{a}{r}\right)^3\right|+3\alpha\left(\gamma A_0\left(\frac{a}{r}\right)^{3\gamma}+A_0\left(1-\left(\frac{a}{r}\right)^{3\gamma}\right)-\frac{\Sigma_{m+}-\Sigma_m}{1-f}\right)\leq\sigma_0 \tag{3.11}$$

The shakedown limit is reached in when the yield function vanishes simultaneously for the extreme values of loading:

$$\left|\frac{3\gamma A_0}{2}\left(\frac{a}{r}\right)^{3\gamma}\right|+3\alpha\left(\gamma A_0\left(\frac{a}{r}\right)^{3\gamma}+A_0\left(1-\left(\frac{a}{r}\right)^{3\gamma}\right)\right)\leq\sigma_0 \tag{3.12}$$

$$\left|\frac{3\gamma A_0}{2}\left(\frac{a}{r}\right)^{3\gamma}-\frac{3}{2}\frac{\Delta\Sigma_m}{1-f}\left(\frac{a}{r}\right)^3\right|+3\alpha\left(\gamma A_0\left(\frac{a}{r}\right)^{3\gamma}+A_0\left(1-\left(\frac{a}{r}\right)^{3\gamma}\right)-\frac{\Delta\Sigma_m}{1-f}\right)\leq\sigma_0 \tag{3.13}$$

Because $(a/r)^n$ decreases quickly when r increases, the previous condition is satisfied anywhere in the body if it is fulfilled at $r=a$:

$$\left|\left(\frac{3\gamma A_0}{2}\right)^2\right|+3\alpha\left(\gamma A_0\right)\leq\sigma_0$$

$$\left|\left(\frac{3\gamma A_0}{2}-\frac{3}{2}\frac{\Delta\Sigma_m}{1-f}\right)^2\right|+3\alpha\left(\gamma A_0-\frac{\Delta\Sigma_m}{1-f}\right)\leq\sigma_0$$

Combining the two previous equations, the shakedown limit for pure hydrostatic loading reads:

$$\frac{\Delta\Sigma_m}{\sigma_0}\leq\frac{3\left(1-f\right)}{\left(3/2+3\alpha\right)\left(3/2-3\alpha\right)} \tag{3.14}$$

It is worth to observe the relationship between the shakedown limit on the cycle amplitude and the elastic limit (3.5):

$$\Delta\Sigma_m\leq\Delta\Sigma_m^{SD}=\Sigma_{m+}^E-\Sigma_{m-}^E=\frac{3\left(1-f\right)\sigma_0}{\left(3/2+3\alpha\right)\left(3/2-3\alpha\right)} \tag{3.15}$$

3.1.2 Collapse by development of a mechanism

Moreover, because the stress field chosen in (3.7), all the macro-element is plastified when the *limit load* Σ_m^L is reached:

$$\Sigma_{m\pm}^L=\frac{\sigma_0}{3\alpha}\left(1-f^\gamma\right)=\frac{\sigma_0}{3\alpha}\left(1-f^{2\alpha/(2\alpha\pm1)}\right) \tag{3.16}$$

It is clear that the collapse by fatigue occurs only if:

$$\Sigma_{m-}\geq\Sigma_{m-}^L\quad and\quad\Sigma_{m+}=\Sigma_{m-}+\Delta\Sigma_m^{SD}\leq\Sigma_{m+}^L \tag{3.17}$$

If $\Sigma_{m-}=0$, owing to (3.14) and (3.16), the fatigue collapse occurs under the condition:

$$\frac{3\left(1-f\right)}{\left(3/2+3\alpha\right)\left(3/2-3\alpha\right)}\leq\frac{1}{3\alpha}\left(1-f^{2\alpha/(2\alpha+1)}\right) \tag{3.18}$$

And if $\Sigma_{m-}=-\Sigma_{m+}$, the fatigue collapse occurs provided:

$$\begin{aligned} &-\frac{3\left(1-f\right)}{2\left(3/2+3\alpha\right)\left(3/2-3\alpha\right)}\geq\frac{1}{3\alpha}\left(1-f^{2\alpha/(2\alpha-1)}\right)\\ \textit{and}\quad &\frac{3\left(1-f\right)}{2\left(3/2+3\alpha\right)\left(3/2-3\alpha\right)}\leq\frac{1}{3\alpha}\left(1-f^{2\alpha/(2\alpha+1)}\right) \end{aligned} \tag{3.19}$$

3.2 Macroscopic shakedown criterion under general cyclic loadings

3.2.1 The trial stress and residual stress fields

For the general case, it is not possible to obtain the exact solution because of the non linearity of Drucker-Prager yield function. The choice of a trial stress field is crucial. It must be rather rich to capture the main physical effect but depends on a few number of parameters in order to obtain a closed-form formula for the macroscopic criterion.

Taking into account the symmetry of the hollow sphere model, the trial stress field is considered as the sum of the two following fields:

- A heterogeneous part inspired from the exact field under pure hydrostatic loadings which is expressed in spherical coordinates:

$$\boldsymbol{\sigma}^{(1)}=\bar{\boldsymbol{\rho}}^{(1)}+\boldsymbol{\sigma}^{E(1)} \tag{3.20}$$

  where the residual stress field in the inner region $a\leq r\leq c$ is inspired from the exact solution Cheng et al. (2012) in the pure hydrostatic loading:

$$\begin{aligned} \bar{\boldsymbol{\rho}}^{(1)}=A_0\left(\left(1-\left(\frac{a}{r}\right)^{3\gamma}\right)\mathbf{1}+\frac{3}{2}\gamma\left(\frac{a}{r}\right)^{3\gamma}\left(\boldsymbol{e}_\theta\otimes\boldsymbol{e}_\theta+\boldsymbol{e}_\phi\otimes\boldsymbol{e}_\phi\right)\right)\\ -\frac{\Sigma_{m+}}{1-f}\left(\mathbf{1}+\frac{1}{2}\left(\frac{a}{r}\right)^3\left(\boldsymbol{e}_\theta\otimes\boldsymbol{e}_\theta+\boldsymbol{e}_\phi\otimes\boldsymbol{e}_\phi-2\,\boldsymbol{e}_r\otimes\boldsymbol{e}_r\right)\right) \end{aligned} \tag{3.21}$$

  A_0 being a constant to be determined.

  The stress field in the fictitious elastic body is given

$$\boldsymbol{\sigma}^{E(1)}=\frac{\Sigma_m}{1-f}\left(\mathbf{1}+\frac{1}{2}\left(\frac{a}{r}\right)^3\left(\mathbf{e}_\theta\otimes\mathbf{e}_\theta+\mathbf{e}_\phi\otimes\mathbf{e}_\phi-2\,\boldsymbol{e}_r\otimes\boldsymbol{e}_r\right)\right) \tag{3.22}$$

- The other part under the pure deviatoric loadings is expressed in spherical coordinates:

$$\boldsymbol{\sigma}^{(2)} = \bar{\boldsymbol{\rho}}^{(2)} + \boldsymbol{\sigma}^{E(2)} \tag{3.23}$$

where a statically admissible stress field in the fictitious body, deduced from the Papkovich-Neuber solution (Soutas-Little, 1999) for the hollow sphere under the pure deviatoric load, was proposed in the previous work (Zhang et al., 2018) in the following form, in the spherical coordinates (r,θ,ϕ) with orthonormal frame $\{\mathbf{e}_r,\mathbf{e}_\theta,\mathbf{e}_\phi\}$:

$$\begin{aligned}
\boldsymbol{\sigma}^{E(2)} = -\frac{sign(J_3)\Sigma_e}{3(1-f)} \Bigg\{ & \left[\frac{a^3\left(18a^2+5r^2(-5+\nu)\right)(1+3\cos(2\theta))}{2r^5(-7+5\nu)} - \frac{1+3\cos(2\theta)}{2} \right] (\mathbf{e}_r\otimes\mathbf{e}_r) \\
& + \left[\frac{a^3\left(27a^2+5r^2(1-2\nu)-3\left(21a^2+5r^2(-1+2\nu)\right)\cos^2(\theta)\right)}{2r^5(-7+5\nu)} + \frac{-1+3\cos(2\theta)}{2} \right] (\mathbf{e}_\theta\otimes\mathbf{e}_\theta) \\
& + \left[\frac{a^3\left(9a^2+25r^2(-1+2\nu)-45\left(a^2+r^2(-1+2\nu)\right)\cos^2(\theta)\right)}{2r^5(-7+5\nu)} + 1 \right] \left(\mathbf{e}_\phi\otimes\mathbf{e}_\phi\right) \\
& + \left[\frac{3a^3\left(12a^2-5r^2(1+\nu)\right)\sin(2\theta)}{2r^5(-7+5\nu)} + \frac{3\sin(2\theta)}{2} \right] (\mathbf{e}_r\otimes\mathbf{e}_\theta+\mathbf{e}_\theta\otimes\mathbf{e}_r) \Bigg\}
\end{aligned} \tag{3.24}$$

where ν is Poisson's coefficient, Σ_e the macroscopic equivalent stress and J_3 the third invariant of the macroscopic stress deviator.

Similar to the residual stress field for the pure hydrostatic loading (3.21), the new deviatoric residual stress field consists of two parts:

$$\bar{\boldsymbol{\rho}}^{(2)} = \bar{\boldsymbol{\rho}}^{(2a)} + \bar{\boldsymbol{\rho}}^{(2b)}\,, \tag{3.25}$$

where $\bar{\boldsymbol{\rho}}^{(2a)}$ is the extreme value of the elastic stress field in the fictitious elastic body, taking the following form in spherical coordinates:

$$\begin{aligned}
\bar{\boldsymbol{\rho}}^{(2a)} = \frac{sign(J_{3+})\Sigma_{e+}}{3(1-f)} \Bigg\{ & \left[\frac{a^3\left(18a^2+5r^2(-5+\nu)\right)(1+3\cos(2\theta))}{2r^5(-7+5\nu)} - \frac{1+3\cos(2\theta)}{2} \right] (\mathbf{e}_r\otimes\mathbf{e}_r) \\
& + \left[\frac{a^3\left(27a^2+5r^2(1-2\nu)-3\left(21a^2+5r^2(-1+2\nu)\right)\cos^2(\theta)\right)}{2r^5(-7+5\nu)} + \frac{-1+3\cos(2\theta)}{2} \right] (\mathbf{e}_\theta\otimes\mathbf{e}_\theta) \\
& + \left[\frac{a^3\left(9a^2+25r^2(-1+2\nu)-45\left(a^2+r^2(-1+2\nu)\right)\cos^2(\theta)\right)}{2r^5(-7+5\nu)} + 1 \right] \left(\mathbf{e}_\phi\otimes\mathbf{e}_\phi\right) \\
& + \left[\frac{3a^3\left(12a^2-5r^2(1+\nu)\right)\sin(2\theta)}{2r^5(-7+5\nu)} + \frac{3\sin(2\theta)}{2} \right] (\mathbf{e}_r\otimes\mathbf{e}_\theta+\mathbf{e}_\theta\otimes\mathbf{e}_r) \Bigg\}
\end{aligned} \tag{3.26}$$

and the second part $\bar{\boldsymbol{\rho}}^{(2b)}$ is in spherical coordinates:

$$\bar{\boldsymbol{\rho}}^{(2b)} = \rho_{rr}^{2b}\mathbf{e}_r\otimes\mathbf{e}_r + \rho_{\theta\theta}^{2b}\mathbf{e}_\theta\otimes\mathbf{e}_\theta + \rho_{\phi\phi}^{2b}\mathbf{e}_\phi\otimes\mathbf{e}_\phi + \rho_{r\theta}^{2b}\left(\mathbf{e}_r\otimes\mathbf{e}_\theta + \mathbf{e}_\theta\otimes\mathbf{e}_r\right) \tag{3.27}$$

ρ_{rr}^{2b}, $\rho_{\theta\theta}^{2b}$, $\rho_{\phi\phi}^{2b}$ and $\rho_{r\theta}^{2b}$ being the functions of r and θ. We suppose the deviatoric parts $\boldsymbol{s}^{E(2)}$, $\boldsymbol{s}^{(2b)}$ of $\boldsymbol{\sigma}^{E(2)}$, $\bar{\boldsymbol{\rho}}^{(2b)}$ have the following relation:

$$\boldsymbol{s}^{(2b)} = A_1\,K(r)\,\boldsymbol{s}^{E(2)} \quad and \quad \sigma_m(\bar{\boldsymbol{\rho}}^{(2b)}) = A_1\,K(r)\,\sigma_m(\boldsymbol{\sigma}^{E(2)}) \tag{3.28}$$

where $K(r)$ is a function of r and A_1 the constant to be determined, noticing that the existence of $\bar{\boldsymbol{\rho}}^{(2b)}$ and $K(r)$ was provided in (Zhang et al., 2017a).

Consequently, in the matrix Ω_M, the resultant two parameters-based trial stress field in the matrix can be written as:

$$\boldsymbol{\sigma} = \boldsymbol{\sigma}^{(1)} + \boldsymbol{\sigma}^{(2)}\,, \tag{3.29}$$

Note that a vanishing stress field is considered in the void ω.

In spherical coordinates, the complete stress field (3.29) reads for $a \le r \le c$:

$$\begin{aligned}
\boldsymbol{\sigma} = &\left[\left(\frac{a^3\left(18a^2+5r^2\left(-5+\nu\right)\right)\left(1+3\cos(2\theta)\right)}{2\,r^5\left(-7+5\nu\right)} - \frac{1+3\cos(2\theta)}{2}\right)\frac{sign(J_{3+})\Sigma_{e+} - sign(J_3)\Sigma_e}{3(1-f)}\right.\\
&\left.+\rho_{rr}^{2b} + \left(1-\left(\frac{a}{r}\right)^{3\gamma}\right)A_0 - \frac{\Sigma_{m+}-\Sigma_m}{1-f}\left(1-\left(\frac{a}{r}\right)^3\right)\right]\left(\mathbf{e}_r\otimes\mathbf{e}_r\right)\\
&+\left[\frac{a^3\left(27a^2+5r^2\left(1-2\nu\right)-3\left(21a^2+5r^2\left(-1+2\nu\right)\right)\cos^2(\theta)\right)}{2\,r^5\left(-7+5\nu\right)}\frac{sign(J_{3+})\Sigma_{e+} - sign(J_3)\Sigma_e}{3(1-f)}\right.\\
&\frac{\left(3\cos(2\theta)-1\right)}{2}\frac{sign(J_{3+})\Sigma_{e+} - sign(J_3)\Sigma_e}{3(1-f)} + \rho_{\theta\theta}^{2b} + \left(1-\left(\frac{a}{r}\right)^{3\gamma} + \frac{3}{2}\gamma\left(\frac{a}{r}\right)^{3\gamma}\right)A_0\\
&\left.-\frac{\Sigma_{m+}-\Sigma_m}{1-f}\left(1+\frac{1}{2}\left(\frac{a}{r}\right)^3\right)\right]\left(\mathbf{e}_\theta\otimes\mathbf{e}_\theta\right)\\
&+\left[\left(\frac{a^3\left(9a^2+25r^2\left(-1+2\nu\right)-45\left(a^2+r^2\left(-1+2\nu\right)\right)\cos^2(\theta)\right)}{2\,r^5\left(-7+5\nu\right)}+1\right)\frac{sign(J_{3+})\Sigma_{e+} - sign(J_3)\Sigma_e}{3(1-f)}\right.\\
&\left.+\rho_{\phi\phi}^{2b} + \left(1-\left(\frac{a}{r}\right)^{3\gamma} + \frac{3}{2}\gamma\left(\frac{a}{r}\right)^{3\gamma}\right)A_0 - \frac{\Sigma_{m+}-\Sigma_m}{1-f}\left(1+\frac{1}{2}\left(\frac{a}{r}\right)^3\right)\right]\left(\mathbf{e}_\phi\otimes\mathbf{e}_\phi\right)\\
&+\left[\left(\frac{3\sin(2\theta)}{2} + \frac{3a^3\left(12a^2-5r^2\left(1+\nu\right)\right)\sin(2\theta)}{2\,r^5\left(-7+5\nu\right)}\right)\frac{sign(J_{3+})\Sigma_{e+} - sign(J_3)\Sigma_e}{3(1-f)} + \rho_{r\theta}^{2b}\right]\left(\mathbf{e}_r\otimes\mathbf{e}_\theta + \mathbf{e}_\theta\otimes\mathbf{e}_r\right)
\end{aligned} \tag{3.30}$$

For a variable hydrostatic loading combined with a constant shear loading, we consider the load do-

main defined by two elementary loads $\mathbf{\Sigma}_+$ and $\mathbf{\Sigma}_-$, and the axisymmetric macroscopic stress tensor, resulting from (3.30), takes the form:

$$\mathbf{\Sigma}_\pm = \Sigma_{m\pm}\mathbf{1} - sign(J_{3\pm})\frac{\Sigma_{e\pm}}{3}\left(\mathbf{e}_r\otimes\mathbf{e}_r + \mathbf{e}_\theta\otimes\mathbf{e}_\theta - 2\mathbf{e}_\phi\otimes\mathbf{e}_\phi\right) \tag{3.31}$$

From (3.28) and (3.30), it is readily seen that the mean stress and the equivalent stress read for $a \le r \le c$:

$$\begin{aligned}\sigma_m = {} & \gamma A_0\left(\frac{a}{r}\right)^{3\gamma} + A_0\left(1-\left(\frac{a}{r}\right)^{3\gamma}\right) - \frac{\Sigma_{m+}-\Sigma_m}{1-f} \\ & - \frac{5a^3(\nu+1)\left(3cos^2\theta-1\right)}{r^3(-7+5\nu)}\left(\frac{sign(J_{3+})\Sigma_{e+}-sign(J_3)\Sigma_e}{3(1-f)} + K(r)\,A_1\right)\end{aligned} \tag{3.32}$$

$$\begin{aligned}\sigma_e^2 = {} & \left(\frac{3\gamma A_0}{2}\left(\frac{a}{r}\right)^{3\gamma} - \frac{3}{2}\frac{\Sigma_{m+}-\Sigma_m}{1-f}\left(\frac{a}{r}\right)^3\right)^2 + \left(\frac{sign(J_{3+})\Sigma_{e+}-sign(J_3)\Sigma_e}{(1-f)} + 3K(r)\,A_1\right)^2 P_2(r,\theta) \\ & + \left(3\gamma A_0\left(\frac{a}{r}\right)^{3\gamma} - 3\frac{\Sigma_{m+}-\Sigma_m}{1-f}\left(\frac{a}{r}\right)^3\right)P_1(r,\theta)\left(\frac{sign(J_{3+})\Sigma_{e+}-sign(J_3)\Sigma_e}{(1-f)} + 3K(r)\,A_1\right)\end{aligned} \tag{3.33}$$

where

$$P_1(r,\theta) = \frac{3(-5\nu+10\nu(\frac{a}{r})^3+18(\frac{a}{r})^5-20(\frac{a}{r})^3+7)}{7-5\nu}\frac{(3\cos^2(\theta)-1)}{2} \tag{3.34}$$

$$\begin{aligned}P_2(r,\theta) = \Bigg\{ & \Bigg[(\frac{1125}{2}\nu-\frac{1175}{2})(\frac{a}{r})^3+(-\frac{1175}{2}\nu-\frac{2205}{2})(\frac{a}{r})^5+(225\nu^2-1125\nu+\frac{3375}{4})(\frac{a}{r})^6 \\ & +(1125\nu-\frac{2475}{2})(\frac{a}{r})^8+\frac{1215}{4}(\frac{a}{r})^{10}\Bigg]\cos^4(\theta)+\Bigg[(-150\nu^2-165\nu+525)(\frac{a}{r})^3 \\ & +(675\nu-945)(\frac{a}{r})^5+(-225\nu^2+900\nu-\frac{1125}{2})(\frac{a}{r})^6+(-810\nu+675)(\frac{a}{r})^8 \\ & -\frac{135}{2}(\frac{a}{r})^{10}\Bigg]\cos^2(\theta)+\Bigg[(25\nu^2-70\nu+49)+(50\nu^2-\frac{115}{2}\nu-\frac{35}{2})(\frac{a}{r})^3+(-\frac{135}{2}\nu+\frac{189}{2})(\frac{a}{r})^5 \\ & +(100\nu^2-175\nu-\frac{475}{4})(\frac{a}{r})^6+(45\nu-\frac{615}{2})(\frac{a}{r})^8+\frac{351}{4}(\frac{a}{r})^{10}\Bigg]\Bigg\}\frac{9}{(5\nu-7)^2}\end{aligned} \tag{3.35}$$

3.2.2 Closed-form expression of the homogenized shakedown criterion

Considering the yield function (3.1), the shakedown condition reads:

$$\begin{aligned}&\left[\left(\frac{3\gamma A_0}{2}\left(\frac{a}{r}\right)^{3\gamma}-\frac{3}{2}\frac{\Sigma_{m+}-\Sigma_m}{1-f}\left(\frac{a}{r}\right)^3\right)^2+\left(\frac{sign(J_{3+})\Sigma_{e+}-sign(J_3)\Sigma_e}{3(1-f)}+K(r)\,A_2\right)^2 P_2(r,\theta)\right.\\&\left.+\left(3\gamma A_0\left(\frac{a}{r}\right)^{3\gamma}-3\frac{\Sigma_{m+}-\Sigma_m}{1-f}\left(\frac{a}{r}\right)^3\right)P_1(r,\theta)\left(\frac{sign(J_{3+})\Sigma_{e+}-sign(J_3)\Sigma_e}{3(1-f)}+K(r)\,A_2\right)\right]^{1/2}\\&+3\alpha\left[\gamma A_0\left(\frac{a}{r}\right)^{3\gamma}+A_0\left(1-\left(\frac{a}{r}\right)^{3\gamma}\right)-\frac{\Sigma_{m+}-\Sigma_m}{1-f}\right.\\&\left.-\frac{5a^3(\nu+1)\left(3cos^2\theta-1\right)}{r^3(-7+5\nu)}\left(\frac{sign(J_{3+})\Sigma_{e+}-sign(J_3)\Sigma_e}{3(1-f)}+K(r)\,A_1\right)\right]\le\sigma_0\end{aligned}\tag{3.36}$$

The collapse occurs by fatigue when the yield function vanishes simultaneously for the extreme values of loading:

$$\begin{aligned}&\left[\left(\frac{3\gamma A_0}{2}\left(\frac{a}{r}\right)^{3\gamma}\right)^2+(K(r)\,A_1)^2\,P_2(r,\theta)+3\gamma A_0\left(\frac{a}{r}\right)^{3\gamma}P_1(r,\theta)\,(K(r)\,A_1)\right]^{1/2}\\&+3\alpha\left[\gamma A_0\left(\frac{a}{r}\right)^{3\gamma}+A_0\left(1-\left(\frac{a}{r}\right)^{3\gamma}\right)-\frac{5a^3(\nu+1)\left(3cos^2\theta-1\right)}{r^3(-7+5\nu)}K(r)\,A_1\right]=\sigma_0\end{aligned}\tag{3.37}$$

$$\begin{aligned}&\left[\left(\frac{3\gamma A_0}{2}\left(\frac{a}{r}\right)^{3\gamma}-\frac{3}{2}\frac{\Delta\Sigma_m}{1-f}\left(\frac{a}{r}\right)^3\right)^2+\left(\frac{\Delta(sign(J_3)\Sigma_e)}{3(1-f)}+K(r)\,A_2\right)^2 P_2(r,\theta)\right.\\&\left.+\left(3\gamma A_0\left(\frac{a}{r}\right)^{3\gamma}-3\frac{\Delta\Sigma_m}{1-f}\left(\frac{a}{r}\right)^3\right)P_1(r,\theta)\left(\frac{\Delta(sign(J_3)\Sigma_e)}{3(1-f)}+K(r)\,A_2\right)\right]^{1/2}\\&+3\alpha\left[\gamma A_0\left(\frac{a}{r}\right)^{3\gamma}+A_0\left(1-\left(\frac{a}{r}\right)^{3\gamma}\right)-\frac{\Delta\Sigma_m}{1-f}\left(\frac{a}{r}\right)^3\right.\\&\left.-\frac{5a^3(\nu+1)\left(3cos^2\theta-1\right)}{r^3(-7+5\nu)}\left(\frac{\Delta sign(J_3)\Sigma_e}{3(1-f)}+K(r)\,A_1\right)\right]=\sigma_0\end{aligned}\tag{3.38}$$

Because $(a/r)^n$ decreases quickly when r increases, the previous condition is satisfied anywhere in the body if it is fulfilled at $r=a$, we obtain:

$$\begin{aligned}&\left[\frac{9}{4}\left(\gamma A_0\right)^2+(K(a)\,A_1)^2\,P_2(a,\theta)+3\,\gamma A_0\,P_1(a,\theta)\,(K(a)\,A_1)\right]^{1/2}\\&+3\alpha\left[\gamma A_0-\frac{5(\nu+1)\left(3cos^2\theta-1\right)}{(-7+5\nu)}K(a)\,A_1\right]=\sigma_0\end{aligned}\tag{3.39}$$

$$\begin{aligned}&\left[\frac{9}{4}\left(\gamma A_0-\frac{\Delta\Sigma_m}{1-f}\right)^2+\left(\frac{\Delta(sign(J_3)\Sigma_e)}{3(1-f)}+K(a)\,A_1\right)^2 P_2(a,\theta)\right.\\&\left.+3\left(\gamma A_0-\frac{\Delta\Sigma_m}{1-f}\right)P_1(a,\theta)\left(\frac{\Delta(sign(J_3)\Sigma_e)}{3(1-f)}+K(a)\,A_1\right)\right]^{1/2}\\&+3\alpha\left[\gamma A_0-\frac{\Delta\Sigma_m}{1-f}-\frac{5\,(\nu+1)\left(3cos^2\theta-1\right)}{(-7+5\nu)}\left(\frac{\Delta(sign(J_3)\Sigma_e)}{3(1-f)}+K(a)\,A_1\right)\right]=\sigma_0\end{aligned}\tag{3.40}$$

Due to the linear elastic response when shakedown occurs, one has:

$$\tau=\frac{\gamma A_0}{K(a)\,A_1}=\frac{\gamma A_0-\frac{\Delta\Sigma_m}{1-f}}{\frac{\Delta(sign(J_3)\Sigma_e)}{3(1-f)}+K(a)\,A_1}=\frac{-\frac{\Delta\Sigma_m}{1-f}}{\frac{\Delta(sign(J_3)\Sigma_e)}{3(1-f)}}\tag{3.41}$$

Replacing γA_0 and $\gamma A_0-\frac{\Delta\Sigma_m}{1-f}$, (3.39) and (3.40) can be written as:

$$\begin{aligned}&\left[\frac{9}{4}\tau^2+3\tau P_1(a,\theta)+P_2(a,\theta)-9\alpha^2\left(\tau-\frac{5\,(\nu+1)\left(3cos^2\theta-1\right)}{(-7+5\nu)}\right)^2\right](K(a)A_1)^2\\&+6\alpha\sigma_0\left[\tau-\frac{5\,(\nu+1)\left(3cos^2\theta-1\right)}{(-7+5\nu)}\right]K(a)A_1-\sigma_0^2=0\end{aligned}\tag{3.42}$$

$$\begin{aligned}&\left[\frac{9}{4}\tau^2+3\tau P_1(a,\theta)+P_2(a,\theta)-9\alpha^2\left(\tau-\frac{5\,(\nu+1)\left(3cos^2\theta-1\right)}{(-7+5\nu)}\right)^2\right]\left(\frac{\Delta(sign(J_3)\Sigma_e)}{3(1-f)}+K(a)\,A_1\right)^2\\&+6\alpha\sigma_0\left[\tau-\frac{5\,(\nu+1)\left(3cos^2\theta-1\right)}{(-7+5\nu)}\right]\left(\frac{\Delta(sign(J_3)\Sigma_e)}{3(1-f)}+K(a)\,A_1\right)-\sigma_0^2=0\end{aligned}\tag{3.43}$$

Solving (3.42) with respect to $K(a)A_1$, we obtain:

$$\frac{K(a)\,A_1}{\sigma_0}=\frac{-6\alpha\sigma_0\left(\tau-\frac{5(\nu+1)\left(3cos^2\theta-1\right)}{(-7+5\nu)}\right)-2\sqrt{\frac{9}{4}\tau^2+3\tau P_1(a,\theta)+P_2(a,\theta)}}{2\left(\frac{9}{4}\tau^2+3\tau P_1(a,\theta)+P_2(a,\theta)-9\alpha^2\left(\tau-\frac{5(\nu+1)\left(3cos^2\theta-1\right)}{(-7+5\nu)}\right)^2\right)}\tag{3.44}$$

where the negative sign is chosen.

Likewise, solving (3.43) with respect to $K(a)A_1$, we obtain:

$$\frac{\Delta(sign(J_3)\Sigma_e)}{3(1-f)\sigma_0}+\frac{K(a)\,A_1}{\sigma_0}=\frac{-6\alpha\sigma_0\left(\tau-\frac{5(\nu+1)\left(3cos^2\theta-1\right)}{(-7+5\nu)}\right)+2\sqrt{\frac{9}{4}\tau^2+3\tau P_1(a,\theta)+P_2(a,\theta)}}{2\left(\frac{9}{4}\tau^2+3\tau P_1(a,\theta)+P_2(a,\theta)-9\alpha^2\left(\tau-\frac{5(\nu+1)\left(3cos^2\theta-1\right)}{(-7+5\nu)}\right)^2\right)}\tag{3.45}$$

where the positive sign is chosen.

Eliminating $K(a)A_1$ between the two latter equations (3.44) and (3.45), we obtain:

$$\frac{\Delta(sign(J_3)\Sigma_e)}{3(1-f)\sigma_0} = \frac{2\sqrt{\frac{9}{4}\tau^2+3\tau P_1(a,\theta)+P_2(a,\theta)}}{\frac{9}{4}\tau^2+3\tau P_1(a,\theta)+P_2(a,\theta)-9\alpha^2\left(\tau-\frac{5(\nu+1)(3cos^2\theta-1)}{(-7+5\nu)}\right)^2} \tag{3.46}$$

Combining (3.41), leads to the closed-form macroscopic fatigue criterion:

$$\begin{cases} \dfrac{\Delta\Sigma_m}{\sigma_0} = -\tau(1-f)\dfrac{2\sqrt{\frac{9}{4}\tau^2+3\tau P_1(a,\theta)+P_2(a,\theta)}}{\frac{9}{4}\tau^2+3\tau P_1(a,\theta)+P_2(a,\theta)-9\alpha^2\left(\tau-\frac{5(\nu+1)(3cos^2\theta-1)}{(-7+5\nu)}\right)^2} \\ \dfrac{\Delta(sign(J_3)\Sigma_e)}{\sigma_0} = 3(1-f)\dfrac{2\sqrt{\frac{9}{4}\tau^2+3\tau P_1(a,\theta)+P_2(a,\theta)}}{\frac{9}{4}\tau^2+3\tau P_1(a,\theta)+P_2(a,\theta)-9\alpha^2\left(\tau-\frac{5(\nu+1)(3cos^2\theta-1)}{(-7+5\nu)}\right)^2} \end{cases} \tag{3.47}$$

In which two events may occur:

- When $J_{3+} > 0$, the condition is satisfied if it is fulfilled at the equator $\theta = \pi/2$ where the left part of the previous shakedown condition (3.39) and (3.40) takes its maximum value, where

$$P_1(a,\frac{\pi}{2}) = \frac{3(5\nu+5)}{2(5\nu-7)} \qquad P_2(a,\frac{\pi}{2}) = \frac{225(7\nu^2-13\nu+7)}{(5\nu-7)^2}$$

- When $J_{3+} < 0$, the condition is satisfied if it is fulfilled at the poles $\theta = 0$ and $\theta = \pi$ where the left part of the previous shakedown condition (3.39) and (3.40) takes its maximum value, where

$$P_1(a,0) = \frac{3(5\nu+5)}{-5\nu+7} \qquad P_2(a,0) = \frac{225(\nu^2+2\nu+1)}{(5\nu-7)^2}$$

The above macroscopic criterion (3.47) is established to predict the fatigue limit for hollow sphere with Drucker-Prager matrix in a parametric form which depends on the generalized macroscopic stress triaxiality $\tau = -\frac{3\Delta\Sigma_m}{\Delta sign(J_3)\Sigma_e}$. More precisely, the fatigue limit stress curve can be obtained from this macroscopic criterion for different fixed values of τ.

The set of equations (3.47) constitutes the main finding in this study.

3.2.3 Some particular cases

In (3.47), $\frac{\Delta\Sigma_m}{\sigma_0}$ and $\frac{\Delta sign(J_3)\Sigma_e}{\sigma_0}$ appear as a pair of generalized macro-stress which are conjugate to generalized macroscopic stress triaxiality τ. Considering the special values $|\tau| = \infty$, $\tau = 0$ and $\alpha = 0$, the obtained criterion can be examined with explicit, simple results:

- $|\tau| = \infty$: The macroscopic criterion (3.47) is reduced to:

$$\begin{cases} \dfrac{\Delta\Sigma_m}{\sigma_0} = \dfrac{3\left(1-f\right)}{\left(3/2+3\alpha\right)\left(3/2-3\alpha\right)} \\ \dfrac{\Delta(sign(J_3)\Sigma_e)}{\sigma_0} = 0 \end{cases} \tag{3.48}$$

which gives the yield points corresponding to the macroscopic fatigue limit under pure hydrostatic cyclic loadings and is as same as the one given in Section 3.1.

- $\tau = 0$: The macroscopic criterion (3.47) is reduced to:

$$\begin{cases} \dfrac{\Delta\Sigma_m}{\sigma_0} = 0 \\ \dfrac{\Delta(sign(J_3)\Sigma_e)}{\sigma_0} = 3(1-f)\dfrac{2\sqrt{P_2(a,\theta)}}{P_2(a,\theta) - 9\alpha^2\left(\frac{5(\nu+1)\left(3cos^2\theta-1\right)}{(-7+5\nu)}\right)^2} \end{cases} \tag{3.49}$$

which gives the yield points: $\frac{\Delta\Sigma_m}{\sigma_0} = 0$, $\frac{\Delta(sign(J_3)\Sigma_e)}{\sigma_0} = \frac{6(1-f)\sqrt{P_2(a,\pi/2)}}{P_2(a,\pi/2)-9\alpha^2\left(\frac{10(\nu+1)}{(-7+5\nu)}\right)^2}$ corresponding to the macroscopic fatigue limit under pure shear cyclic loadings.

- $\alpha = 0$: In this case, we consider the porous material with an incompressible matrix, and the pressure-sensitive parameter friction angle ϕ vanishes. The macroscopic criterion (3.47) is reduced to:

$$\begin{cases} \dfrac{\Delta\Sigma_m}{\sigma_0} = -\tau(1-f)\dfrac{2\sqrt{\frac{9}{4}\tau^2+3\tau P_1(a,\theta)+P_2(a,\theta)}}{\frac{9}{4}\tau^2+3\tau P_1(a,\theta)+P_2(a,\theta)} \\ \dfrac{\Delta sign(J_3)\Sigma_e}{\sigma_0} = 3(1-f)\dfrac{2\sqrt{\frac{9}{4}\tau^2+3\tau P_1(a,\theta)+P_2(a,\theta)}}{\frac{9}{4}\tau^2+3\tau P_1(a,\theta)+P_2(a,\theta)} \end{cases} \tag{3.50}$$

which can be written in the following form:

$$\left(\frac{3}{4}\frac{\Delta\Sigma_m}{1-f}\right)^2 - \frac{3}{2}\frac{\Delta\Sigma_m}{1-f}\frac{\Delta(sign(J_3)\,\Sigma_e)}{2\left(1-f\right)}P_1(a,\frac{\pi}{2}) + P_2(a,\frac{\pi}{2})\left(\frac{\Delta(sign(J_3)\,\Sigma_e)}{2\left(1-f\right)}\right)^2 = \sigma_0^2 \tag{3.51}$$

where

  - When $J_{3+} > 0$, the condition is satisfied if it is fulfilled at the equator $\theta = \pi/2$ where the left part of the previous condition (3.51) takes its maximum value, where

$$P_1(a,\frac{\pi}{2}) = \frac{5\nu+5}{2(5\nu-7)} \qquad P_2(a,\frac{\pi}{2}) = \frac{25(7\nu^2-13\nu+7)}{(5\nu-7)^2}$$

– When $J_{3+} < 0$, the condition is satisfied if it is fulfilled at the poles $\theta = 0$ and $\theta = \pi$ where the left part of the previous condition (3.51) takes its maximum value, where

$$P_1(a,0) = \frac{5\nu+5}{-5\nu+7} \qquad P_2(a,0) = \frac{25(\nu^2+2\nu+1)}{(5\nu-7)^2}$$

which is the same result obtained in the recent research (Zhang et al., 2017a) of the fatigue limit of porous materials with von Mises matrix.

3.3 Illustration and assessment of the effective shakedown criterion

The goal of this section is to illustrate the shakedown yield and to validate the accuracy of the analytical results by comparison with numerical ones. To this end, incremental elastic-plastic finite element simulations are carried out by the use of the software Abaqus Standard (Hibbett et al., 1998).

3.3.1 Numerical model

The common solution strategy used to numerical study of nonlinear structures under variable thermo-mechanical loads is the path-following incremental analysis, which reconstructs in a step-by-step manner the structural response to the applied path loading. This numerical procedure is employed out in this work.

Thanks to the geometrical symmetry of the hollow sphere, numerical computations are conducted by considering a quarter of an axisymmetric model with a spherical void as shown on Fig.2.4. The geometry is discretized by 20000 for-nodes axisymmetric elements. This mesh grid is found to be sufficient accurate to obtain reliable numerical results. Moreover, the desired macroscopic stress triaxiality $T = \Sigma_m/\Sigma_e$ is kept constant during simulations through the application of the homogenous boundary strain rate $\boldsymbol{v} = \boldsymbol{D}\cdot\boldsymbol{x}$ on the outer boundary $\partial\Omega$ and by the use of the subroutine MPC (Multi-Points Constraints) implemented in Abaqus software. This numerical procedure is already described in (Guo et al., 2008) and successfully used in many works Guo et al. (2008); Cheng et al. (2015a); Zhang et al. (2017b,a). The computations are performed for different porosities $f \in \{0.001, 0.01, 0.1\}$, different friction angles $\phi \in \{10°, 20°, 30°\}$ and with $\sigma_0 = 20$ MPa, $E = 14$ GPa and $\nu = 0.2$. Moreover, the following loading cases are considered for instance: alternating load $R = -1$, pulsating one $R = 0$ and intermediate cyclic loads with $R = 1/5$ and $R = -1/5$.

Unlike, previous works in the literature which are concerned only by the former cycles during the transient phase, here 100 cycles of cyclic loadings are performed for each chosen stress triaxiality T. The

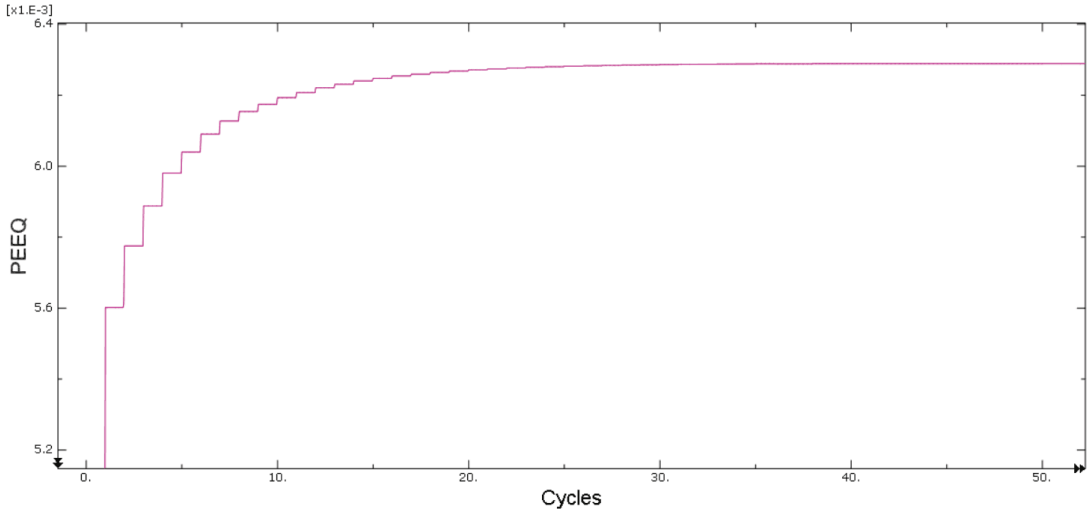

Figure 3.1: Accumulated Equivalent Plastic Strain (PEEQ) under pulsating load when shakedown occurs for $f = 0.01$, $\phi = 20°$ and $T = 1.3333$

state of the long-term behavior is checked by increasing of the amplitude of the imposed deformation on the external boundary until the collapse by fatigue or a mechanism is observed. In practice, the evolution of the equivalent plastic deformation, and the evolution of the components of the plastic strain tensor in the whole structure provide information on the status of the structure as shown in Fig.3.1 and Fig.3.2.

3.3.2 Results and discussion

Figures 3.3 to *Figure* 3.5 plotted the macroscopic shakedown domain computed from the established macroscopic fatigue criterion (3.47) under alternating loading ($R = -1$) for several void volume fractions ($f \in \{0.001, 0.01, 0.1\}$) and friction angles ($\phi \in \{10°, 20°, 30°\}$). It is worth noting that the collapse by development of a mechanism do not occur in this situation, so the safety domain is only defined by the fatigue criterion. The effective shakedown criterion is found much smaller and completely inside the yield loci obtained under monotonic loads. Many interesting conclusions can be drawn. Firstly, an excellent agreement between the analytic solutions and numerical results is observed. Small differences are observed for larger porosity $f = 0.1$ (*Figure* 3.5) around the pure deviatoric limit state. This can be explained by the applied pure deviatoric elastic stress field $\boldsymbol{\sigma}^{E(2)}$ (3.24). Obviously, it can be improved by considering an exact elastic solution for pure deviatoric load. Besides, the numerical points are strictly inside the analytical ones, and the built criterion can be considered as a quasi-lower bound for the fatigue limit due to the choice of the statical approach based on Melan's theorem. Interestingly, in the particular case of pure hydrostatic loading, the numerical results fit the exact value $\Delta\Sigma_m^{SD} = \frac{3(1-f)}{(3/2+3\alpha)(3/2-3\alpha)}$. This

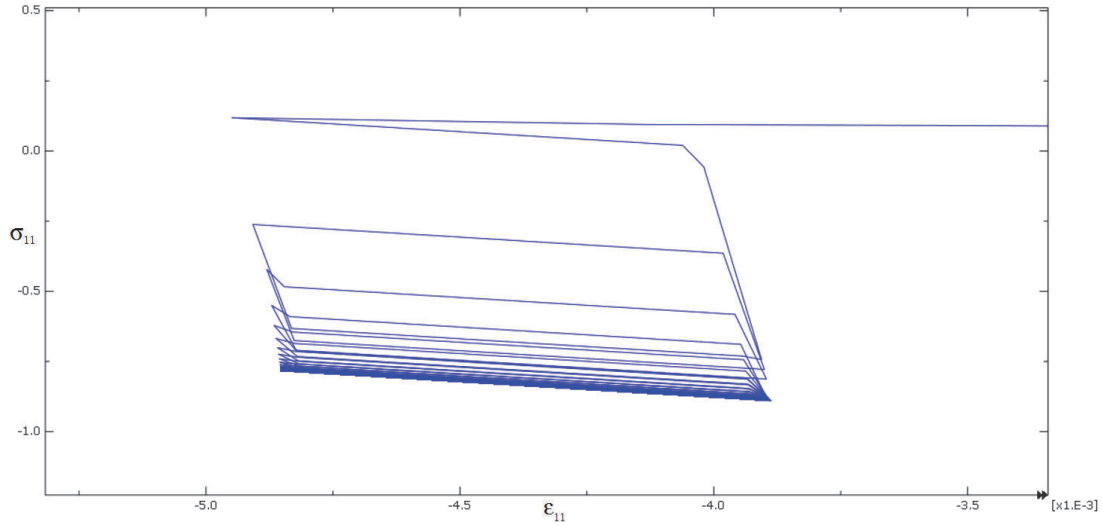

Figure 3.2: ε_{11} under pulsating load on the internal boundary at $\theta = \pi/2$ when shakedown occurs for $f = 0.01$, $\phi = 20°$ and $T = 1.3333$

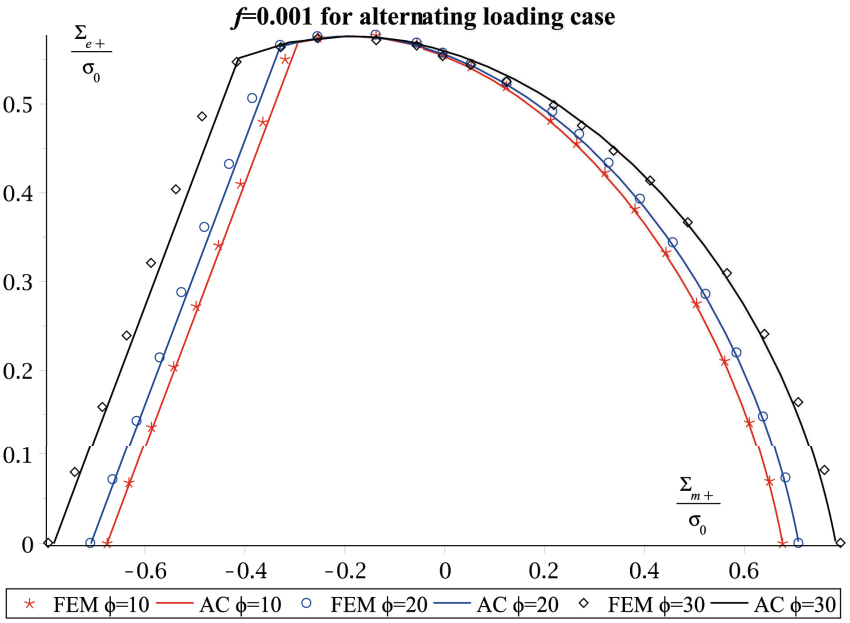

Figure 3.3: Comparison between the yield surfaces obtained by the analytic criterion (3.47) and by step-by-step finite element simulations under alternating loadings ($R = -1$) for porosity $f = 0.001$ and $\phi \in \{10°, 20°, 30°\}$.

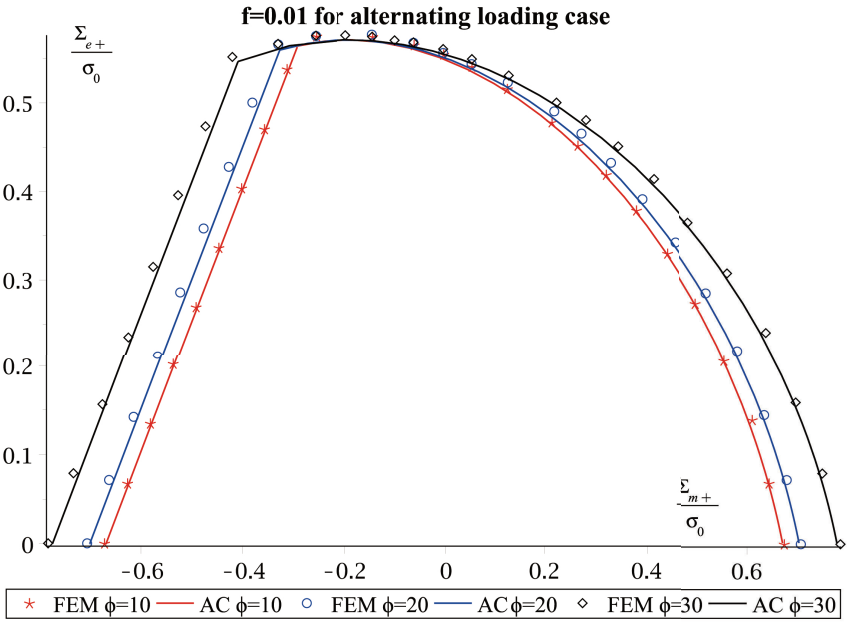

Figure 3.4: Comparison between the yield surfaces obtained by the analytic criterion (3.47) and by step-by-step finite element simulations under alternating loadings ($R = -1$) for porosity $f = 0.01$ and $\phi \in \{10°, 20°, 30°\}$.

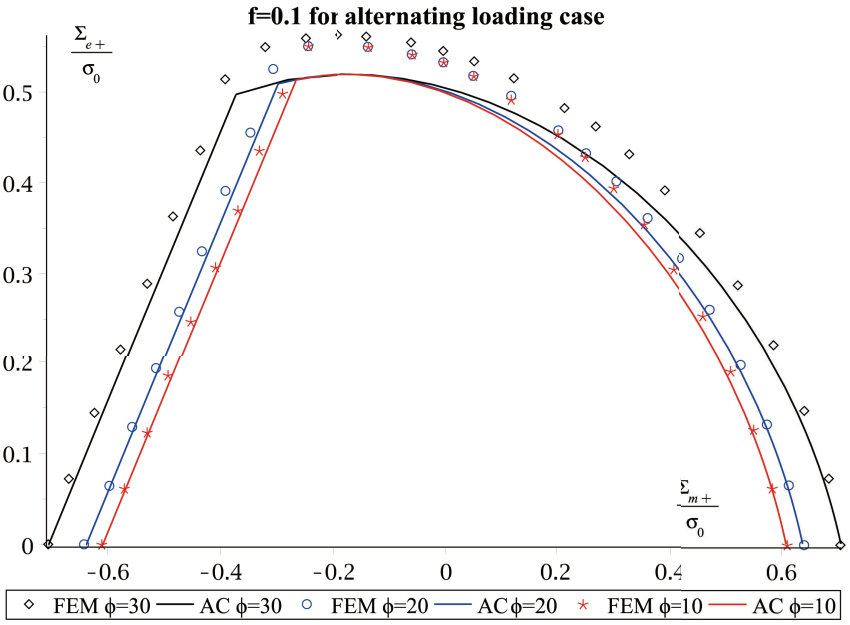

Figure 3.5: Comparison between the yield surfaces obtained by the analytic criterion (3.47) and by step-by-step finite element simulations under alternating loadings ($R = -1$) for porosity $f = 0.1$ and $\phi \in \{10°, 20°, 30°\}$.

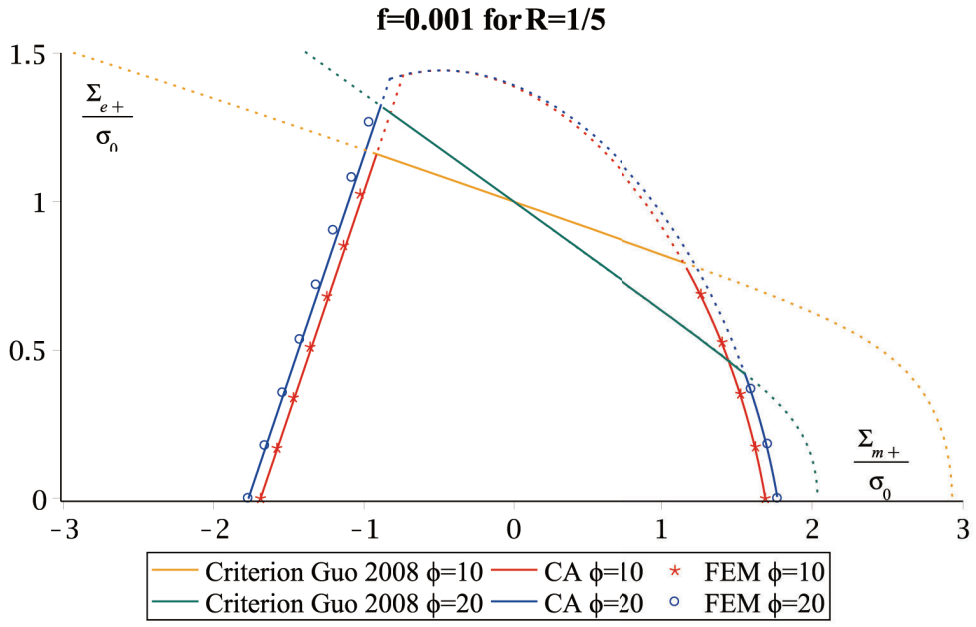

Figure 3.6: Interaction curve for the intermediate loads with $R = 1/5$ for porosity $f = 0.001$. The analytic safe domain is bounded by solid lines.

fact is foreseeable since the trial stress field and the residual stress tensor contain the exact solution for the hollow sphere under hydrostatic load.

As shown on these figures, the strength under cyclic loadings shrinks with decreasing ϕ. On the contrary, the friction angle does not have strong influence of the analytical fatigue limit around the value of $T = 0$ (pure shear).

Figures 3.6 to 3.8 display the comparison between analytical results and numerical ones of the shakedown limit for the intermediate load corresponding to $R = 1/5$. Also, the results corresponding to $R = -1/5$ are plotted in Figs.3.9 to 3.11.

Two major features must be underlined here. Unlike the alternating load (for which $R = -1$), the safety domain is obtained at the intersection of the domain defined by the new fatigue criterion and the one proposed in Guo et al. (Guo et al., 2008), corresponding to the collapse by development of a mechanism at the first cycle. In all figures shown hereafter, **the analytic safe domain is bounded by solid lines**. The second important remark is that the shakedown safe domain is considerably reduced compared to the gauge surface corresponding to the failure under monotonic loading. This ductility reduction is more pronounced in the dominant compression zone ($\Sigma_m < 0$). In addition, these curves confirm that the effect of the friction angle on the safe domain is negligible. The same conclusion can be deduced for the pulsating loading case (see Appendix 1).

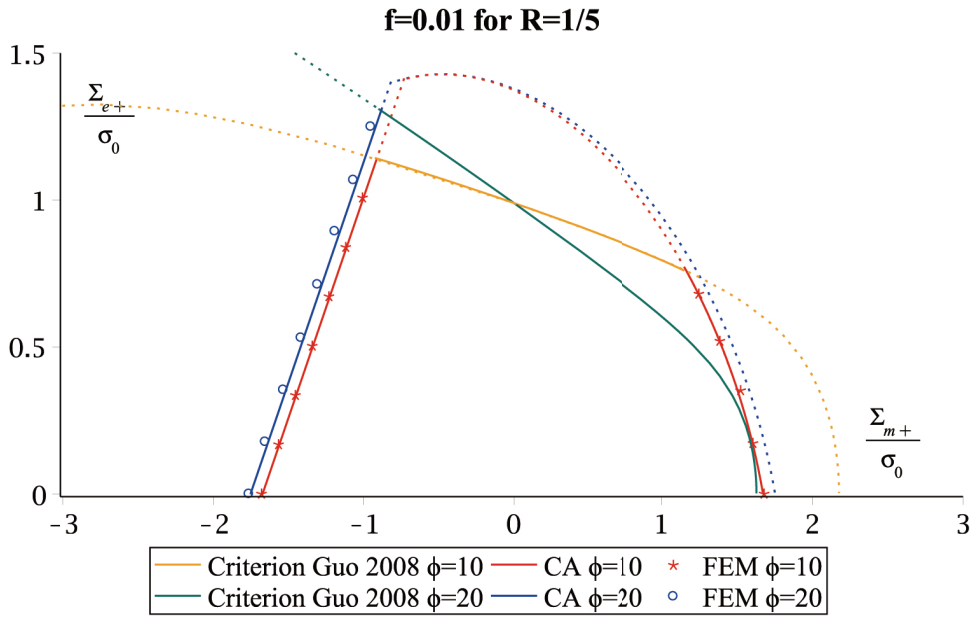

Figure 3.7: Interaction curve for the intermediate loads with $R = 1/5$ for porosity $f = 0.01$. The analytic safe domain is bounded by solid lines.

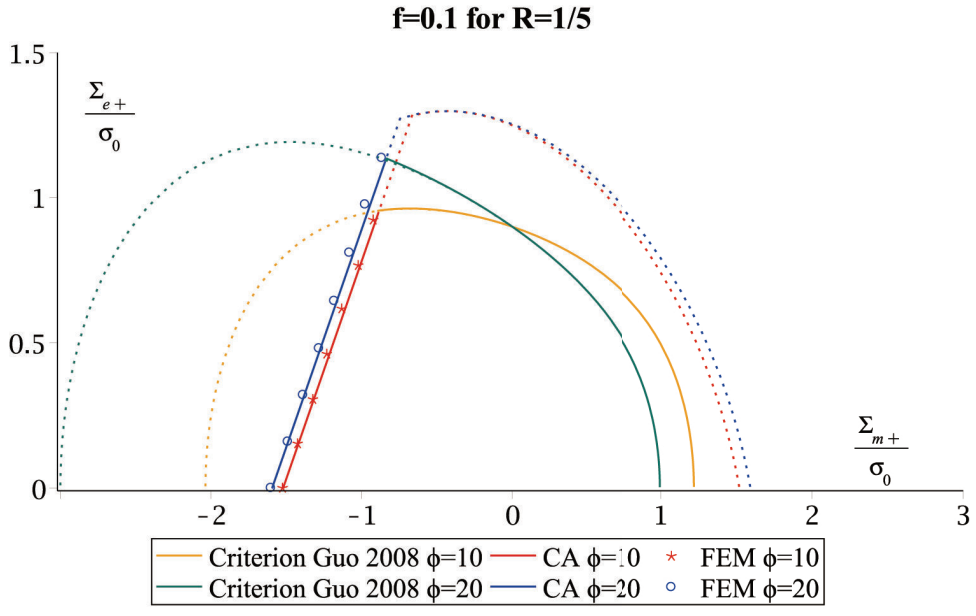

Figure 3.8: Interaction curve for the intermediate loads with $R = 1/5$ for porosity $f = 0.1$. The analytic safe domain is bounded by solid lines.

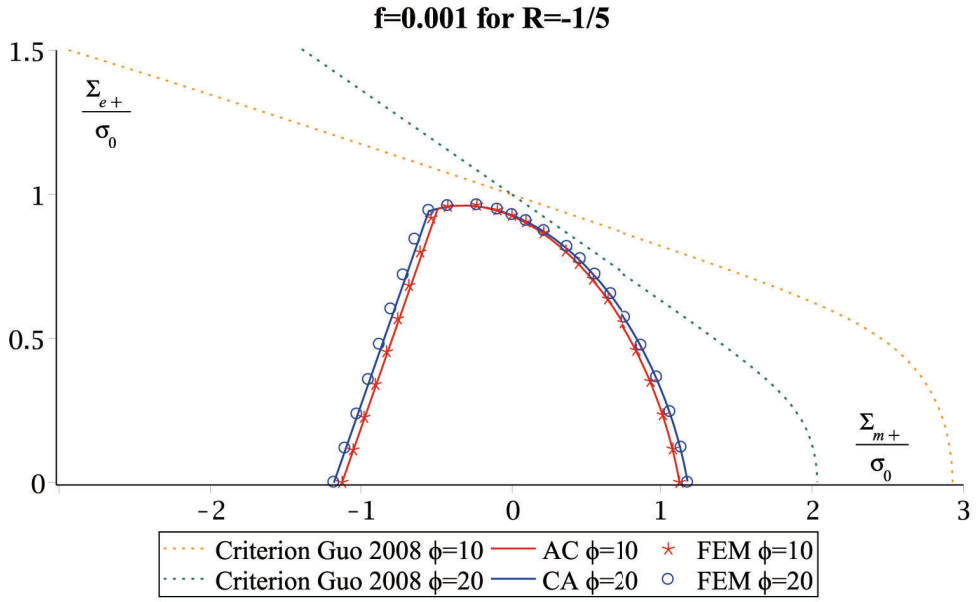

Figure 3.9: Interaction curve for the intermediate loads with $R = -1/5$ for porosity $f = 0.001$. The analytic safe domain is bounded by solid lines.

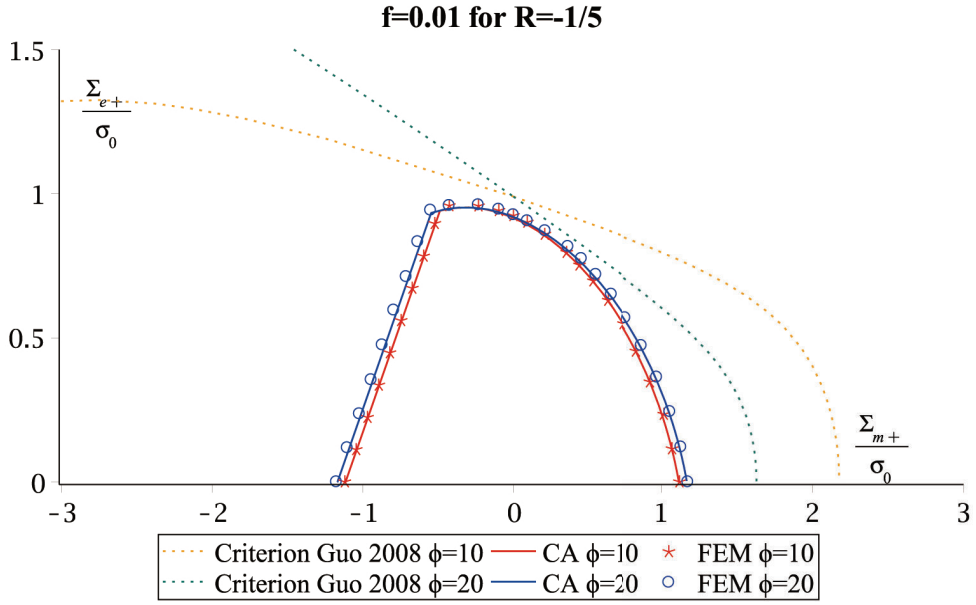

Figure 3.10: Interaction curve for the intermediate loads with $R = -1/5$ for porosity $f = 0.01$. The analytic safe domain is bounded by solid lines.

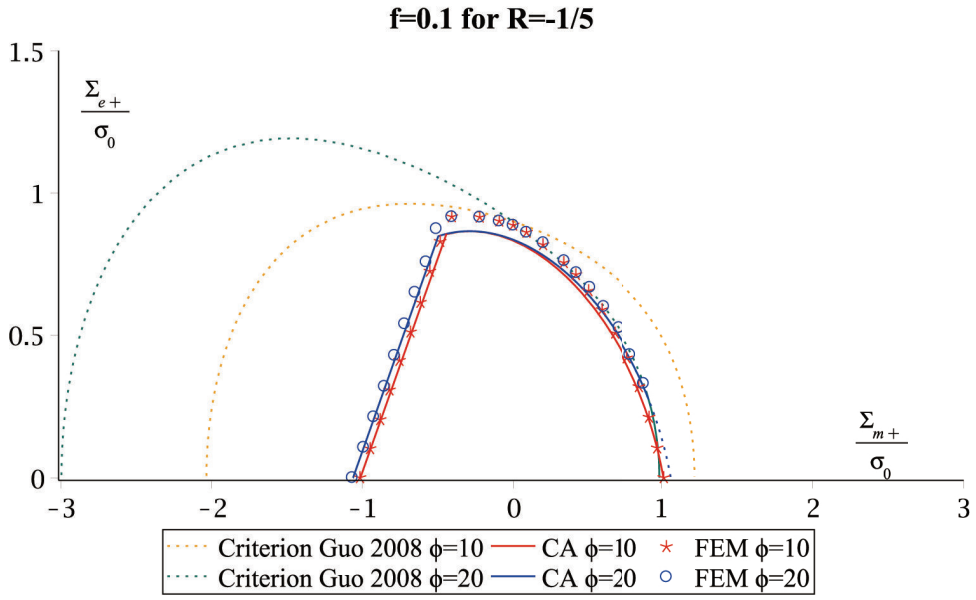

Figure 3.11: Interaction curve for the intermediate loads with $R = 1/5$ for porosity $f = 0.1$. The analytic safe domain is bounded by solid lines.

It is worthy noting, that for all loading cases with various material data, the macroscopic safe domain is convex. Further, it is legitimate to wonder whether there is a noticeable difference between the macroscopic shakedown domains for porous materials with Drucker-Prager model or von Mises criterion. To answer this question, Figs.3.12 depicts the analytic safe domains obtained under cyclic loads with Drucker-Prager and von Mises constitutive laws. The difference between the models is noticeable but not considerable as it could be expected because off the presence of the first invariant of the stress in the Drucker-Prager yield function. This remark should be taken with precaution because, as we have seen above, the real safe domain is a result of interaction between the homogenized shakedown domain and the limit analysis effective yield.

For completeness, the influence of Poisson's ratio on the macroscopic shakedown criterion is studied. Figure 3.13 depicted the analytical and numerical safe domain boundary for different values of Poisson's coefficient $\nu \in \{0.15, 0.25, 0.35, 0.4\}$ for the intermediate loading case $R = -1/5$ with $f = 0.01$ and friction angle $\phi \in \{10°, 20°\}$. It can be seen that the strength domain shrinks slightly with the increase of ν within the dominant compression zone ($\Sigma_m < 0$) while the homogenized criterion is insensitive to Poisson's ratio variations in the traction region ($\Sigma_m > 0$). These observations has been confirmed by considering other loading cases and different angle friction, but not reported in the present paper for seek of shortness.

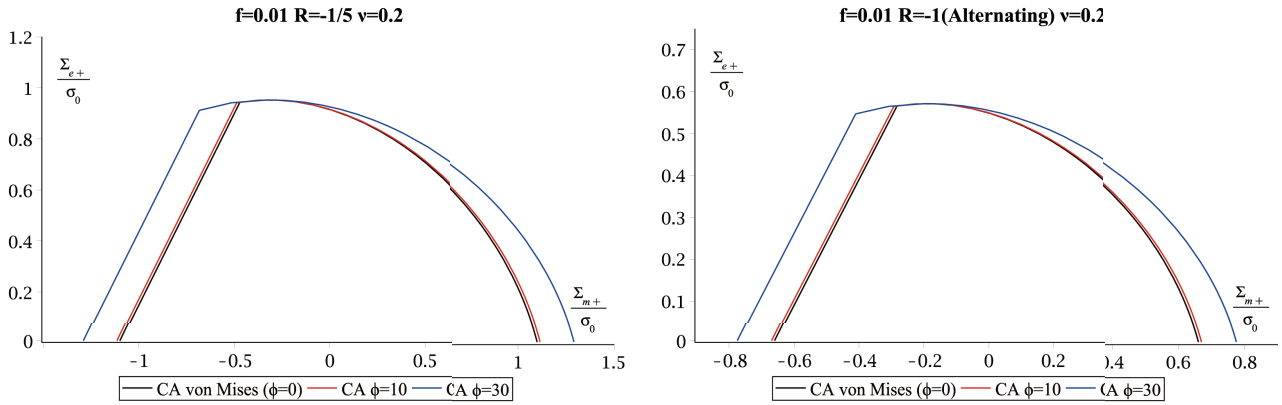

Figure 3.12: Comparison of the effective shakedown criterion with Drucker-Prager dilatant matrix with the one with von Mises model.

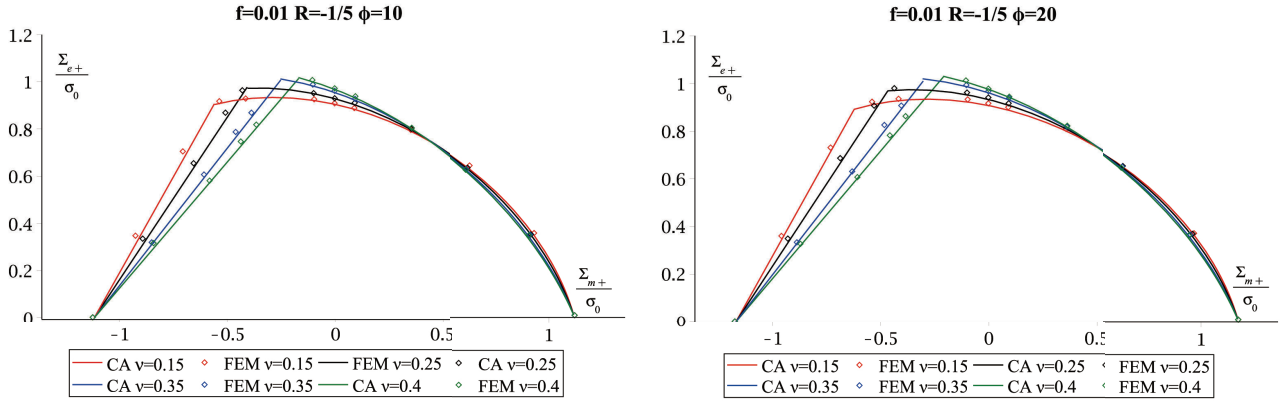

Figure 3.13: Effect of Poisson's coefficient on the macroscopic shakedown domain for the intermediate loading case $R = -1/5$.

3.4 Conclusion

In this chapter we derived a homogenized shakedown criterion for ductile porous material with pressure-sensitive dilatant matrix under cyclic repeated loadings, considering the hollow sphere unit cell. The closed-form fatigue criterion in parametric form, depending on the porosity, friction angle, Poisson's ratio and the sign of the third invariant of the macroscopic stress tensor, is able to predict the shakedown limit for all intermediate repetitive fluctuation of loads lying between the alternating and the pulsating loads ($-1 \leq R < 1$). The safety domain is bounded by this fatigue criterion and by the macroscopic yield strength proposed by Guo et al (Guo et al., 2008) corresponding to the collapse by development of a mechanism at the first cycle, inside of which the material is always stable. It is worthy to note that the obtained results allow us to retrieve, as a particular case, the fatigue criterion of porous material with a von Mises matrix (Zhang et al., 2017b). Further, the macroscopic shakedown loci predicted by our

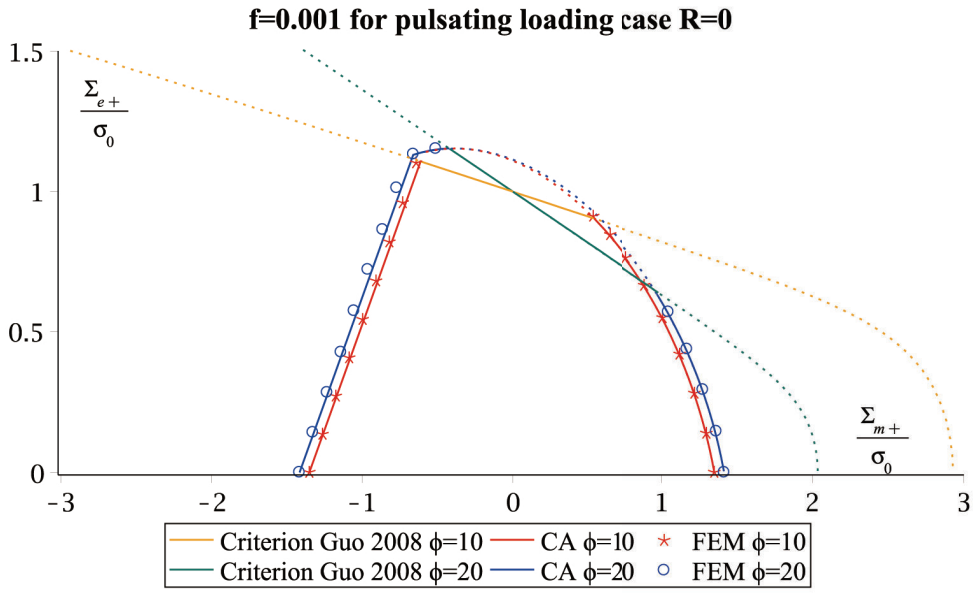

Figure 14: Interaction curve under pulsating loadings ($R = 0$) for porosity $f = 0.001$. The analytic safe domain by solid lines.

analysis is slightly effected by friction angle variations, however, the safe domain is considerably reduced compared to the one obtained by limit analysis for monotonic load conditions (Guo et al., 2008). This strength reduction is more pronounced in the dominant compression zone ($\Sigma_m < 0$). The established model have been assessed and validated against numerical solutions derived by micomrchanics-based finite element computations by considering a quarter of the hollow sphere subjected to homogeneous strain rate boundary conditions for various configurations of porosity and frictions angles.

It should be also remarked that small but noticeable differences for high porosity around the pure deviatoric limit are observed. Subsequently, in the outlook, attention will be focused on the refinement of the trial stress fields for pure deviatoric load in order to improve the model. The consideration of the kinematical hardening including the backstresses constitutes also a challenging subject for future developments. Finally, the use of the so-called Direct Methods for the computational of numerical shakedown rigorous bounds is in preparation for future papers.

Appendix 1: Comparison of the shakedown criterion (3.47) with numerical results for the pulsating loading case ($R = 0$)

Figures 14 to *Figure* 16 display the comparison between analytical results and numerical ones of the shakedown limit for porosities $f = 0.001$, $f = 0.01$ and $f = 0.1$ for pulsating loading case ($R = 0$).

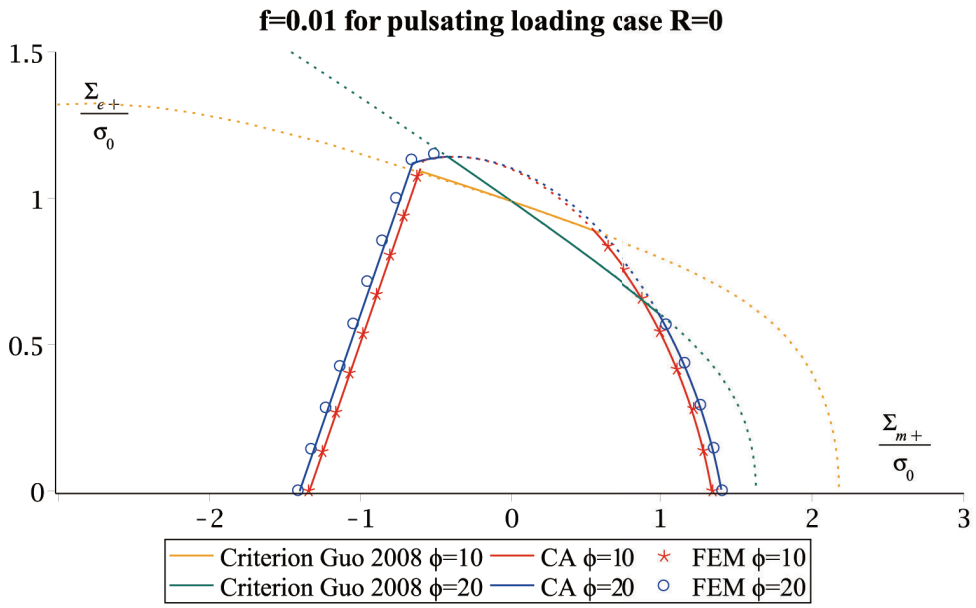

Figure 15: Interaction curve under pulsating loadings ($R = 0$) for porosity $f = 0.01$. The analytic safe domain is bounded by solid lines.

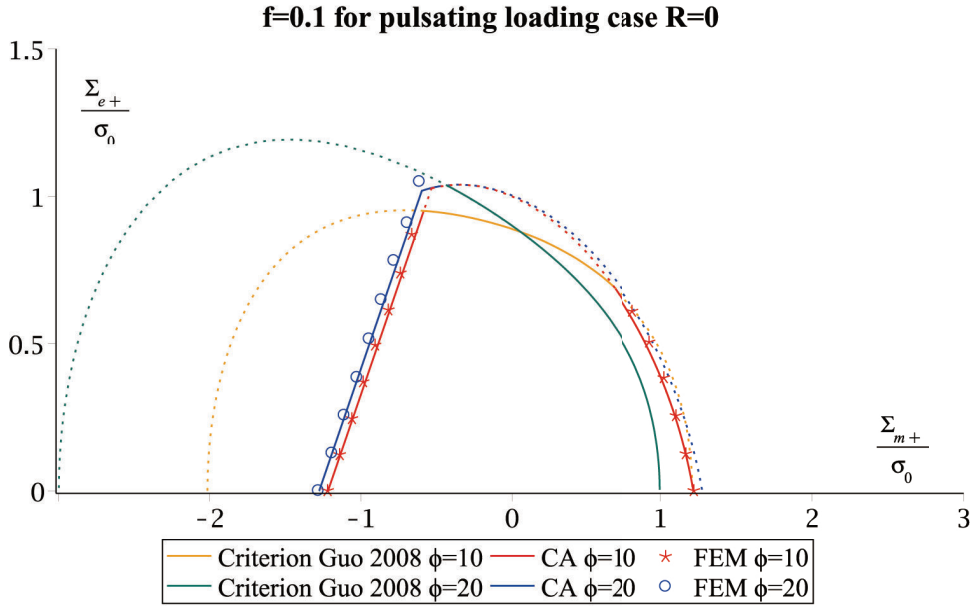

Figure 16: Interaction curve under pulsating loadings ($R = 0$) for porosity $f = 0.1$. The analytic safe domain is bounded by solid lines.

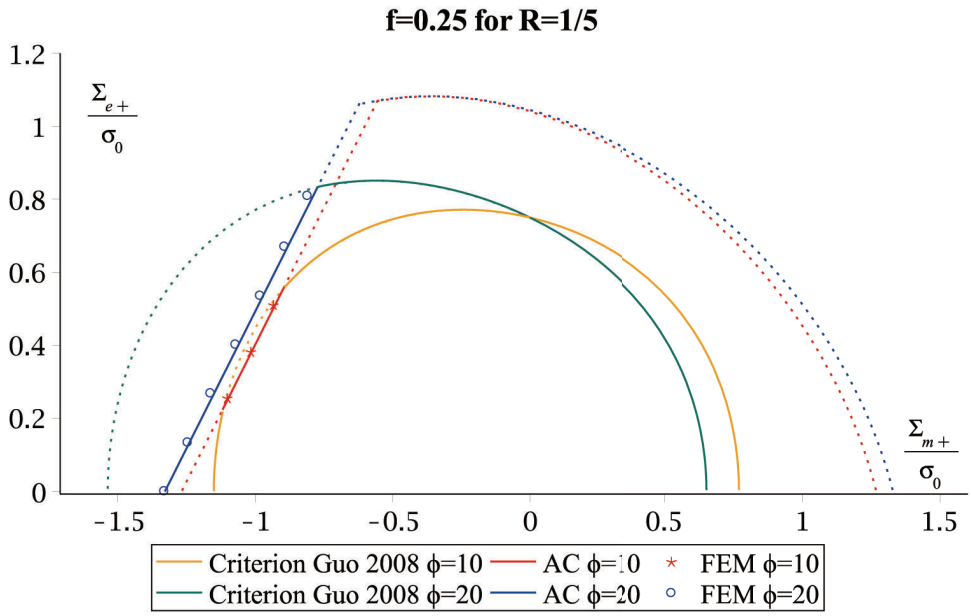

Figure 17: Interaction curve under the intermediate loadings with $R = -1.5$ for porosity $f = 0.25$. The analytic safe domain by solid lines.

Appendix 2: The macroscopic safe domain for the porosity $f = 0.25$

For completeness, in this appendix, we plot the safe domain of the porous material with high porosity $f = 0.25$ and for loads parameters $R = 0, 1.5, -1.5$. The safe domain is obtained by the interaction between the macroscopic shakedown criterion (3.47) and the surface obtained under monotonic loads (Guo et al., 2008).

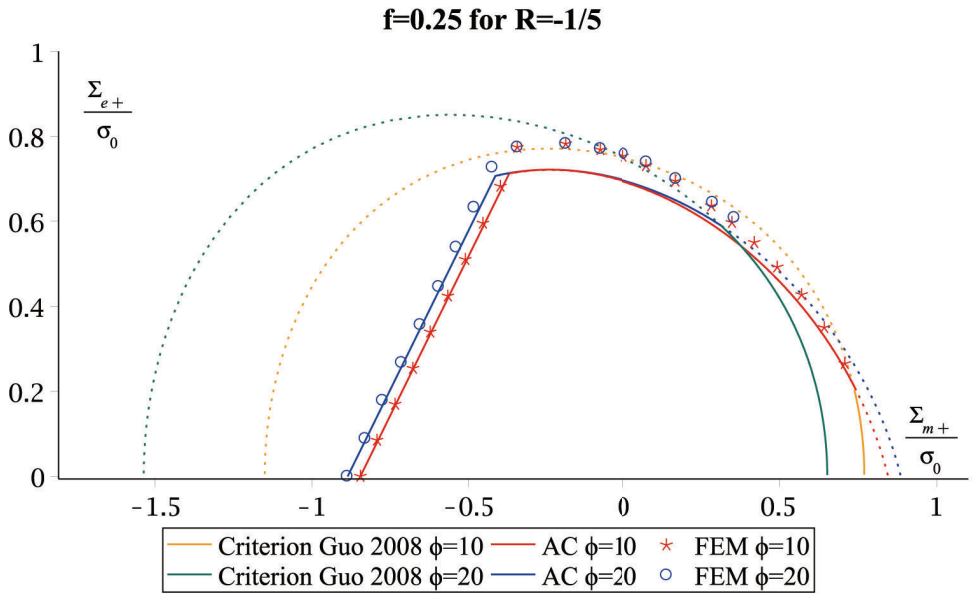

Figure 18: Interaction curve under pulsating loadings ($R = -1.5$) for porosity $f = 0.25$. The analytic safe domain by solid lines.

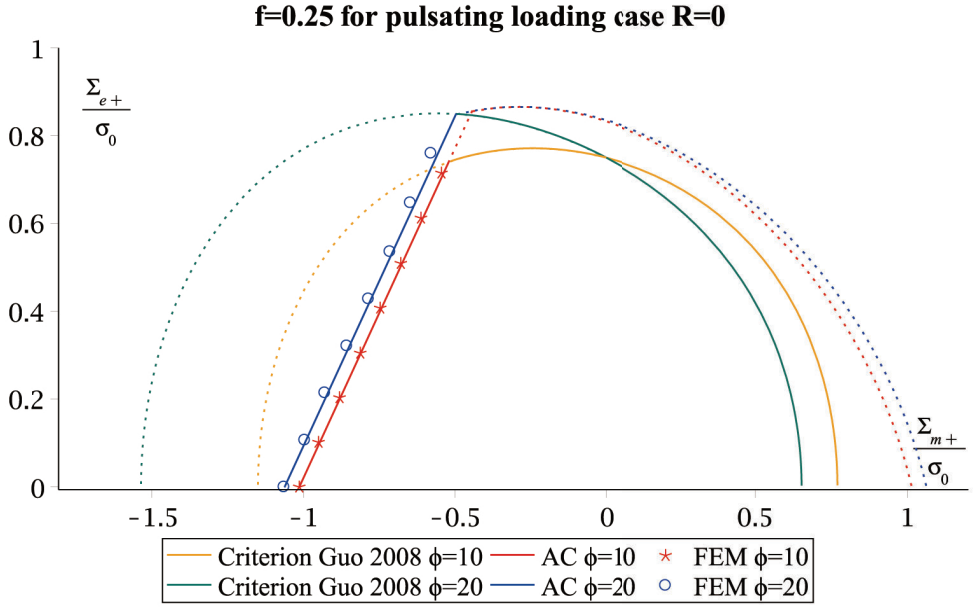

Figure 19: Interaction curve under pulsating loadings ($R = 0$) for porosity $f = 0.25$. The analytic safe domain by solid lines.

Chapter 4

Numerical shakedown analysis of porous materials under two macroscopic varying loadings by non-linear optimizaion

This chapter aims at providing a direct numerical method to predict the shakedown safety domain of porous materials under under two macroscopic independently varying loadings based on Melan's theorem. Considering the critical loading path of the load domain instead of the whole history, the statical shakedown condition yields an optimization problem, of which the objective function is the shakedown limit factor, with the discretization of a three dimensional model of von Mises matrix. We adopt the macroscopic hydrostatic and deviatoric loads to capture the effects of compressive/tensive and shear effects. By the application of a non-linear optimizer IPOPT using the interior-point method, the proposed optimization is solved efficiently to give not only the limit load factor, but also the corresponding residual stress tensor for the shakedown state. In order to access the reliability of the present method, two special loading cases (alternating-alternating and pulsating-pulsating) are especially and fully discussed. The obtained results are illustrated and compared to the incremental step-by-step FEM computations within the same load program.

4.1 Introduction

In this chapter, our attention is focus on establishing a direct numerical method to estimate the shakedown load by reforming the statical theorem as mathematical programming problem to find the mini-

mum value of an objective function. As in the research of shakedown behavior of pavements under two independently varying loads, Nguyen et al. (Nguyen et al., 2008) have proposed a numerical procedure to determine the limit factor by discretizing the a three dimensional model and solving an large size optimization problem, which is achieved by the interior-point method (Wächter and Biegler, 2006). In the same sprit, we adopt König's statement that shakedown occurs for a given load domain if and only if it occurs for its convex envelope (Konig and Kleiber, 1978), which allows us to consider only the vertices of the load domain in order to eliminate the time dependence of loadings. For the purpose of the general use in the future, we consider a three dimensional hollow sphere model as a reference volume of the porous material, so that the procedure can be implemented for other irregular models. Similar to the previous study of the shakedown behavior under one cyclic load, we apply a referential macroscopic hydrostatic and deviatoric stress to produce the elastic stress tensors realized by a 3D Abaqus MPC (multi-points constraints) user subroutine (Liu et al., 2016), which can simulate the general compressive/tensive and shear effects, respectively. Then the discretization of the the structure by a large number of finite elements and constraints leads the shakedown analysis to a large size optimization problem, which can be solved by the non-linear optimizer IPOPT (Schenk and Gärtner, 2004), based on the interior point algorithm.

The chapter is presented in the following way. In Section 4.2, we recall again Melan's statical theorem and the transformed expression, which is the starting point of the direct shakedown analysis. In Section 4.3, the shakedown problem is discretized on mathematical optimization programming and the non-linear algorithm is introduced. Section 4.4 is concerned with the application of the present numerical program to two special loading cases (alternating-alternating and pulsating-pulsating). Results are illustrated and compared with the existing solution and the step-by-step incremental FEM computations in order to access its reliability, despite it is a bit time consuming. Finally, concluding remarks and perspectives are finally summarized in the last section.

4.2 Basic definitions and formulations

As indicated in Figure 2.1, we consider an elastic perfectly plastic material occupying a hollow sphere model of inner radius $r = a$ and outer radius $r = b$ with the porosity $f = (a/b)^3$ for porous materials. This reference unit volume Ω is enclosed by the surface $\partial\Omega$ and composed of a void ω embedded in a matrix $\Omega_M = \Omega - \omega$. The boundary $\partial\omega$ of the void ω is assumed to be a free traction boundary.

For the elementary cell Ω having experienced elasto-plastic deformation, the stress field $\boldsymbol{\sigma}$ can be consider as the sum of two parts: an elastic part $\boldsymbol{\sigma}^E$, in a corresponding fictitious elastic body, which

satisfies Hooke's law, and a complementary part $\boldsymbol{\rho}$ called residual stress field:

$$\boldsymbol{\sigma} = \boldsymbol{\sigma}^E + \boldsymbol{\rho} \tag{4.1}$$

In the absence of the volume force $\boldsymbol{f}$, considering the equilibrium equations and boundary conditions, the residual stress tensor must satisfy the following conditions at any time:

$$\begin{cases} div\, \boldsymbol{\rho} = \mathbf{0} \quad in \Omega \\ \boldsymbol{\rho} \cdot \boldsymbol{n} = \mathbf{0} \quad on \partial\omega \end{cases} \tag{4.2}$$

where $\boldsymbol{n}$ is the unit outward normal vector of the matrix.

4.2.1 Load domain for shakedown analysis and Melan's theorem

We describe a varying load as in Subsection 2.2. Let us denote p_0 and q_0 as two reference loads, for instance, then the two independent variable loads can be described by $p(t) = \mu_1(t)p_0$ and $q(t) = \mu_2(t)q_0$. The rectangular reference load domain $\mathscr{P}_0$ is indicated in Figure 2.2(a), where $\bar{\mu}_n^-$ and $\bar{\mu}_n^+$ are constant lower and upper bounds. Then, because of the linearity of the elastic response in the fictitious body when shakedown occurs, the total stress field can be assumed as:

$$\boldsymbol{\sigma} = \alpha\boldsymbol{\sigma}^E + \boldsymbol{\rho} \tag{4.3}$$

where $\alpha > 1$ is the load factor. Hence, Melan's lower bound theorem of shakedown (Melan, 1936) can be expressed as follows:

If a time-independent residual stress field $\bar{\boldsymbol{\rho}}$, which satisfies the conditions (4.2), and a load factor α can be found, such that for all loads in the domain $\mathscr{P}$, the yield criterion holds everywhere in Ω at anytime:

$$F(\alpha\boldsymbol{\sigma}^E + \bar{\boldsymbol{\rho}}) < 0 \tag{4.4}$$

then the body shakes down within the given domain $\mathscr{P}$. The greatest value of admissible α is called shakedown factor, noted α_{SD}.

4.2.2 Mathematical transformed optimization

To eliminate the explicit time dependence of the loadings, König et al. (Konig and Kleiber, 1978) proposed a transformed theorem:

Shakedown occurs for any load path in a given convex load domain $\mathscr{P}$ if it occurs for a cyclic load path containing all vertices of $\mathscr{P}$,

which allows us to verify only all the load vertices to predict the save domain for shakedown instead of the entire loading history. As shown in Figure 2.2(b), for two independently varying loads (p and q), we consider a special loading cycle passing through all vertices ($\hat{P}_1$ to $\hat{P}_4$) of $\mathscr{P}$:

$$\mathscr{P}(\boldsymbol{x}, t) = \sum_{k=1}^{m} \delta(t_k)\hat{P}_k(\boldsymbol{x}) \tag{4.5}$$

in which $m = 2^n$ is the totals vertices of $\mathscr{P}$, n is the total number of independent varying loads and $\delta(t_k)$ is the Dirac function:

$$\delta(t_k) = \begin{cases} 1, & if\ t = t_k \\ 0, & if\ t \neq t_k \end{cases} \tag{4.6}$$

where t_k indicates the time instant when the load cycle pass through the vertex $\hat{P}_k$.

To determine the shakedown factor α^{SD}, combining (4.4) and (4.5), the problem can be transformed to an mathematical optimization problem:

$$\begin{aligned} &\max_{\bar{\rho},\alpha} \quad \alpha \\ &s.t. \quad div\ \bar{\rho} = 0 \quad in\Omega \\ &\qquad \bar{\boldsymbol{\rho}} \cdot \boldsymbol{n} = \boldsymbol{0} \quad on\partial\omega \\ &\qquad F(\alpha\boldsymbol{\sigma}^E(\boldsymbol{x}, \hat{P}_k) + \bar{\boldsymbol{\rho}}) \leq 0 \quad in\Omega, \quad \forall k = 1, 2, ...m \end{aligned} \tag{4.7}$$

Once the shakedown factor α^{SD} is obtained, the shakedown save domain is the largest admissible rectangle as shown in Figure 2.2(b):

$$\mathscr{P}^{SD} = \alpha^{SD}\mathscr{P}_0 \tag{4.8}$$

4.3 Shakedown analysis by mathematical programming

In this chapter, we study the shakedown behavior of the hollow sphere submitted to varying macroscopic hydrostatic and deviatoric loads (Σ_m and Σ_e). The previous optimization method (4.7) has provided a direct procedure to analysis the shakedown load factor without following a step-by-step calculations. Before using the chosen non-linear optimizer IPOPT, a few preparations are still necessary:

1. The calculations of pure elastic response $\boldsymbol{\sigma}_0^{1E}$ and $\boldsymbol{\sigma}_0^{2E}$ subjected to unit macroscopic hydrostatic

load Σ_m^0 and deviatoric load Σ_e^0 are carried out by Abaqus standard (Hibbett et al., 1998). All the possible loading conditions can be simulated by an appropriate selected combination of lower and upper bounds $\mu_1^{\pm}$ and $\mu_2^{\pm}$.

2. In Melan's sense, the key point of the statical shakedown approach is to find the admissible time-independent stress field $\bar{\boldsymbol{\rho}}$. The equilibrium and boundary condition (4.2) need to be discretized for the use of Finite Element Method.

3. At last, in order to apply the Interior point method, the FEM formulations in Step 2 and the yield condition should be reformulated to fulfill the require of this chosen optimizer.

4.3.1 Elastic responses subjected to macroscopic referential loads and the selection of vertices in load domain

In our study, we chose the pure macroscopic hydrostatic load Σ_m and deviatoric load Σ_e to simulate the compressive/tensive and shear effects. Due to the geometrical symmetric hollow sphere model, only one-eighths of the cell is considered to produce the elastic response with Abaqus standard.

To fulfill the pure hydrostatic and deviatoric loading condition on the model, a 3D MPC (Multi-Points Constraints) user subroutine is applied on the external boundary, such that we can maintain the macroscopic stress triaxiality $T = \Sigma_m/\Sigma_e$ during the monotonic loading procedure. Note that the implementation of this 3D MPC procedure has already been described by Liu et al (Liu et al., 2016) in the study of void behaviors of ductile porous materials from low to high triaxialities.

We apply reference pure hydrostatic and axisymmetric deviatoric loads (Σ_m^0 and Σ_e^0) on the model (Figure4.1) to produce the corresponding elastic response $\boldsymbol{\sigma}_{m0}^E$ and $\boldsymbol{\sigma}_{e0}^E$, respectively. In practice, we impose $\Sigma_m^0 = \Sigma_e^0$.

As it is defined in (Liu et al., 2016), we also donate the stress ratios by the the macroscopic principal stresses:

$$\varphi_1 = \frac{\Sigma_1}{\Sigma_3}, \quad \varphi_2 = \frac{\Sigma_2}{\Sigma_3} \tag{4.9}$$

Then, the macroscopic mean stress Σ_m and equivalent stress Σ_e are expressed:

$$\begin{aligned} \Sigma_m &= 1/3\,(\Sigma_1 + \Sigma_2 + \Sigma_3) \\ \Sigma_e &= \sqrt{2}/2\,\sqrt{(\Sigma_1 - \Sigma_2)^2 + (\Sigma_2 - \Sigma_3)^2 + (\Sigma_1 - \Sigma_3)^2} \end{aligned} \tag{4.10}$$

So the macroscopic stress triaxiality T can be defined as following:

$$T = \frac{\Sigma_m}{\Sigma_e} = \frac{\sqrt{2}}{3} \frac{\left(\varphi_1 + \varphi_2 + 1\right) Sign\left(\Sigma_3\right)}{\sqrt{\left(\varphi_1 - \varphi_2\right)^2 + \left(\varphi_1 - 1\right)^2 + \left(\varphi_2 - 1\right)^2}} \tag{4.11}$$

where $Sign\left(\Sigma_3\right) = \Sigma_3 / \mid \Sigma_3 \mid$.

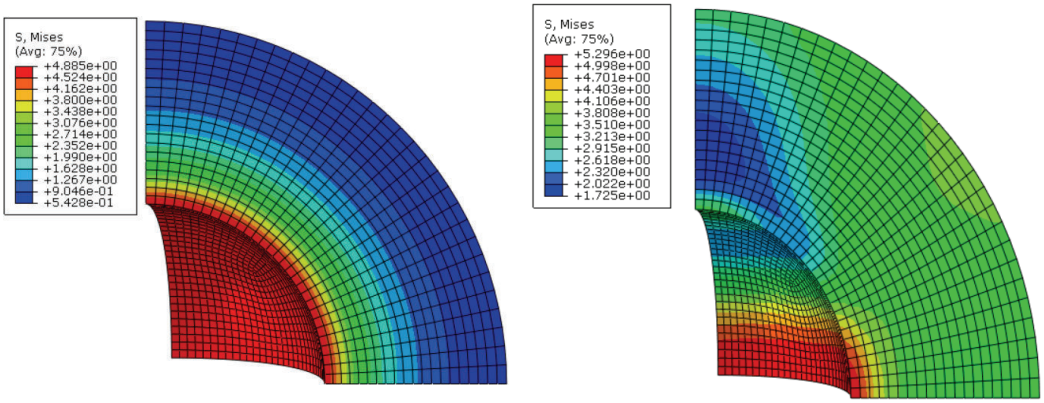

(a) Subjected to hydrostatic load for $T = +\infty$

(b) Subjected to deviatoric load for $T = 0$

Figure 4.1: Elastic solution of one-eighth hollow sphere model due to reference loads

The detailed implementations of macroscopic stress triaxiality to perform the reference load are provided in Appendix 1.

Once the lower and upper bounds $\mu_1^{\pm}$, $\mu_2^{\pm}$ are chosen, the vertices of the reference load domain $\mathscr{P}_0$ on the Σ_m-Σ_e plan can be expressed by:

$$\hat{P}_k = (\mu_1^{\pm}\Sigma_m^0, \mu_2^{\pm}\Sigma_e^0), \quad k = 1,2,3,4 \tag{4.12}$$

Due to proportionality between elastic loads and stresses, the corresponding elastic stresses at each corner of the rectangle are obtained by:

$$\boldsymbol{\sigma}_k^E = \mu_1^{\pm}\boldsymbol{\sigma}_{m0}^E + \mu_2^{\pm}\boldsymbol{\sigma}_{e0}^E, \quad k = 1,2,3,4 \tag{4.13}$$

To relate two independent varying loads for different load rectangle, we impose:

$$\mu_1^+ = cos\vartheta, \quad \mu_2^+ = sin\vartheta \tag{4.14}$$

So the macroscopic stress triaxiality T on the vertex can be expressed by:

$$T = \Sigma_e^+ / \Sigma_m^+ = \mu_1^+ / \mu_2^+ = tan\vartheta \tag{4.15}$$

where Σ_m^+ and Σ_e^+ are maximum hydrostatic and deviatoric stress of the load domain. In practice, we repeat the procedure to get several shakedown limit loads by modifying the values of parameters μ_1^-/μ_1^+ and μ_2^-/μ_2^+, which change the position of the load domain on the Σ_m-Σ_e plan, as well as different T.

4.3.2 Discretization of the shakedown formulations

In this subsection, we discretize and reform (4.7) to build the finite element formulations of the shakedown problem. Because of the auto equilibrium of elastic solution produced by Abaqus, let us start from the conditions of the residual stress field $\bar{\boldsymbol{\rho}}$, and then the yield condition.

For 3D brick element with 8 nodes, we transform the residual stress and strain tensor in vector form:

$$\bar{\rho}_{ij} = \begin{cases} \bar{\rho}_i, & if\ i = j \\ \bar{\rho}_{i+j}, & if\ i \neq j \end{cases}, \qquad \varepsilon_{ij} = \begin{cases} \varepsilon_i, & if\ i = j \\ \varepsilon_{i+j}, & if\ i \neq j \end{cases} \quad i,j = 1,2,3 \tag{4.16}$$

Due to the purely elastic behavior when shakedown occurs, the time independent residual stress does not contribute to the virtual work, the principle of virtual work reads:

$$\int_\Omega \delta\boldsymbol{\varepsilon}^T \bar{\boldsymbol{\rho}}\, dV = \int_\Omega \delta\boldsymbol{u}^T \boldsymbol{B}^T \bar{\boldsymbol{\rho}}\, dV = 0 \tag{4.17}$$

where $\delta\boldsymbol{\varepsilon}$ is the variation of virtual strain, $\delta\boldsymbol{u}$ is the variation of virtual displacement, and $\boldsymbol{B}$ is the strain-displacement linear differential operator:

$$\boldsymbol{\varepsilon} = \boldsymbol{B}\boldsymbol{u} \tag{4.18}$$

For a 3D brick element, $\boldsymbol{B}$ is given by:

$$\boldsymbol{B} = \begin{bmatrix} \frac{\partial N_1}{\partial x_1} & 0 & 0 & \frac{\partial N_2}{\partial x_1} & 0 & 0 & \dots & \frac{\partial N_8}{\partial x_1} & 0 & 0 \\ 0 & \frac{\partial N_1}{\partial x_2} & 0 & 0 & \frac{\partial N_2}{\partial x_2} & 0 & \dots & 0 & \frac{\partial N_8}{\partial x_2} & 0 \\ 0 & 0 & \frac{\partial N_1}{\partial x_3} & 0 & 0 & \frac{\partial N_2}{\partial x_3} & \dots & 0 & 0 & \frac{\partial N_8}{\partial x_3} \\ \frac{\partial N_1}{\partial x_2} & \frac{\partial N_1}{\partial x_1} & 0 & \frac{\partial N_2}{\partial x_2} & \frac{\partial N_2}{\partial x_1} & 0 & \dots & \frac{\partial N_8}{\partial x_2} & \frac{\partial N_8}{\partial x_1} & 0 \\ 0 & \frac{\partial N_1}{\partial x_3} & \frac{\partial N_1}{\partial x_2} & 0 & \frac{\partial N_2}{\partial x_3} & \frac{\partial N_2}{\partial x_2} & \dots & 0 & \frac{\partial N_8}{\partial x_3} & \frac{\partial N_8}{\partial x_2} \\ \frac{\partial N_1}{\partial x_3} & 0 & \frac{\partial N_1}{\partial x_1} & \frac{\partial N_2}{\partial x_3} & 0 & \frac{\partial N_2}{\partial x_2} & \dots & \frac{\partial N_8}{\partial x_3} & 0 & \frac{\partial N_8}{\partial x_1} \end{bmatrix} \tag{4.19}$$

in which $N_i (i = 1,2..8)$ is the standard shape function of 3 dimensional element.

We note NK, NE, NGE, NG the total number of nodes, elements, number of Gauss points per element and total number of Gauss points. (4.17) can be discretized and expressed a sum of integrals over all elements in Ω:

$$\begin{aligned} \int_{\Omega} \delta\boldsymbol{\varepsilon}^T \bar{\boldsymbol{\rho}}\, dV &\approx \sum_{n=1}^{NE} \left[\delta \boldsymbol{u}^n\right]^T \int_{\Omega_n} \boldsymbol{B}^T \bar{\boldsymbol{\rho}}^n\, dV = 0 \\ \Rightarrow \sum_{n=1}^{NE} \int_{\Omega_n} \boldsymbol{B}^T \bar{\boldsymbol{\rho}}^n\, dV &= \sum_{i=1}^{NE} \sum_{j=1}^{NGE} \boldsymbol{B}_{ij}^T \bar{\boldsymbol{\rho}}_{ij} \omega_{ij} det\boldsymbol{J}_{ij} = \sum_{i=1}^{NE} \sum_{j=1}^{NGE} \boldsymbol{C}_{ij} \boldsymbol{\rho}_{ij} = 0 \end{aligned} \tag{4.20}$$

$\boldsymbol{C}_{ij} = \boldsymbol{B}_{ij}^T \omega_{ij} det\boldsymbol{J}_{ij}$ is defined as the equilibrium matrix for the jth gauss point of the ith element which depends only on the geometry of the body and the applied element type, where ω_{ij} being the weight factor of the corresponding Gauss point and $det\boldsymbol{J}_{ij}$ the determinant of the Jacobian matrix.

According to Nguyen et al. (Nguyen et al., 2008), by assembling the all the elementary equilibrium matrix and the residual stress tensor in (4.20), this equation can be transformed in a global form:

$$\left[C_{ij}^g\right] \bar{\rho}_j = 0, \quad \forall i \in [1, 3NK], \forall j \in [1, 6NG] \tag{4.21}$$

The superposition of the elastic stresses at ith Gauss point $\boldsymbol{\sigma}_i^E$ with the corresponding residual stress $\bar{\boldsymbol{\rho}}_i$ constitute a safe state of stresses for each vertex $\hat{P}_k$:

$$F(\alpha \boldsymbol{\sigma}_i^E(\hat{P}_k) + \bar{\boldsymbol{\rho}}_i) \leq 0, \quad \forall i \in [1, NG], \quad \forall k \in [1,4] \tag{4.22}$$

With the consideration of the boundary condition, the $6NG \times 3NK$ dimension global equilibrium matrix $\left[C_{ij}^g\right]$ can be reduced to $6NG \times (3NK - NRES)$, where $NRES$ donates the number of restrained degrees of freedom. As a result, combining (4.21) with (4.22), we rewrite the shakedown optimization problem (4.7):

$$\begin{aligned} &\max_{\bar{\rho}_j, \alpha} \quad \alpha \\ &s.t. \begin{array}{l} \left[C_{ij}^g\right] \bar{\rho}_j = 0 \\ F_r(\alpha \sigma_j^E(\hat{P}_k) + \bar{\rho}_j) \leq 0 \end{array} \\ &\forall j \in [1, 6NG], \quad \forall k \in [1,4], \quad \forall i \in [1, NC] \end{aligned} \tag{4.23}$$

where $NC = 3KS - NRES$. Noticing that there are $6NG + 1$ unknowns corresponding to $\bar{\rho}_j$ and α, respectively. Additionally, $r = 1, 2, ..., 4NG$ donates the total number of yield constraints of the considered

body.

4.3.3 Solution of the shakedown problem by Interior-point method

Referring to (Nguyen et al., 2008; Wächter and Biegler, 2006), the non-linear optimizer IPOPT based on a primal-dual interior-point method provides a efficient solution for solving large-scale non-linear optimization problems in the following form:

$$\begin{aligned} \min_{\bar{\boldsymbol{x}}} \quad & f(\bar{\boldsymbol{x}}) \\ s.t \quad & \boldsymbol{c}(\bar{\boldsymbol{x}}) = \boldsymbol{0} \end{aligned} \tag{4.24}$$

Therefore, in order to fit the shakedown problem to this optimizer, we add the slack variables $\boldsymbol{s}$ to the yield inequality constraints, and the shakedown optimization problem takes the final expression:

$$\begin{aligned} &\min_{\bar{\boldsymbol{x}}} \quad f(\bar{\boldsymbol{x}}) = -\alpha \\ &s.t. \quad c_i(\bar{\boldsymbol{x}}) = \begin{cases} \left[C_{ij}^{g}\right]\bar{\rho}_j = 0, & for \quad i = 1, NC \\ F_r(\alpha\,\sigma_j^E(\hat{P}_k) + \bar{\rho}_j) - s_r = 0, & for \quad i = NC+1, NC+4NG \end{cases} \end{aligned} \tag{4.25}$$

where $\bar{\boldsymbol{x}} = (\bar{\boldsymbol{\rho}}, \alpha, \boldsymbol{s})$ is called vector of primal variables. Before calling the IPOPT optimizer, the last step is to calculate the gradient of objective $\nabla f(\bar{\boldsymbol{x}})$, the gradient of constraints $\boldsymbol{A}_k$, Hessian $\boldsymbol{W}_k$, and to initialize $\bar{\boldsymbol{x}}$. For more details, see Appendix 2.

Consequently, the solution of the shakedown optimization can be described by the following flowchart (Figure 4.2).

4.4 Special loading examples and discussions

In this section, some numerical examples under different loads by applying the present shakedown analysis method are provided. We consider 2 special loading situations:

- Alternating-alternating load, where $\mu_1^-/\mu_1^+ = \mu_2^-/\mu_2^+ = -1$. the rectangular reference load domain $\mathscr{P}_0$ is symmetric about the axis-Σ_m and axis-Σ_e on the Σ_m-Σ_e plan (Figure 4.3(a));
- Pulsating-pulsating load, where $\mu_1^-/\mu_1^+ = \mu_2^-/\mu_2^+ = 0$, $\mathscr{P}_0$ is situated in only one quadrant of the Σ_m-Σ_e plan (Figure 4.3(b));

For each loading case, we repeat the program with different triaxialites $T = \Sigma_m/\Sigma_e = \mu_2^+/\mu_1^+$ to get

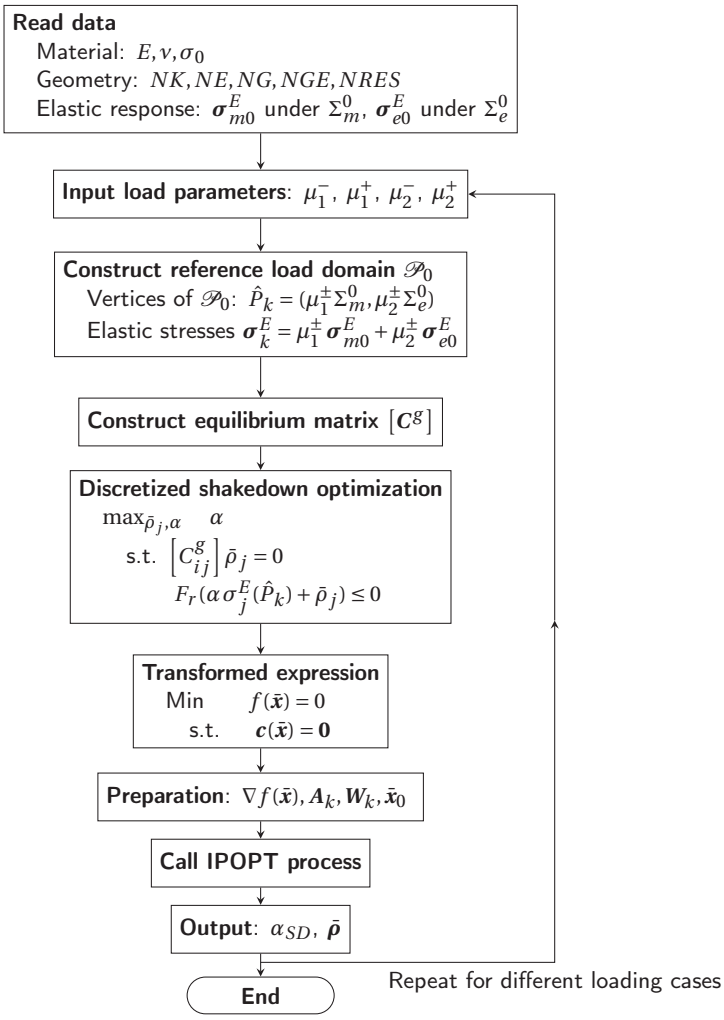

Figure 4.2: Flowchart of the shakedown analysis by interior-point method

several shakedown limit load to illustrate the safety domain on the Σ_m-Σ_e plan for porosity $f = 0.01$ and $f = 0.1$, respectively.

Moreover, in order to verify the reliability of this numerical method, we also perform the incremental step-by-step computations to analyze the transient phase before shakedown. As shown on Figure **??**, a critical loading path $1 \to 2 \to 3 \to 4 \to 1$, passing by all the vertices of load domain $\mathscr{P}$, is considered. We repeat this critical cyclic loading, and if the body shakes down, the current load is within the safety shakedown domain. By increasing the loading factor until the shakedown phenomenon does not occur, the shakedown limit load is obtained. Thus, we may compare the shakedown limit by the two means. The key parameter of the step-by-step computation is the evolution of accumulated equivalent plastic strain(PEEQ). If the the accumulated plastic strain does not vary any more after certain cycles of critical loadings, we consider the body shakes down.

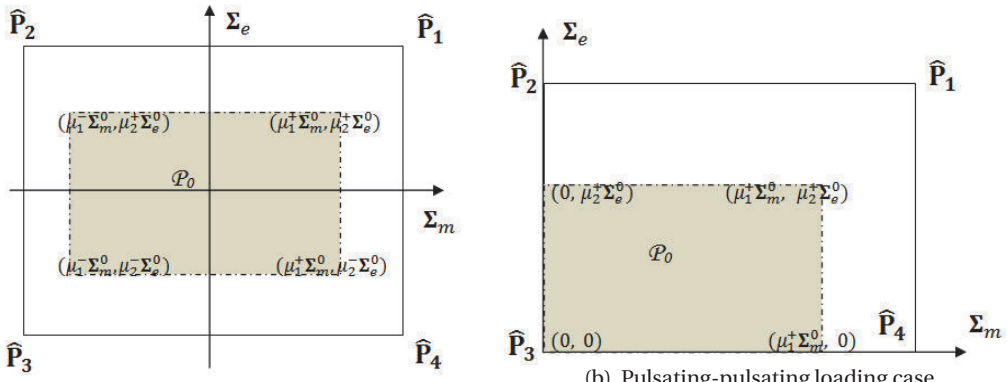

(a) Alternating-alternating loading case

(b) Pulsating-pulsating loading case

Figure 4.3: Reference load under special loading condition

In the following simulations, the material parameters are the Young's modulus: $E = 210GPa$, Poisson's ratio: $\nu = 0.3$ and the yield stress $\sigma_0 = 480MPa$. An initially one-eighth hollow sphere model is discretized by 2981 nodes and 2430 elements.

4.4.1 Alternating hydrostatic load coupled with alternating deviatoric load ($\mu_1^-/\mu_1^+ = \mu_2^-/\mu_2^+ = -1$)

In the research of the macroscopic analytical criterion for the determination of shakedown limit of porous materials subjected to one cyclic loading (Zhang et al., 2017b,a), it is noticed that the shakedown criterion is quite sensitive to the choice elastic stress field, and for alternating loading case ($\mu_1^-/\mu_1^+ = -1$), the shakedown safety domain even coincides with the elastic one. As a result, for two independently varying loading case, it is reasonable to start from the coupled alternating hydrostatic and deviatoric loadings, and compare with the elastic domain. The same model applied for elastic solution is adopted for the determination of the elastic limit by the finite element method. We increase the monotonic load until the plastic strain firstly appears to obtain the macroscopic elastic limit.

Figure 4.4 and 4.5 display the results of the present shakedown analysis computation and step-by-step incremental FEM method, as well as the elastic limit under monotone load for $f = 0.01$ and 0.1, respectively.

Firstly, we observe a quite good agreement between the shakedown limit obtained by the two methods. That is to say, the present shakedown optimization program is reliable to predict the shakedown safety domain for this alternating-alternating loading case.

Moreover, if presented in the same figure 4.6, it is clearly seen that, unlike Zhang's one-varying-load shakedown analytical limit (Zhang et al., 2017b), which is separated on two parts depending on the sign

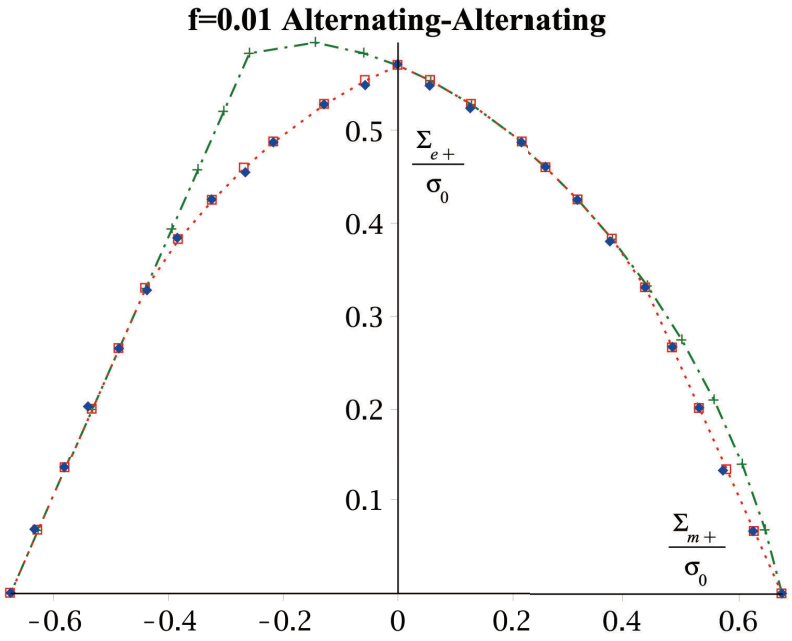

Figure 4.4: Interaction curve for porosity $f = 0.01$. Blue diamond: present direct analysis results; Green line: numerical elastic limit; Red box: shakedown limit by step-by-step computation.

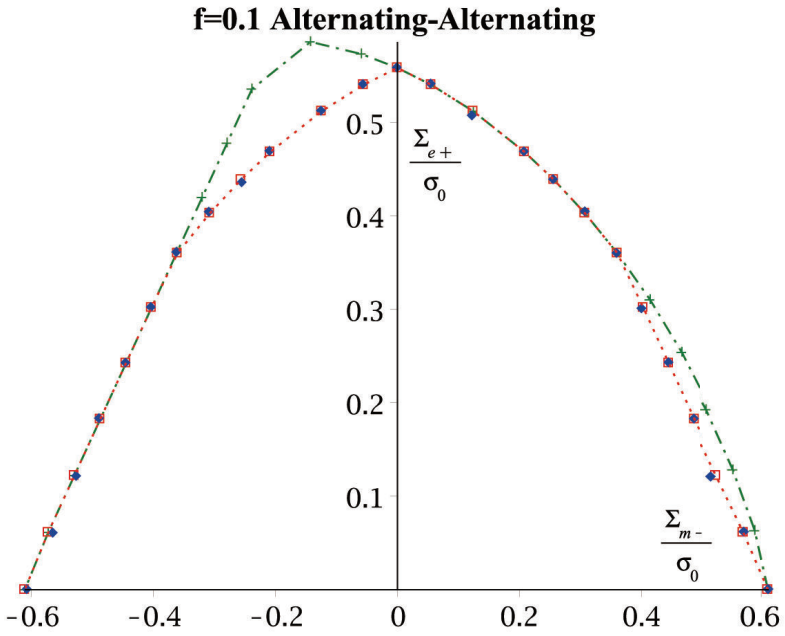

Figure 4.5: Interaction curve for porosity $f = 0.1$. Blue diamond: present direct analysis results; Green line: numerical elastic limit; Red box: shakedown limit by step-by-step computation.

of the third invariant of the macroscopic stress deviator J_3, we notice that the numerical shakedown limit under two independently varying loads is totally symmetric about the axe-Σ_e. However, the corresponding rectangular shakedown load domain for each loading case is still strictly inside the elastic domain. Thus, for alternating-alternating loading case, the applied load can not exceed the elastic limit, or the shakedown will not occur. And the corresponding stresses for all the Gauss points calculated by the program are of cause nearly zero. This is also proved by the step-by-step procedure: once the cyclic load exceed the monotone elastic limit, the plastic strain remains changing during each cycle, and the dissipation cumulates at the same time. So the accommodation arrives immediately, which will also lead to the structure's collapse. In other word, we can not observe the shakedown phenomenon in this loading case.

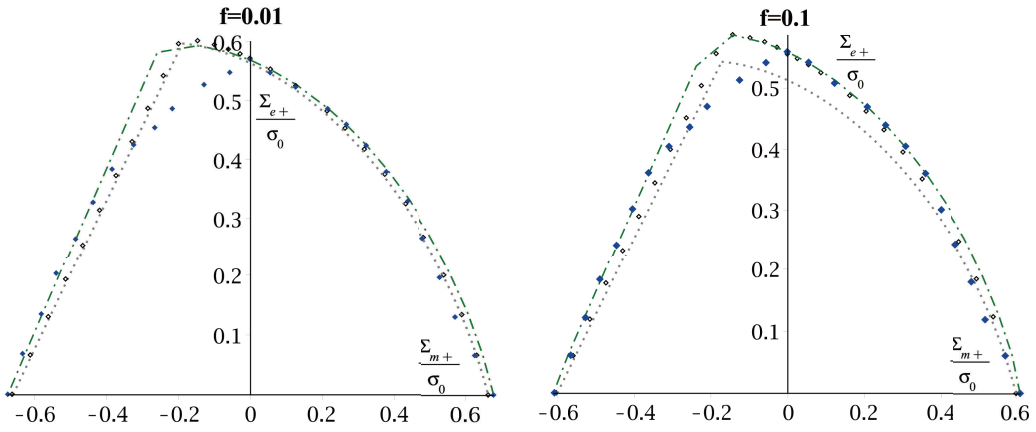

Figure 4.6: Comparison between the present results and one-varying-load shakedown limit in (Zhang et al., 2017b) for alternating loading case. Blue diamond: present direct analysis results; Green line: numerical elastic limit; Gray line and black box: Zhang's analytical criterion and corresponding numerical shakedown limit under one cyclic load.

In the analytical solution of the shakedown problem, we know the accuracy of the prediction is not significantly affected by the trial residual field but strongly depends on the choice of elastic stress field approximation, which is determined by the refinement of the mesh in the present numerical simulations. Although it is difficult to obtain the exact analytical solution of the shakedown limit, we can still compare the numerical results with the analytical one for pure hydrostatic loading case ($\mu_2 = 0$). In (Zhang et al., 2017b), the authors prove that shakedown limit Σ^{SD} under cyclic hydrostatic load and the elastic limit Σ^E have the following relation:

$$\Sigma_m^{SD} = \Sigma_m^E = \frac{2}{3}(1-f)\sigma_0 \tag{4.26}$$

Table 4.1 presents the variation of shakedown limit load with respect to the number of elements for pure

Porosity		Σ_m^{SD}/σ_0 for 0.01			Σ_m^{SD}/σ_0 for 0.1		
Elements	Nodes	$\frac{2}{3}(1-f)$	Optimization	Step-by-step	$\frac{2}{3}(1-f)$	Optimization	Step-by-step
750	1001	0.6600	0.7011	0.7035	0.6000	0.6385	0.6298
1408	1800	0.6600	0.6854	0.6861	0.6000	0.6210	0.6200
2430	2981	0.6600	0.6737	0.6739	0.6000	0.6168	0.6169
4356	5161	0.6600	0.6739	0.6721	0.6000	0.6158	0.6151

Table 4.1: Shakedown limit Σ_m^{SD}/σ_0 under pure hydrostatic loads with respect to different number of elements for porosities $f = 0.01$ and 0.1

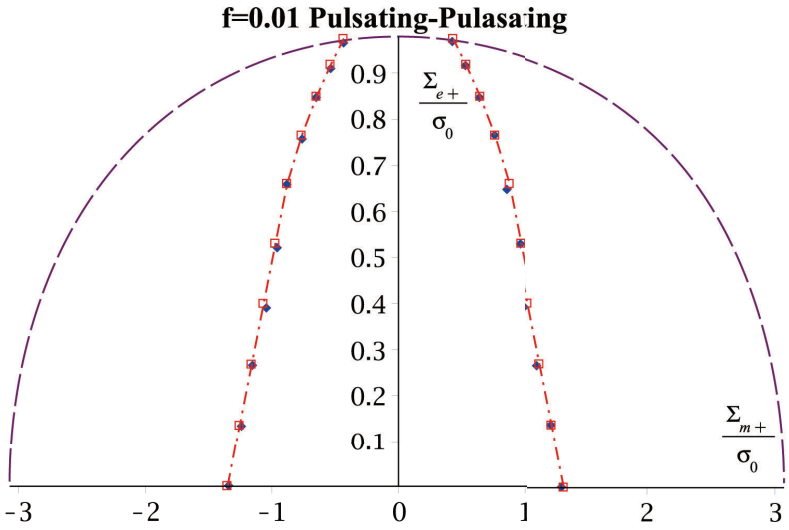

Figure 4.7: Interaction curve for porosity $f = 0.01$. Blue diamond: present direct analysis results; Red box: shakedown limit by step-by-step computation; Purple line: Shen's criterion of limit analysis.

hydrostatic loading case ($\mu_2 = 0$)

4.4.2 Pulsating hydrostatic load coupled with pulsating deviatoric load ($\mu_1^-/\mu_1^+ = \mu_2^-/\mu_2^+ = 0$)

In this subsection, we consider the pulsating-pulsating loading case ($\mu_1^-/\mu_1^+ = \mu_2^-/\mu_2^+ = 0$), where the load domain is in a single quadrant.

Figure 4.7 and 4.8 show the main result of the proposed analysis computation and step-by-step elastic-plastic FEM method, as well as Shen's limit analysis corresponding to the collapse under monotone load (Shen et al., 2015). Noticing that, the shakedown optimization program is overall validated by the step-by-step computation, except for several loading cases, where small differences can be observed. And for high triaxialities, the safety domain is defined by the limit analysis instead of the one of shakedown. Similar to the previous subsection, the shakedown limit load is also symmetric about the axe-Σ_e.

In the one-varying load situation, the amplitude of shakedown cyclic load for pulsating case doubles

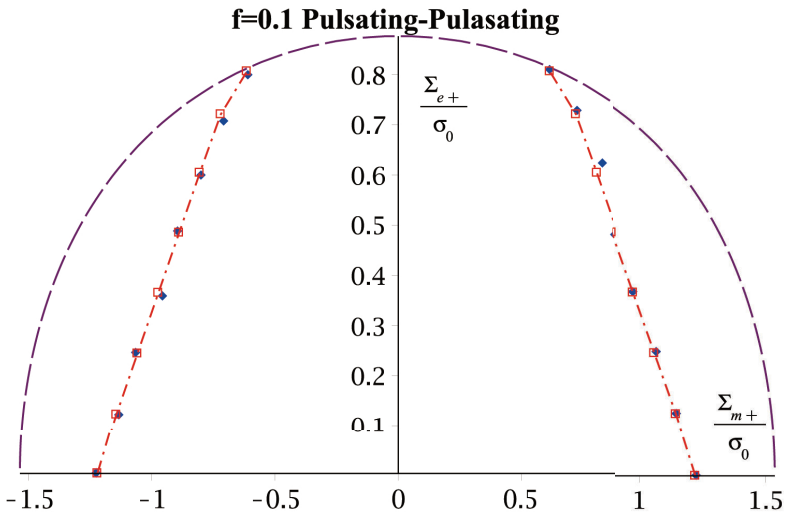

Figure 4.8: Interaction curve for porosity $f = 0.1$. Blue diamond: present direct analysis results; Red box: shakedown limit by step-by-step computation; Purple line: Shen's criterion of limit analysis.

the alternating one. We wonder if this relation remains valid for two independently varying loading case. From Figure 4.9, it is readily seen that the pulsating-pulsating shakedown limit load still holds the double relation of the alternating-alternating one, except for some high triaxialities cases due to the collapse by development of a mechanism, as in limit analysis.

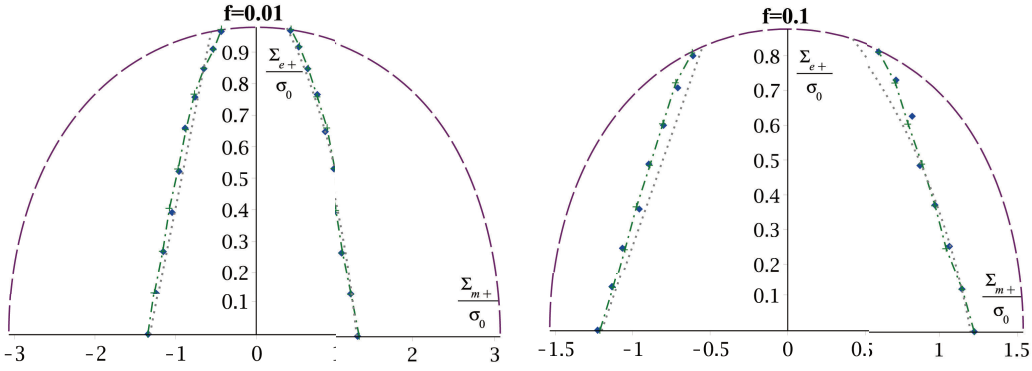

Figure 4.9: Comparison between the present results for pulsating-pulsating loading and double of the one for alternating-alternating loading case. Blue diamond: present direct analysis results for pulsating-pulsating loading; Green line: double of the numerical shakedown limit in the previous subsection; Gray line: Zhang's analytical criterion under one cyclic load; Purple line: Shen's criterion of limit analysis.

4.4.3 Discussions and remarks

In the previous two subsections, we have assessed the predictive capability of the new shakedown optimization program by comparing with the step-by-step computation results for alternating-alternating

Loading case	Alternating-alternating		Pulsating-pulsating	
Triaxiality	Iterations	Time(s)	Iterations	Time(s)
4.3333	5391	13614	7763	19262
1.3333	5069	8464	6079	11720
0.5833	2937	6063	9116	17415

Table 4.2: Comparison of computation time and number of iterations between alternating-alternating and pulsating-pulsating loading case for porosity $f = 0.1$

and pulsating-pulsating loading cases, respectively. Apart from the good agreement between them, some remarks are also made about the results:

1. The present program aiming at finding the shakedown load factor α_{SD} for alternating-alternating loading case is much more efficient than for pulsating-pulsating case. As shown on Table 4.2, the computation time and the corresponding number of iterations for the same macroscopic triaxiality is much less for alternating-alternating case.

This can be explained by the initial value of the shakedown load factor α_0 of the program (see Appendix 4.5). For alternating-alternating loading case, the shakedown limit load is just the elastic limit load. And the initial value α_0 is set to be the elastic factor, which is very close to the objective solution. As a result, it does not take too many iterations compared with other loading cases.

2. For pulsating-pulsating loading case, the optimization results are not as accurate as in the other case. And sometimes, the program even ends with divergence. According to Nguyen (Nguyen et al., 2008), all the six components of the corresponding residual stress tensor are nonzero for this loading condition, which may lead the shakedown problem to be badly scaled and even degenerate, because of the initiation of the residual stress variables. Besides, the starting point of shakedown factor can be especially too small for the vertex $\hat{P}_3 = (0,0)$ of the load domain. And the linear solver of the program will create too many fill-in, which can also be a consequence of a degenerate problem.

To author's knowledge, the solution to the problem is an appropriate choice of the reference load $\mathscr{P}_0$ so that the shakedown load factor α^{SD} is not too large or too small. In practice, once the program ends with bad result, we may restart the program by adjusting the reference load. Besides, to increase the accuracy of the error tolerance of the optimizer can provide a more precise result, which will also lead to a longer computation time.

3. Although it is a little burdensome to solve a axisymmetric problem with a three dimensional model, the proposed program can be implemented easily to all the models of porous material with general loading condition, for which it is difficult to derive the analytical solution (sphere model with irregular void, for example). In addition, the number of independently varying load is not limited to 2, and of cause,

more unknowns and constraints are created, which has a higher requirement of the capacity of computations.

4.5 Conclusion and perspective

In this study, we present an novel numerical procedure for shakedown analysis of porous material under two independently varying loads by using a non-linear optimizer IPOPT, which provides efficiently not only the shakedown load factor but also the corresponding residual stress. A one-eighth 3D hollow sphere model with von Mises matrix is considered by combining referential macroscopic hydrostatic load and deviatoric load to simulate all the loading conditions.

By adopting the transformed Melan's static theorem based on the time-independent residual stress, the shakedown problem has been rewritten to a large-scale optimization problem by verification of the vertices of load domain instead of the whole loading history. The proposed method has been well tested by the step-by-step incremental computations especially for alternating-alternating and pulsating-pulsating loading cases. From the obtained results, some special relation under one cyclic loading condition still holds for the present study. Despite of some divergence problems, the choice of IPOPT optimizer can solve the the optimization problem of a large number of unknowns and constraints practically and efficiently.

In the perspective, the attention is focus on shakedown of ductile porous materials considering a irregular model involving the kinematical hardening as to the numerical procedure. Moreover, another interesting extension will concern the analytical solution of the shakedown limit under multi-varying independent loads.

Appendix 1: Numerical implementation of macroscopic stress triaxiality for 3D models in (Liu et al., 2016)

To maintain the macroscopic stress triaxiality in constant during the proportional loading for the 3 dimensional Finite element program by Abaqus, a procedure of 3D multi-point constraint of the displacement on the external boundary is required.

The total work rate $\dot{W}$ of a 3 dimensional model can be expressed by the doc product of a pair of 3

dimensional generalized force $\boldsymbol{P} = V(\Sigma_1, \Sigma_2, \Sigma_3)$ and displacement rate vectors $\dot{\boldsymbol{Q}} = \left(\dot{E}_1, \dot{E}_2, \dot{E}_3\right)$:

$$\dot{W} = \boldsymbol{P}^T \dot{\boldsymbol{Q}} = V \boldsymbol{\Sigma} : \dot{\boldsymbol{E}} \tag{27}$$

where V is the volume of the chosen model.

In order to put into practice of the multi-point constraint condition, as proposed in the research of the MPC procedure of axisymmetric cell (Cheng and Guo, 2007), it is necessary to introduce an extra "ghost" node into the finite element model with the degrees of freedom (q_1, q_2, q_3) and corresponding forces (p_1, p_2, p_3). For further use, we impose the equality of total work rate between this "ghost" node and the entire considered model:

$$\boldsymbol{p}^T \dot{\boldsymbol{q}} = \boldsymbol{P}^T \dot{\boldsymbol{Q}} \tag{28}$$

For large deformation, one has the following relation in rate forms:

$$\dot{u}_i = \dot{E}_i (u_i + X_i) \tag{29}$$

And for small deformation:

$$\dot{u}_i = \dot{E}_i u_i \tag{30}$$

where $\dot{E}_i \, (i = 1,2,3)$ is the macroscopic principal strain rate. It is shrewed to impose the reactions of the first two DOFs at the "ghost" node are null:

$$p_1 = p_2 = 0 \tag{31}$$

Under this condition, according to (Liu et al., 2016), the unimodular transformation matrix $\mathscr{R}$ is:

$$\mathscr{R} = \begin{bmatrix} sin^2\phi + cos^2\phi cos\theta & cos\phi sin\phi(cos\theta - 1) & cos\phi sin\theta \\ cos\phi sin\phi(cos\theta - 1) & cos^2\phi + sin^2\phi cos\theta & sin\phi sin\theta \\ -cos\phi sin\theta & -sin\phi sin\theta & cos\theta \end{bmatrix} \tag{32}$$

where

$$\begin{aligned} \phi &= atan(\Sigma_2 / \Sigma_1) = atan\left(\varphi_2 / \varphi_1\right) \\ \theta &= atan\left(\sqrt{\Sigma_1^2 + \Sigma_2^2} / \Sigma_3\right) = atan\left(sign(\Sigma_3)\sqrt{\varphi_1^2 + \varphi_2^2}\right) \end{aligned} \tag{33}$$

The fixed stress ratio φ_1 and φ_2 are given in (4.9). Then, the generalized force $\boldsymbol{P}$ and displacement rate $\dot{\boldsymbol{Q}}$ can be expressed by the ones of the "ghost" point and the transformation matrix:

$$\boldsymbol{P} = \mathscr{R}\boldsymbol{p}, \quad \dot{\boldsymbol{Q}} = \mathscr{R}\dot{\boldsymbol{q}} \tag{34}$$

Considering the third nonzero component of the total work rate $\dot{W}$, the third principal stress of the model can be computed directly by:

$$V\Sigma_3 = \frac{p_3\, sign(\Sigma_3)}{\sqrt{\varphi_1^2+\varphi_2^2+1}} \tag{35}$$

As a result, to fulfill the fixed macroscopic stress triaxiality proportional loading requirement, we take q_3 at the "ghost" point as the loading parameter, and φ_1, φ_2, $sign(\Sigma_3)$ to control the triaxiality.

In practice, to produce the elastic response $\boldsymbol{\sigma}^E_{m0}$ under the pure hydrostatic load as shown in Figure 4.1(a), where $\Sigma_e = 0$, we impose $\varphi_1 = 1$, $\varphi_2 = 1$ and $Sign(\Sigma_3) = 1$; Likewise, for obtain $\boldsymbol{\sigma}^E_{e0}$ under axisymmetric deviatoric load in Figure 4.1(a), where $\Sigma_m = 0$, taking $\varphi_1 = -0.5$, $\varphi_2 = -0.5$ and $Sign(\Sigma_3) = -1$.

Appendix 2: Application of Interior-point method to shakedown optimization

For an optimization problem:

$$\begin{aligned} \min_{\bar{\boldsymbol{x}}\in\mathscr{R}^n} \quad & f(\bar{\boldsymbol{x}}) \\ s.t. \quad & c_i(\bar{\boldsymbol{x}}) = 0, \quad i = 1, m \quad : \boldsymbol{\lambda} \\ & \bar{x}_j^L \le \bar{x}_j \le \bar{x}_j^U, \quad j = 1, n \quad : \boldsymbol{z} \end{aligned} \tag{36}$$

According to (Nguyen et al., 2008),the interior-point method, carried out by IPOPT with the help of direct linear solver PARDISO (Schenk and Gärtner, 2004), provides an efficient possibility to solve this problem with a large number of unknowns and constraints. Before calling the optimizer, as well as the transformation of the inequalities (4.25), the gradient of constraints $\boldsymbol{A}_k = \nabla \boldsymbol{c}(\bar{\boldsymbol{x}})$, Hessian $\boldsymbol{W}_k$, initialization of $\bar{\boldsymbol{x}}$.

- Gradient of constraints $\boldsymbol{A}_k$.

The expression of the gradient of constraints $\boldsymbol{A}_k = \nabla \boldsymbol{c}(\bar{\boldsymbol{x}})$ is given by

$$\boldsymbol{A}_k = \begin{bmatrix} & & & \frac{\partial F_1}{\partial \bar{x}_1} & \frac{\partial F_2}{\partial \bar{x}_1} & \cdots & \frac{\partial F_{4NG}}{\partial \bar{x}_1} \\ & \boldsymbol{C}^T & & \frac{\partial F_1}{\partial \bar{x}_2} & \frac{\partial F_2}{\partial \bar{x}_2} & \cdots & \frac{\partial F_{4NG}}{\partial \bar{x}_2} \\ & & & \vdots & \vdots & \cdots & \vdots \\ 0 & \cdots & 0 & \frac{\partial F_1}{\partial \bar{x}_{6NG+1}} & \frac{\partial F_2}{\partial \bar{x}_{6NG+1}} & \cdots & \frac{\partial F_{4NG}}{\partial \bar{x}_{6NG+1}} \\ 0 & \cdots & 0 & -1 & 0 & \cdots & 0 \\ 0 & \cdots & 0 & 0 & -1 & \ddots & 0 \\ \vdots & \vdots & \vdots & \vdots & \ddots & \ddots & \vdots \\ 0 & \cdots & 0 & 0 & \cdots & \cdots & -1 \end{bmatrix} \tag{37}$$

in which $\boldsymbol{C}$ and F are the global self-equilibrium matrix and yield constraints defined in (4.25).

- Hessian $\boldsymbol{W}_k$of Lagrangian function.

  We donate Lagrangian function $L(\bar{\boldsymbol{x}}, \boldsymbol{\lambda}, \boldsymbol{z})$ for the original optimization problem (36):

$$L(\bar{\boldsymbol{x}}, \boldsymbol{\lambda}, \boldsymbol{z}) = f(\bar{\boldsymbol{x}}) + \boldsymbol{c}(\bar{\boldsymbol{x}})^T - \boldsymbol{z} \tag{38}$$

  Then Hessian $\boldsymbol{W}_k \in \mathscr{R}^{n \times n}$ of the Lagrangian function L is given by

$$\begin{aligned} \boldsymbol{W}_k = \nabla^2_{\bar{x}\bar{x}} L = \nabla^2_{\bar{x}\bar{x}} f(\bar{\boldsymbol{x}}_k) + & \sum_{i=1}^{NC+4NG} \lambda_i \nabla^2_{\bar{x}\bar{x}} \boldsymbol{c}_i(\bar{\boldsymbol{x}}_k) F_i(\bar{\boldsymbol{x}}_k) \\ = & \sum_{i=1}^{NC} \lambda_i \nabla^2_{\bar{x}\bar{x}} C_{kl} + \sum_{i=NC+1}^{NC+4NG} \lambda_i \nabla^2_{\bar{x}\bar{x}} F_i(\bar{\boldsymbol{x}}_k) \\ & \sum_{i=NC+1}^{NC+4NG} \lambda_i \nabla^2_{\bar{x}\bar{x}} F_i(\bar{\boldsymbol{x}}_k) \end{aligned} \tag{39}$$

- Initialization of $\bar{\boldsymbol{x}}$.

  The initial point of all the unknowns $\bar{\boldsymbol{x}}_0 = (\bar{\boldsymbol{\rho}}_0, \alpha_0, \boldsymbol{s}_0)$ should be chosen far away from the boundary due to the requirement to strictly satisfy the bound constraints of the interior-point method.

  For the shakedown load factor α_0, it starts from the elastic factor at the first vertex $\hat{P}_1$ of the load domain, and the initial residual stress is set to be the corresponding elastic response:

$$\begin{aligned} \alpha_0 &= \alpha^E_{\hat{P}_1} \\ \bar{\boldsymbol{\rho}}_0 &= \boldsymbol{\sigma}^E_{\hat{P}_1} \end{aligned} \tag{40}$$

Then, the initial values for the slack variables $\boldsymbol{s}_0$ are chosen by the yield criterion:

$$s_{0r} = F_r(\alpha_0 \sigma_j^E(\bar{\boldsymbol{x}}, \hat{P}_1) + \bar{\rho}_{0j}) \tag{41}$$

General conclusion

The main objective of this thesis is to provide a micro-macro shakedown approach for ductile porous materials with von Mises and Drucker-Prager matrix based on Melan's statical theorem, analytically and numerically. Following Dang Van (Dang-Van, 1973), we try to maximize the admissible load domain, which turns out to be a fatigue criterion of the considered hollow sphere model in Gurson's spirit (Gurson et al., 1977).

We start from the simplest case: the hollow sphere model with von Mises matrix concerning alternating ($R = -1$) and pulsating loads ($R = 0$). The exact solution for the pure hydrostatic loading condition is firstly derived, then combined with the additional trial terms to capture the shear effects. From Melan's theorem, the key point is to construct a time-independent admissible residual stress field. Besides, the macroscopic shakedown criterion depends strongly on the microscopic elastic solution, of which the deviatoric part is inspired from Papkovich-Neuber solution (Soutas-Little, 1999) (This solution has been applied to provide the elastic stress field under pure deviatoric load. See Appendix A). Then, to extend the proposed model to general cyclically repeated loads ($-1 \leq R < 1$), we constructed a more appropriate trial residual stress field by relaxing the boundary condition. It can be seen from the improved model that the shakedown limit is the inferior one of the double elastic limit and ultimate limit under monotonic load: $\alpha_{SD} = inf(2\alpha_E, \alpha_l)$. Interestingly, we find that for alternating loading case, the shakedown safety domain coincides with the elastic domain, which confirms that the shakedown phenomenon will not occur under this loading case, but the plastic fatigue, instead. To avoid the repetition, this part is combined and provided in Chapter 2.

Furthermore, we have derived a macroscopic model for the associated Drucker-Prager material (Chapter 3). Thanks to the previous study about the elastic solution with the same hollow sphere model, we achieve our goal by including the influence of the friction angle in the derived approach. The final closed form expression of the macroscopic shakedown criteria, together with the one of limit analysis under monotonic proportional load (Shen et al., 2015), defines the safety domain for the considered model

under general cyclic loads. The new closed-form macroscopic criteria derived in Chapter 2 and 3 both depend on the two stress invariants Σ_m and Σ_e, the sign of the third invariant of the stress deviator J_3, the porosity f and Poisson's ratio ν. All the established model have been assessed and validated against numerical solutions derived from micromechanics-based finite element computations by considering a quarter of the hollow sphere subjected to homogeneous strain rate boundary conditions for various configurations of porosity and friction angles by the means of Abaqus with a user-defined-subroutine MPC (Cheng and Guo, 2007).

In the last chapter, for a more complex combination of independent loads, where the statically admissible stress fields are difficult to be constructed, we provide a numerical shakedown analysis by considering König's extension (Konig and Kleiber, 1978) of Melan's theorem. The statical shakedown condition is transformed as a large-size non-linear optimization problem, which is solved efficiently by the optimizer IPOPT using the interior-point method. The obtained results are compared to the step-by-step incremental computations especially for alternating-alternating and pulsating-pulsating loading cases.

In the future, several tracks of research can be considered to improve the study of shakedown of porous materials:

- Although experiments (Kobayashi et al., 1991; Schmidt et al., 1991) have shown that in ductile metals, the strain to fracture is considerably lower, for a given load level, if this load is reached under cyclic conditions than if it is reached monotonically, the experimental data of porous materials are still in a lack. As a result, on the ground of shakedown of ductile porous materials, we can only compare today the analytical results with the numerical ones. However, our theoretical predictions could suggest new experimental testing in order to assess the fatigue strength of porous materials.

- In Chapter 2 and 3, small but noticeable differences between the criteria and numerical results are remarked ($f = 0.1$). We can improve the accuracy of the present criterion with a larger porosity by constructing a better trial stress field for the deviatoric part. On the other hand, another interesting extension is applying this established method to non-associated Drucker-Prager matrix with the consideration of the bipotential-based limit analysis method (Cheng et al., 2015a) and non-linear homogenization techniques. By adopting a trial velocity field and the use of Koiter's kinematic approach, the influence of the dilatancy angle could be taken into consideration.

- In Chapter 4, we focus our attention only on von Mises matrix. Then the next step may be applying this optimization program to Drucker-Prager material, for which an additional bound on hydrostatic stress σ_m is needed (Nguyen and Ponter, 2007). Besides, it can be used for non-axisymmetric

loads to show the influence of the Lode angle (Cheng et al., 2015b) (the third invariant of the stress deviator instead of the sign) in three dimensional context.

- Lastly, another interesting extension is to consider voided single crystals (Paux et al., 2015) as in Dang Van's criterion. The idea relies on applying shakedown theory to fatigue analysis of the structures (Dang-Van, 2002). For example, applications to high cycle fatigue: some multiaxial fatigue criteria (Papadopoulos, 1994) are essentially based on the hypothesis of elastic shakedown at the mesoscopic scale and therefore a bounded cumulated dissipation; as for the low cycle fatigue, we can speak of a plastic shakedown at both mesoscopic and macroscopic scale and a cumulated energy bounded by the failure energy permitting a direct determination of the fatigue limit.

Bibliography

Abdel-Karim, M., Ohno, N., 2000. Kinematic hardening model suitable for ratchetting with steady-state. International Journal of Plasticity 16 (3-4), 225–240.

Atluri, S. N., 1984. On constitutive relations at finite strain: hypo-elasticity and elasto-plasticity with isotropic or kinematic hardening. Computer methods in applied mechanics and engineering 43 (2), 137–171.

Axelsson, K., Samuelsson, A., 1979. Finite element analysis of elastic–plastic materials displaying mixed hardening. International Journal for Numerical Methods in Engineering 14 (2), 211–225.

Benzerga, A. A., Besson, J., 2001. Plastic potentials for anisotropic porous solids. European Journal of Mechanics-A/Solids 20 (3), 397–434.

Besson, J., Guillemer-Neel, C., 2003. An extension of the green and gurson models to kinematic hardening. Mechanics of materials 35 (1-2), 1–18.

Bleich, H., 1932. Über die bemessung statisch unbestimmter stahltragwerke unter berücksichtgung des elastisch-plastischen verhaltens des baustoffes. Bauingenieur 13 (19).

Bleyer, J., Pham, D. T., De Buhan, P., Florence, C., 2015. Yield design of periodically heterogeneous plates. In: Direct Methods for Limit and Shakedown Analysis of Structures. Springer, pp. 143–158.

Chaboche, J.-L., 1991. On some modifications of kinematic hardening to improve the description of ratchetting effects. International journal of plasticity 7 (7), 661–678.

Charkaluk, E., Constantinescu, A., Maïtournam, H., Van, K. D., 2009. Revisiting the dang van criterion. Procedia Engineering 1 (1), 143–146.

Chen, M., Hachemi, A., Weichert, D., 2013. Shakedown and optimization analysis of periodic composites. In: Limit State of Materials and Structures. Springer, pp. 45–69.

Cheng, L., Danas, K., Constantinescu, A., Kondo, D., 2017. A homogenization model for porous ductile solids under cyclic loads comprising a matrix with isotropic and linear kinematic hardening. International Journal of Solids and Structures 121, 174–190.

Cheng, L., de Saxcé, G., Kondo, D., 2014. A stress-based variational model for ductile porous materials. International Journal of Plasticity 55, 133–151.

Cheng, L., Guo, T., 2007. Void interaction and coalescence in polymeric materials. International Journal of Solids and Structures 44 (6), 1787–1808.

Cheng, L., Jia, Y., Oueslati, A., De Saxcé, G., Kondo, D., 2012. Plastic limit state of the hollow sphere model with non-associated drucker–prager material under isotropic loading. Computational Materials Science 62, 210–215.

Cheng, L., Jia, Y., Oueslati, A., De Saxcé, G., Kondo, D., 2015a. A bipotential-based limit analysis and homogenization of ductile porous materials with non-associated drucker–prager matrix. Journal of the Mechanics and Physics of Solids 77, 1–26.

Cheng, L., Monchiet, V., Morin, L., De Saxcé, G., Kondo, D., 2015b. An analytical lode angle dependent damage model for ductile porous materials. Engineering Fracture Mechanics 149, 119–133.

Chinh, P. D., 2007. Shakedown theory for elastic plastic kinematic hardening bodies. International Journal of Plasticity 23 (7), 1240–1259.

Coffin Jr, L., 1954. A study of cyclic thermal stresses in a ductile metal. Transactions ASME 76.

Cook, R. D., Malkus, D. S., Plesha, M. E., Witt, R. J., 1974. Concepts and applications of finite element analysis. Vol. 4. Wiley New York.

Dafalias, Y., 1983. Corotational rates for kinematic hardening at large plastic deformations. Journal of Applied Mechanics 50 (3), 561–565.

Dang-Van, K., 1973. Sur la résistance ala fatigue des métaux. Extrait de sciences et techniques de l'armement.

Dang-Van, K., 1993. Macro-micro approach in high-cycle multiaxial fatigue. In: Advances in multiaxial fatigue. ASTM International.

Dang-Van, K., 2002. Application of shakedown theory to fatigue analysis of structures. In: Inelastic Behaviour of Structures under Variable Repeated Loads. Springer, pp. 377–393.

de Buhan, P., Hassen, G., 2013. A multiphase model for assessing the overall yield strength of soils reinforced by linear inclusions. In: Limit State of Materials and Structures. Springer, pp. 165–178.

De Saxcé, G., 1995. The bipotential method, a new variational and numerical treatment of the dissipative laws of materials. In: Proc. 10th Int. Conf. on Mathematical and Computer Modelling and Scientific Computing,(Boston, 1995).

De Saxcé, G., Feng, Z.-Q., 1998. The bipotential method: a constructive approach to design the complete contact law with friction and improved numerical algorithms. Mathematical and computer modelling 28 (4-8), 225–245.

Devaux, J., Gologanu, M., Leblond, J., Perrin, G., 1997. On continued void growth in ductile metals subjected to cyclic loadings. In: IUTAM Symposium on Nonlinear Analysis of Fracture. Springer, pp. 299–310.

Drucker, D., Prager, W., Greenberg, H., 1952. Extended limit design theorems for continuous media. Quarterly of applied mathematics 9 (4), 381–389.

Drucker, D. C., 1951. A more fundamental approach to plastic stress-strain relations. In: Proc. 1st US National Congress of Applied Mechanics. pp. 487–491.

Drucker, D. C., 1956. On uniqueness in the theory of plasticity. Quarterly of Applied Mathematics 14 (1), 35–42.

Drucker, D. C., 1963. On the postulate of stability of material in the mechanics of continua. Tech. rep., BROWN UNIV PROVIDENCE RI.

Druyanov, B., Roman, I., 1998. On adaptation (shakedown) of a class of damaged elastic plastic bodies to cyclic loading. European Journal of Mechanics-A/Solids 17 (1), 71–78.

Eterovic, A. L., Bathe, K.-J., 1990. A hyperelastic-based large strain elasto-plastic constitutive formulation with combined isotropic-kinematic hardening using the logarithmic stress and strain measures. International Journal for Numerical Methods in Engineering 30 (6), 1099–1114.

Fritzen, F., Forest, S., Böhlke, T., Kondo, D., Kanit, T., 2012. Computational homogenization of elasto-plastic porous metals. International Journal of Plasticity 29, 102–119.

Garajeu, M., 1995. Contribution a l'etude du comportement non lineaire de milieux poreux avec ou sans renfort. Ph.D. thesis, Aix-Marseille 2.

Gărăjeu, M., Suquet, P., 1997. Effective properties of porous ideally plastic or viscoplastic materials containing rigid particles. Journal of the Mechanics and Physics of Solids 45 (6), 873–902.

Gilles, P., Jullien, B., Mottet, G., 1992. Analysis of cyclic effects on ductile tearing strength by a local approach of fracture. In: Advances in Fracture/Damage Models for the Analysis of Engineering Problems. Vol. 137. ASME Publication AMD, pp. 269–284.

Gokhfeld, D., 1966. Some problems of shakedown of plates and shells. In: Proc. VI-th Soviet Conf. Plates Shells, Nauka. pp. 284–291.

Gologanu, M., Leblond, J.-B., Perrin, G., Devaux, J., 1997. Recent extensions of gurson's model for porous ductile metals. In: Continuum micromechanics. Springer, pp. 61–130.

Guo, T., Faleskog, J., Shih, C., 2008. Continuum modeling of a porous solid with pressure-sensitive dilatant matrix. Journal of the Mechanics and Physics of Solids 56 (6), 2188–2212.

Gurson, A. L., et al., 1977. Continuum theory of ductile rupture by void nucleation and growth: Part i: Yield criteria and flow rules for porous ductile media. Journal of engineering materials and technology 99 (1), 2–15.

Gvozdev, A., 1960. The determination of the value of the collapse load for statically indeterminate systems undergoing plastic deformation. International Journal of Mechanical Sciences 1 (4), 322–335.

Hachemi, A., Chen, M., Chen, G., Weichert, D., 2014. Limit state of structures made of heterogeneous materials. International Journal of Plasticity 63, 124–137.

Hachemi, A., Schwabe, F., Weichert, D., 2000. Failure investigation of fiber-reinforced composite materials by shakedown analysis. In: Inelastic Analysis of Structures under Variable Loads. Springer, pp. 107–119.

Halphen, B., 1980. Periodic solutions in plasticity and viscoplasticity. In: Variational Methods in the Mechanics of Solids. Elsevier, pp. 273–277.

Hassan, T., Kyriakides, S., 1992. Ratcheting in cyclic plasticity, part i: uniaxial behavior. International journal of plasticity 8 (1), 91–116.

Hibbett, Karlsson, Sorensen, 1998. ABAQUS/standard: User's Manual. Vol. 1. Hibbitt, Karlsson & Sorensen.

Hill, R., 1948. A variational principle of maximum plastic work in classical plasticity. The Quarterly Journal of Mechanics and Applied Mathematics 1 (1), 18–28.

Hill, R., 1950. The mathematical theory of plasticity, oxford university press, oxford, 1950.

Hill, R., 1951. Lxxxviii. on the state of stress in a plastic-rigid body at the yield point. The London, Edinburgh, and Dublin Philosophical Magazine and Journal of Science 42 (331), 868–875.

Hill, R., 1967. The essential structure of constitutive laws for metal composites and polycrystals. Journal of the Mechanics and Physics of Solids 15 (2), 79–95.

Hjiaj, M., Fortin, J., De Saxcé, G., 2003. A complete stress update algorithm for the non-associated drucker–prager model including treatment of the apex. International Journal of Engineering Science 41 (10), 1109–1143.

Hodge, P., 1959. Plastic analysis of structures mc-graw hill. New York.

Hodge Jr, P., 1954. Shakedown of elastic-plastic structures. Residual stresses in metals and metal construction.

Keralavarma, S., Benzerga, A., 2010. A constitutive model for plastically anisotropic solids with non-spherical voids. Journal of the Mechanics and Physics of Solids 58 (6), 874–901.

Kobayashi, H., Kusumoto, T., Nakazawa, H., 1991. Cyclic j-r-curve and upper limit characteristic of fatigue crack growth in 2-1/2 cr-mo steel. International journal of pressure vessels and piping 52 (3), 337–356.

Koiter, W., 1960. General theorems for elastic-plastic solids, progress in solid mechanics, 1.

Koiter, W. T., 1953. Stress-strain relations, uniqueness and variational theorems for elastic-plastic materials with a singular yield surface. Quarterly of applied mathematics 11 (3), 350–354.

Konig, J., Kleiber, M., 1978. New method of shakedown analysis. BULLETIN DE L ACADEMIE POLONAISE DES SCIENCES-SERIE DES SCIENCES TECHNIQUES 26 (4), 275–281.

König, J., Siemaszko, A., 1988. Strainhardening effects in shakedown processes. Ingenieur-Archiv 58 (1), 58–66.

Lacroix, R., Leblond, J.-B., Perrin, G., 2016. Numerical study and theoretical modelling of void growth in porous ductile materials subjected to cyclic loadings. European Journal of Mechanics-A/Solids 55, 100–109.

Laitusis, C. C., Morgan, D. L., Bridgeman, B., Zanna, J., Stone, E., 2007. Examination of fatigue effects from extended-time accommodations on the sat reasoning test™. ETS Research Report Series 2007 (2).

Lance, R., Onat, E., 1963. Analysis of plastic shallow conical shells. Journal of Applied Mechanics 30 (2), 199–209.

Leblond, J.-B., Germain, P., 2003. Mécanique de la rupture fragile et ductile. Hermès science publications.

Leblond, J.-B., Perrin, G., Devaux, J., 1995. An improved gurson-type model for hardenable ductile metals. European journal of mechanics. A. Solids 14 (4), 499–527.

Lemaitre, J., Chaboche, J.-L., 1994. Mechanics of solid materials. Cambridge university press.

Liu, Z., Wong, W., Guo, T., 2016. Void behaviors from low to high triaxialities: Transition from void collapse to void coalescence. International Journal of Plasticity 84, 183–202.

Madou, K., Leblond, J.-B., 2012a. A gurson-type criterion for porous ductile solids containing arbitrary ellipsoidal voids—i: limit-analysis of some representative cell. Journal of the Mechanics and Physics of Solids 60 (5), 1020–1036.

Madou, K., Leblond, J.-B., 2012b. A gurson-type criterion for porous ductile solids containing arbitrary ellipsoidal voids—ii: determination of yield criterion parameters. Journal of the Mechanics and Physics of Solids 60 (5), 1037–1058.

Magnier, V., Charkaluk, E., De Saxcé, G., 2014. Bipotential versus return mapping algorithms: Implementation of non associated flow rules. International Journal of Solids and Structures 51 (15-16), 2857–2864.

Maier, G., Carvelli, V., Cocchetti, G., 2000. On direct methods for shakedown and limit analysis. EUROPEAN JOURNAL OF MECHANICS. A, SOLIDS 19, S79–S100.

Maitournam, H., 2013. Mécanique des structures anélastiques.

Manson, S., 1954. Nat. advise. comm. aero. tech., 2.933.

Martin, J., 1975. Plasticity: Fundamentals and General Results. MIT Press, Cam-bridge, Ma.

Mbiakop, A., Constantinescu, A., Danas, K., 2015. On void shape effects of periodic elasto-plastic materials subjected to cyclic loading. European Journal of Mechanics-A/Solids 49, 481–499.

Melan, E., 1936. Theory statisch unbestimmter systeme aus ideal plastischen baustoff. Sitz Ber Akad. Wiss, 145–195.

Mises, R. v., 1928. Mechanik der plastischen formänderung von kristallen. ZAMM-Journal of Applied Mathematics and Mechanics/Zeitschrift für Angewandte Mathematik und Mechanik 8 (3), 161–185.

Monchiet, V., Cazacu, O., Charkaluk, E., Kondo, D., 2008. Macroscopic yield criteria for plastic anisotropic materials containing spheroidal voids. International Journal of Plasticity 24 (7), 1158–1189.

Monchiet, V., Charkaluk, E., Kondo, D., 2007. An improvement of gurson-type models of porous materials by using eshelby-like trial velocity fields. Comptes Rendus Mecanique 335 (1), 32–41.

Monchiet, V., Gruescu, C., Charkaluk, E., Kondo, D., 2006. Approximate yield criteria for anisotropic metals with prolate or oblate voids. Comptes Rendus Mecanique 334 (7), 431–439.

Neal, B., 1956. The plastic methods of structural analysis. Chapman and Hall, London.

Nguyen, A. D., Hachemi, A., Weichert, D., 2008. Application of the interior-point method to shakedown analysis of pavements. International Journal for Numerical Methods in Engineering 75 (4), 414–439.

Nguyen, A. D., Ponter, U. D. A., 2007. Lower-bound shakedown analysis of pavements by using the interior point method. Doctor thesis, RWTH Aachen University, Aachen.

Nguyen, Q. S., 2000. Stability and nonlinear solid mechanics. Wiley.

Onat, E., 1960. Plastic analysis of shallow conical shells. Transactions of the American Society of Civil Engineers 126 (1), 1111–1122.

Orowan, E., 1939. Theory of the fatigue of metals. Proceedings of the Royal Society of London. Series A, Mathematical and Physical Sciences, 79–106.

Papadopoulos, I. V., 1994. A new criterion of fatigue strength for out-of-phase bending and torsion of hard metals. International Journal of Fatigue 16 (6), 377–384.

Pastor, F., Thoré, P., Kondo, D., Pastor, J., 2013. Limit analysis and conic programming for gurson-type spheroid problems. In: Limit State of Materials and Structures. Springer, pp. 207–218.

Paux, J., Morin, L., Brenner, R., Kondo, D., 2015. An approximate yield criterion for porous single crystals. European Journal of Mechanics-A/Solids 51, 1–10.

Polizzotto, C., 2010. Shakedown analysis for a class of strengthening materials within the framework of gradient plasticity. International Journal of Plasticity 26 (7), 1050–1069.

Prager, W., Kieffer, J., Epain, R., 1958. Problèmes de plasticité théorique. Dunod.

Ruiz, C. C. d. L. P., Silveira, J. L. L., 2018. Shakedown analysis for porous materials. European Journal of Mechanics-A/Solids 69, 124–134.

Save, M. A., Massonnet, C. E., De Saxcé, G., 1997. Plastic limit analysis of plates, shells and disks. Vol. 43. Elsevier.

Sawczuk, A., 1969. Evaluation of upper bounds to shakedown loads for shells. Journal of the Mechanics and Physics of Solids 17 (4), 291–301.

Schenk, O., Gärtner, K., 2004. Solving unsymmetric sparse systems of linear equations with pardiso. Future Generation Computer Systems 20 (3), 475–487.

Schmidt, R., Wilkowski, G., Mayfield, M., 1991. al-the international piping integrity research group (ipirg) program on overview-smirt 11.

Schwer, L. E., Murray, Y. D., 1994. A three-invariant smooth cap model with mixed hardening. International Journal for Numerical and Analytical Methods in Geomechanics 18 (10), 657–688.

Shen, W., Zhang, J., Shao, J., Kondo, D., 2017. Approximate macroscopic yield criteria for drucker-prager type solids with spheroidal voids. International Journal of Plasticity 99, 221–247.

Shen, W. Q., Oueslati, A., De Saxcé, G., 2015. Macroscopic criterion for ductile porous materials based on a statically admissible microscopic stress field. International Journal of Plasticity 70, 60–76.

Simon, J.-W., 2013. Direct evaluation of the limit states of engineering structures exhibiting limited, nonlinear kinematical hardening. International Journal of Plasticity 42, 141–167.

Soutas-Little, R. W., 1999. Elasticity. Courier Corporation.

Stoughton, T. B., 2002. A non-associated flow rule for sheet metal forming. International Journal of Plasticity 18 (5-6), 687–714.

Stoughton, T. B., Yoon, J.-W., 2004. A pressure-sensitive yield criterion under a non-associated flow rule for sheet metal forming. International Journal of Plasticity 20 (4-5), 705–731.

Sun, Y., Wang, D., 1995. Analysis of shear localization in porous materials based on a lower bound approach. International journal of fracture 71 (1), 71–83.

Symonds, P. S., 1951. Shakedown in continuous media. Journal of Applied Mechanics Transactions of the Asme 18 (1), 85–89.

Taleb, L., Hauet, A., 2009. Multiscale experimental investigations about the cyclic behavior of the 304l ss. International Journal of Plasticity 25 (7), 1359–1385.

Thoré, P., Pastor, F., Pastor, J., Kondo, D., 2009. Closed-form solutions for the hollow sphere model with coulomb and drucker–prager materials under isotropic loadings. Comptes Rendus Mécanique 337 (5), 260–267.

Tvergaard, V., 1981. Influence of voids on shear band instabilities under plane strain conditions. International Journal of fracture 17 (4), 389–407.

Tvergaard, V., Needleman, A., 1984. Analysis of the cup-cone fracture in a round tensile bar. Acta metallurgica 32 (1), 157–169.

Vermeer, P. A., De Borst, R., 1984. Non-associated plasticity for soils, concrete and rock. HERON, 29 (3), 1984.

Wächter, A., Biegler, L. T., 2006. On the implementation of an interior-point filter line-search algorithm for large-scale nonlinear programming. Mathematical programming 106 (1), 25–57.

Weichert, D., Maier, G., 2014. Inelastic behaviour of structures under variable repeated loads: direct analysis methods. Vol. 432. Springer.

Yi, S., Duo, W., 1989. A lower bound approach to the yield loci of porous materials. Acta Mechanica Sinica 5 (3), 237–243.

Zhang, J., Oueslati, A., Shen, W., de Saxcé, G., 2018. Exact elastic solution of the axisymmetric and deviatoric loaded hollow sphere. International Journal of Pressure Vessels and Piping.

Zhang, J., Shen, W., Oueslati, A., De Saxce, G., 2017a. A macroscopic criterion of shakedown limit for ductile porous materials subjected to general cyclic loadings. Mechanics of Materials 115, 76–87.

Zhang, J., Shen, W., Oueslati, A., De Saxce, G., 2017b. Shakedown of porous materials. International Journal of Plasticity 95, 123–141.

Appendix A

Exact elastic solution of the axisymmetric and deviatoric loaded hollow sphere

International Journal of Pressure Vessels and Piping 162 (2018) 40–45

Contents lists available at ScienceDirect

International Journal of Pressure Vessels and Piping

journal homepage: www.elsevier.com/locate/ijpvp

Exact elastic solution of the axisymmetric and deviatoric loaded hollow sphere

J. Zhang, A. Oueslati*, W.Q. Shen, G. de Saxcé

Univ. Lille, CNRS, Arts et Métiers Paris Tech, Centrale Lille, FRE 3723 - LML - Laboratoire de Mécanique de Lille, F-59000 Lille, France

ARTICLE INFO

Keywords:
Hollow sphere
Spherical harmonics
Axisymmetric and deviatoric loads
Effective properties
von Mises criterion

ABSTRACT

This paper provides the analytical solution of the elastic hollow sphere subjected to axisymmetric and pure deviatoric surface tractions within the framework of the infinitesimal strains. The expressions of the stress and displacement fields are derived in closed-form in terms of spherical harmonics by using Boussinesq-Neuber-Papkovitch potentials. The obtained solution is valid for thin and thick hollow sphere. It is shown that, for the J_2-plasticity, the hollow spherical shell undergoes incipient first plastic strains at the pole $\theta = \pi/2$ located on the internal surface boundary. In the perspective of shakedown analysis of ductile porous materials, the macroscopic stress and strain fields of the hollow sphere model are obtained from their local counterparts by the volume average operator.

1. Introduction

Over the past few years, there has been a growing interest in Metallic Hollow Sphere Structures (MHSS) due to their light weight and their capacity for energy absorption and heat insulation. These novel foams, composed of an assemblage of hollow spheres, are used in transport engines, aerospace and chemistry [1–3]. For instance, the hollow silicalite spheres are used for ethanol/water separation by pervaporation [4], the hollow spheres ceramics are employed for heat insulation [5], the synthetic magnetic polymeric microsphere can be used for selective enrichment and rapid separation of phosphopeptides [6], etc. New technologies for manufacturing hollow spherical-cell foams with high precision for wide ranges of thickness and diameter have been developed recently [7,8]. In parallel, great efforts have been focused over characterization of different failure modes of these cellular materials which requires a better understanding of deformations of a single hollow sphere.

On the other hand, the hollow sphere shell plays a key role in ductile damage of porous materials. In fact, since the Gurson's pioneering work [9] on ductile damage of voided solids, the unit cell modeling the representative elementary volume (REV) in micro-poromechanics is almost the hollow sphere [10–15] because it is the simplest geometrical model. Further, it allows the derivation of closed-form expressions of the effective yield criteria according to the local strength yield of the solid matrix. In our recent works [16,17], we have adopted the hollow sphere unit cell for the shakedown study of porous materials under cyclic loads. The present work stems from these studies.

Although numerous experimental investigations and numerical studies based on the finite element method have been devoted to the hollow sphere under different loads [18–27], few analytic solutions dealing with the mechanical response to complex and general loads are provided in literature. The analytical elastic plastic solution of hollow sphere under internal and external pressure is classical and can be found in any textbook of mechanics of deformable solids. Wei et al. [28] provided the closed form expressions of the stress and strain distributions within an elastic thin or thick hollow sphere subjected to diametrical point loads. The method of solution is based on Fourier-Legendre expansion for the boundary applied loads. Motivated by Wei et al. solution, Chen et al. [29] have solved the problem of an elastic hollow sphere compressed between two flat platens under the Hertzian contact assumption. Gregory et al. [30] have developed approximate solution for a thin or a moderately thick spherical cap in axisymmetric deformations. An asymptotic expansion in the framework of the thin shell theory with refined boundary conditions has been employed. Later on, in Ref. [31], a similar procedure has been provided for the derivation of an asymptotic solution of a thick hollow sphere compressed by equal and opposite concentrated axial loads. The dynamic response of a thick-walled elastic spherical shell subject to radially symmetric loadings have been studied in Pao et al. [32] by applying the theory of rays.

The purpose of the present work is to derive the analytical solution of a hollow sphere made up of a homogeneous and isotropic material in infinitesimal elasticity under axisymmetric and deviatoric surface tractions. The plan of the paper is as follows. In the next section, a brief review of the internal solution of a solid sphere and the external

* Corresponding author.
E-mail address: abdelbacet.oueslati@univ-lille1.fr (A. Oueslati).

https://doi.org/10.1016/j.ijpvp.2018.02.007
Received 22 November 2017; Received in revised form 13 February 2018; Accepted 15 February 2018
Available online 24 February 2018

solution of the spherical cavity embedded in infinite matrix under axisymmetric loads is presented. The presentation follows the one in Refs. [33] and [34]. In section 3, we firstly setup the problem of a hollow sphere subjected to an axisymmetic and pure deviatoric surface stress distribution on the outer boundary. Then, the closed-form expressions of the displacement and stress field are derived by the combination of the internal and external solutions. The macroscopic stress and strain fields obtained from their local counterparts by the volume average operator are also delivered. Section 4 focuses on von Mises yield condition of the hollow sphere. It is worthy to note that some computations have been checked or performed by making use of the Mathematica software [35,36]. Finally, some concluding remarks are drawn in the last section.

2. The external and internal problems

Boussinesq-Neuber-Papkovitch potentials provide a powerful tool for solving three-dimensional elastic problems. The displacement and stress fields are expressed in terms of harmonic potentials, given by the vector $\boldsymbol{\Psi}$ and the scalar function Φ.

In the absence of volume forces, the displacement field $\boldsymbol{u}$ reads:

$$2\mu\boldsymbol{u} = -(4-\nu)\boldsymbol{\Psi} + \nabla(\boldsymbol{x}\cdot\boldsymbol{\Psi}+\Phi) \tag{1}$$

where $\boldsymbol{x}$ is the position vector, μ is the shear modulus and ν is Poisson ratio.

The harmonicity of the potentials ($\nabla^2\boldsymbol{\Psi} = 0$; $\nabla^2\,\Phi = 0$) insures that Lamé-Navier equations of the linear elasticity are satisfied.

2.1. Spherical harmonics

Consider the spherical coordinates (r, θ, ϕ) where r is the radius, θ the inclination angle, φ the azimuth one, with orthonormal frame $\{\mathbf{e}_r, \mathbf{e}_\theta, \mathbf{e}_\phi\}$ as shown in Fig. 1.

For an axisymmetric potential F (independent of ϕ), the Laplace equation writes:

$$\nabla^2 F(r,\theta) = \frac{\partial^2 F}{\partial r^2}(r,\theta) + \frac{2}{r}\frac{\partial F}{\partial r}(r,\theta) + \frac{cot\theta}{r^2}\frac{\partial F}{\partial \theta}(r,\theta) = 0 \tag{2}$$

Employing the method of separation of variables, the solution of (2) is decomposed in terms of Fourier series with respect of the variable θ as follows:

$$F(r,\theta) = \sum_{n=0}^{\infty} r^n f_n(\theta) \tag{3}$$

Substitution of (3) in (2) yields the following differential equation

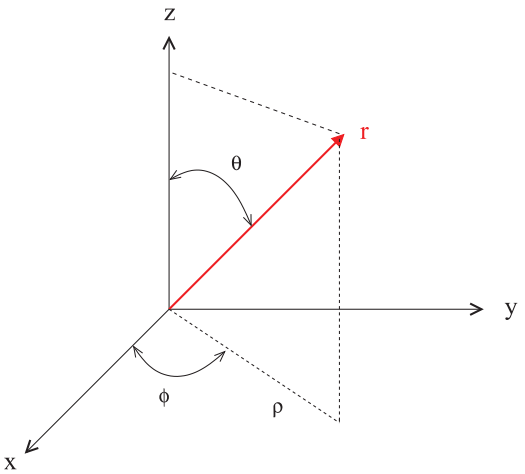

Fig. 1. The spherical coordinates.

$$\frac{1}{sin\theta}\frac{d}{d\theta}\left(sin\theta\frac{df_n}{d\theta}\right) + n(n+1)f_n = 0 \tag{4}$$

By introducing the new variable $\zeta = cos\theta$, equation (4) recasts into:

$$(1-\zeta^2)\frac{d^2 f_n}{d\zeta^2} - 2\frac{df_n}{d\zeta} + n(n+1)f_n = 0 \tag{5}$$

This is the standard Legendre equation for which the continuous fundamental solutions for $|\zeta| \le 1$ (or $0 \le \theta \le \pi$) are the Legendre polynomials of the first kind $P_n(\zeta)$:

$$P_n(\zeta) = \frac{1}{2^n n!}\frac{d^n(\zeta^2-1)}{d\zeta^n} \tag{6}$$

The solutions $r^n P_n(cos\theta)$ $(n \ge 0)$ of the Laplace equation are called the spherical harmonics.

It is worth noting that the harmonics defined by the Legendre Polynomials given by (6) are bounded at the origin $r = 0$. However, if we set $n = -p-1$ for $p \ge 0$ then $n(n+1) = p(p+1)$, and thus the Legendre equation (4) remains unchanged but with p replacing n. This means that the potentials $r^{-n-1}P_n(cos\theta)$ are harmonics and also singular at the origin $r = 0$ for $n \ge 0$.

2.2. Internal solution

The internal problem is concerned with a solid sphere subjected to an axisymmetric traction exerted onto its boundary S_e defined by $r = b$. Let $\boldsymbol{u} = (u_r, u_\theta, 0)$ be the displacement vector explained in the spherical frame. It is shown in Refs. [33,34], that by using Boussinesq-Neuber-Papkovich solution (1), the displacement components are given in terms of Legendre's polynomial series as follows:

$$u_r = \sum_n \left[A_n(n+1)(n-2+4\nu)\,r^{n+1} + B_n n\,r^{n-1}\right] P_n(\zeta) \tag{7}$$

$$u_\theta = \sum_n \left[A_n(n+1)(n+5-4\nu)\,r^{n+1} + B_n\,r^{n-1}\right]\frac{d}{d\theta}P_n(\zeta) \tag{8}$$

The stresses are given by:

$$\frac{1}{2\mu}\sigma_{rr} = \sum_n \left[A_n(n+1)(n^2-n-2-2\nu)\,r^n + B_n n(n-1)\,r^{n-2}\right] P_n(\zeta) \tag{9}$$

$$\frac{1}{2\mu}\sigma_{r\theta} = \sum_n \left[A_n(n^2+2n-1+2\nu)\;r^n + B_n(n-1)\,r^{n-2}\right]\frac{d}{d\theta}P_n(\zeta) \tag{10}$$

$$\begin{aligned}\tfrac{1}{2\mu}\sigma_{\theta\theta} = &-\textstyle\sum_n \left[A_n(n^2+4n+2+2\nu)(n+1)\,r^n + B_n n^2\,r^{n-2}\right] P_n(\zeta)\\ &+ \textstyle\sum_n \left[A_n(n+5-4\nu)\,r^n + B_n\,r^{n-2}\right] cot(\theta)\,\tfrac{d}{d\theta}P_n(\zeta)\end{aligned} \tag{11}$$

$$\begin{aligned}\tfrac{1}{2\mu}\sigma_{\varphi\varphi} = &\textstyle\sum_n \left[A_n(n+1)(n-2-2\nu-4n\nu)\,r^n + B_n n\,r^{n-2}\right] P_n(\zeta)\\ &+ \textstyle\sum_n \left[A_n(n+5-4\nu)\,r^n + B_n\,r^{n-2}\right] cot(\theta)\,\tfrac{d}{d\theta}P_n(\zeta)\end{aligned} \tag{12}$$

Let $\boldsymbol{T} = (\sigma_{rr}(r=b), \sigma_{r\theta}(r=b), 0)$ be the stress vector applied onto the boundary S_e: $r = b$. For convenience, let us denote $f(\theta) = \sigma_{rr}(r=b,\theta)$ and $g(\theta) = \sigma_{r\theta}(r=b,\theta)$.

It follows from equations (9) and (10) that:

$$\begin{aligned}f(\theta) &= 2\mu\textstyle\sum_n \left[A_n(n+1)(n^2-n-2-2\nu)\,b^n + B_n n(n-1)\,b^{n-2}\right] P_n(\zeta)\\ &= \textstyle\sum_n F_n\,P_n(\zeta)\end{aligned} \tag{13}$$

$$\begin{aligned}g(\theta) &= 2\mu\textstyle\sum_n \left[A_n(n^2+2n-1+2\nu)\;b^n + B_n(n-1)\,b^{n-2}\right]\tfrac{d}{d\theta}P_n(\zeta)\\ &= \textstyle\sum_n G_n\,\tfrac{d}{d\theta}P_n(\zeta) = -\sum_n G_n\,\tfrac{dP_n(\zeta)}{d\zeta}sin\theta\end{aligned} \tag{14}$$

It should be emphasized that equations (13) and (14) represent the expansions of the boundary traction functions f and g in spherical harmonics. The evaluation of the series expansions F_n and G_n can be obtained by Ref. [33]:

$$F_n = \frac{2n+1}{2}\int_0^{\pi} f(\theta)\, P_n(cos\theta)\, sin\theta\, d\theta \tag{15}$$

and

$$G_n = \frac{2n+1}{2}\int_0^{\pi} g(\theta)\, \frac{dP_n}{d\theta}\, sin\theta\, d\theta \tag{16}$$

Once the coefficients F_n and G_n are obtained, the evaluation of the coefficients A_n and B_n is straightforward from equations (13) and (14) for each integer n.

2.3. External solution

The exterior problem represents the axisymmetric loaded spherical hole embedded in an infinite solid with vanishing loading at infinity. The radius of the cavity is denoted by $r = a$.

Its corresponding external solution can be obtained directly from the internal solution (7–12) by replacing n by $(n+1)$ [33,34]. Besides, by virtue of the relation $P_{-(n+1)} = P_n$, the internal solution gives the closed-form solution of the displacement and the stress fields as follows:

$$u_r = \sum_n \left[\frac{C_n}{r^n} n(n+3-4\nu) - \frac{D_n}{r^{n+2}}(n+1)\right] P_n(\zeta) \tag{17}$$

$$u_\theta = \sum_n \left[\frac{C_n}{r^n}(-n+4-4\nu) + \frac{D_n}{r^{n+2}}\right] \frac{d}{d\theta} P_n(\zeta) \tag{18}$$

and

$$\frac{1}{2\mu}\sigma_{rr} = \sum_n \left[-\frac{C_n}{r^{n+1}} n(n^2+3n-2\nu) + \frac{D_n}{r^{n+3}}(n+1)(n+2)\right] P_n(\zeta) \tag{19}$$

$$\frac{1}{2\mu}\sigma_{r\theta} = \sum_n \left[\frac{C_n}{r^{n+1}}(n^2-2+2\nu) - \frac{D_n}{r^{n+3}}(n+2)\right] \frac{d}{d\theta} P_n(\zeta) \tag{20}$$

$$\begin{aligned}\frac{1}{2\mu}\sigma_{\theta\theta} = &\sum_n \left[\frac{C_n}{r^{n+1}} n(n^2-2n-1+2\nu) - \frac{D_n}{r^{n+3}}(n+1)^2\right] P_n(\zeta) \\ &- \sum_n \left[\frac{C_n}{r^{n+1}}(-n+4-4\nu) + \frac{D_n}{r^{n+3}}\right] cot(\theta)\, \frac{d}{d\theta} P_n(\zeta)\end{aligned} \tag{21}$$

$$\begin{aligned}\frac{1}{2\mu}\sigma_{\varphi\varphi} = &\sum_n \left[\frac{C_n}{r^{n+1}} n(n+3-4n\nu-2\nu) - \frac{D_n}{r^{n+3}}(n+1)\right] P_n(\zeta) \\ &+ \sum_n \left[\frac{C_n}{r^{n+1}}(-n+4-4\nu) + \frac{D_n}{r^{n+3}}\right] cot(\theta)\, \frac{d}{d\theta} P_n(\zeta)\end{aligned} \tag{22}$$

The boundary stresses exerted onto the spherical cavity surface S_i: $(r = a)$ are given by:

$$\alpha(\theta) = \sigma_{rr}(r=a,\theta), \quad \beta(\theta) = \sigma_{r\theta}(r=a,\theta) \tag{23}$$

The spherical expansions of the function $\alpha(\theta)$ and $\beta(\theta)$ are given by:

$$\begin{aligned}\alpha(\theta) &= 2\mu \sum_n \left[-\frac{C_n}{a^{n+1}} n(n^2+3n-2\nu) + \frac{D_n}{a^{n+3}}(n+1)(n+2)\right] P_n(\zeta) \\ &= \sum_n M_n\, P_n(\zeta)\end{aligned} \tag{24}$$

$$\begin{aligned}\beta(\theta) &= \sum_n \left[\frac{C_n}{a^{n+1}}(n^2-2+2\nu) - \frac{D_n}{a^{n+3}}(n+2)\right] \frac{d}{d\theta} P_n(\zeta) \\ &= \sum_n N_n \frac{d}{d\theta} P_n(\zeta) = -\sum_n N_n \frac{dP_n(\zeta)}{d\zeta} sin\theta\end{aligned} \tag{25}$$

Similar to the internal solution, the coefficients M_n and N_n are obtained by use of equations (15) and (16) and then C_n and D_n are derived from (24) and (25).

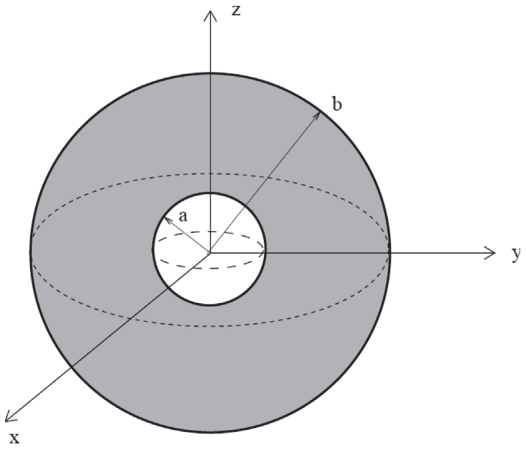

Fig. 2. The hollow sphere unit cell.

3. Closed-form solution of the hollow sphere subjected to an axisymmetric loads

Let a thick hollow sphere of inner radius $r = a$ and outer radius $r = b$ (cf. Fig. 2) be subjected to axisymmetric traction loads. It is convenient to introduce the porosity $f = \frac{a^3}{b^3}$ which is the damage parameter in ductile fracture of voided materials.

The solution of the problem under consideration is achieved by the combination of the internal and external solutions explained in the previous section [33]. Indeed, the stresses applied on the boundaries $S_i(r=a)$ and $S_e(r=b)$ yield four algebraic equations giving the coefficients A_n, B_n, M_n and N_n for each n. The closed form solution involves the spherical expansions of the displacement and stress fields.

In this work, we consider a free traction boundary at S_i, (i.e. $\alpha(\theta) = 0$, $\beta(\theta) = 0$) and an axisymmetric and pure deviatoric surface traction exerted on the external boundary S_e. This stress boundary condition complies with the stress vector $\mathbf{T^d} = \boldsymbol{\sigma^d}\cdot\mathbf{n}$ where $\boldsymbol{n}$ is the outward unit normal vector to the external boundary S_e and the homogeneous deviatoric tensor $\boldsymbol{\sigma^d}$ is taken in the following form, in the cylindrical coordinates (ρ, ϕ, z) with orthonormal frame $\{\mathbf{e}_\rho, \mathbf{e}_\phi, \mathbf{e}_z\}$:

$$\boldsymbol{\sigma}^d = P(\mathbf{e}_\rho \otimes \mathbf{e}_\rho + \mathbf{e}_\phi \otimes \mathbf{e}_\phi - 2\mathbf{e}_z \otimes \mathbf{e}_z), \tag{26}$$

where P is a constant load.

It is easy to establish that, in the spherical frame, the stress vector $\mathbf{T^d} = \boldsymbol{\sigma^d}\cdot\mathbf{n}$ writes:

$$\mathbf{T^d} = -\frac{1}{2}P(3cos(2\theta)+1)\,\mathbf{e}_r + 3Psin(\theta)cos(\theta)\,\mathbf{e}_\theta \tag{27}$$

Thus, we get

$$\begin{cases} f(\theta) = -\frac{1}{2}P(3cos(2\theta)+1) \\ g(\theta) = -3P\, sin(\theta)\, cos(\theta) \\ m(\theta) = 0 \\ n(\theta) = 0 \end{cases} \tag{28}$$

The evaluation of F_n, G_n, M_n and N_n is achieved by the use of equations (15) and (16) or by a simple identification. It turns out that only term for $n = 2$ is not vanishing, and Legendre's polynomial series involves only polynomial of degree 2.

We find:

$$\begin{cases} F_2 = -2P, & G_2 = -P \\ M_2 = 0, & N_2 = 0 \end{cases} \tag{29}$$

By using equations (13), (14), (24) and (25), we obtain

$$A_2 = P\frac{\Delta^A}{\Lambda^A} \tag{30}$$

where

$$\begin{cases} \Delta^A = 15f\,(f^{1/3}+1) \\ \Lambda^A = b^2\mu\nu^2 25(-f^{2/3}+f^{7/3}+f^{8/3}+f^3-f^{1/3}-1) \\ -\,7b^2\mu(-7f^{2/3}+18f^{4/3}-18f^{5/3}+7f^{7/3}+7f^{8/3}+7f^3-18f^2-7f^{1/3} \\ \quad +18f-7) \end{cases}$$

$$B_2 = P\frac{1}{2\mu\left(\frac{126f\,(f^{5/3}+f^2-f^{1/3}-1)}{(f^{1/3}+1)f^{1/3}(25(f^{2/3}+f^{4/3}+1)\nu^2-7(7f^{2/3}+25f^{4/3}+7))+25\nu^2-49}+f-1\right)} \tag{31}$$

$$C_2 = P\frac{5b^3}{4(f^{1/3}-1)\mu\left(-\frac{5(f^{2/3}+f^{1/3}+1)\nu}{f}+\frac{7(f^{2/3}+f^{1/3}+1)}{f}-\frac{126(f^{1/3}+1)^2}{(f^{2/3}+f^{4/3}+f^{5/3}+f^2+f^{1/3}+f+1)(5\nu+7)}\right)} \tag{32}$$

and

$$D_2 = P\frac{\Delta^D}{\Lambda^D} \tag{33}$$

where

$$\begin{cases} \Delta^D = -3b^5f^{5/3}(5\nu+7)(f^{2/3}+f^{4/3}+f^{1/3}+f+1) \\ \Lambda^D = 50(-f^{2/3}+f^{7/3}+f^{8/3}+f^3-f^{1/3}-1)\mu\nu^2 \\ -\,14\mu(-7f^{2/3}+18f^{4/3}-18f^{5/3}+7f^{7/3}+7f^{8/3}+7f^3-18f^2-7f^{1/3} \\ \quad +18f-7) \end{cases}$$

In conclusion, the stress field writes

$$\sigma = \begin{pmatrix} \sigma_{rr} & \sigma_{r\theta} & 0 \\ \sigma_{r\theta} & \sigma_{\theta\theta} & 0 \\ 0 & 0 & \sigma_{\phi\phi} \end{pmatrix} \tag{34}$$

where

$$\frac{1}{2\mu}\sigma_{rr} = \left(-3\nu A_2 r^2 + B_2 + \frac{6D_2}{r^5} + \frac{2(\nu-5)C_2}{r^3}\right)(-1+3cos^2(\theta)) \tag{35}$$

$$\frac{1}{2\mu}\sigma_{r\theta} = \left(-\frac{3}{2}(2\nu+7)A_2 r^2 - \frac{3}{2}B_2 - \frac{3(\nu+1)C_2}{r^3} + \frac{6D_2}{r^5}\right)sin(2\theta) \tag{36}$$

$$\frac{1}{2\mu}\sigma_{\theta\theta} = \left(-3(\nu+7)r^2A_2 - 2B_2 - \frac{(2-4\nu)C_2}{2r^3} - \frac{9D_2}{2r^5}\right)(-1+3cos^2(\theta)) + \left(3(7-4\nu)A_2 r^2 + 3B_2 + \frac{3(2-4\nu)C_2}{r^3} + \frac{3D_2}{r^5}\right)cos^2(\theta) \tag{37}$$

$$\frac{1}{2\mu}\sigma_{\varphi\varphi} = \left(-15\nu A_2 r^2 + B_2 - \frac{5(2\nu-1)C_2}{r^3} - \frac{3D_2}{2r^5}\right)(-1+3cos^2(\theta)) + \left(3(4\nu-7)A_2 r^2 - 3B_2 + \frac{6(2\nu-1)C_2}{r^3} - \frac{3D_2}{r^5}\right)cos^2(\theta) \tag{38}$$

where A_2, B_2, C_2 and D_2 are given by the relations (30,31,32,33).

The stresses distributions are depicted in Figs. 3–6 for $b = 1m$, $f = 0.1$, $P = 1MPa$, $E = 2.1\,10^5 MPa$ and $\nu = 0.3$.

It can be observed that σ_{rr}, $\sigma_{\theta\theta}$ and $\sigma_{\phi\phi}$ are symmetric about the axis $\theta = \pi/2$ while $\sigma_{r\theta}$ is anti-symmetric with respect to the same axis.

In the perspective of limit analysis or shakedown investigations of ductile porous materials, the effective or macroscopic properties of the hollow sphere are obtained as volume averages of their microscopic counterparts.

The overall stress $\boldsymbol{\Sigma}$ writes and strain $\boldsymbol{\Xi}$ are given by:

$$\boldsymbol{\Sigma} = \frac{1}{|\Omega|}\int_\Omega \boldsymbol{\sigma}\ dV, \quad \boldsymbol{\Xi} = \frac{1}{|\Omega|}\int_\Omega \boldsymbol{\varepsilon}\ dV. \tag{39}$$

It then follows:

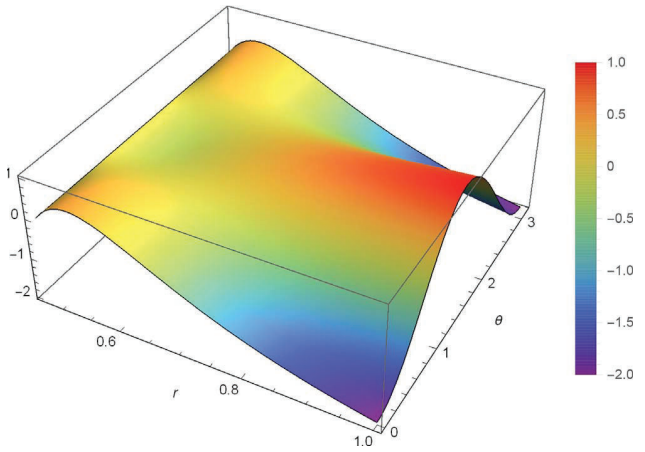

Fig. 3. Distribution of the stress σ_{rr}.

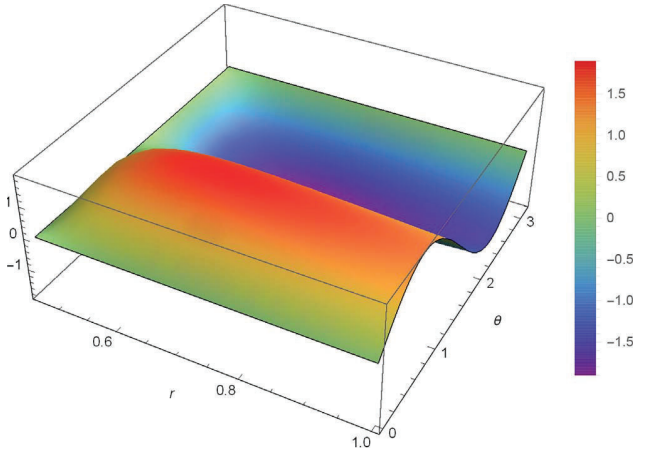

Fig. 4. Distribution of the stress $\sigma_{r\theta}$.

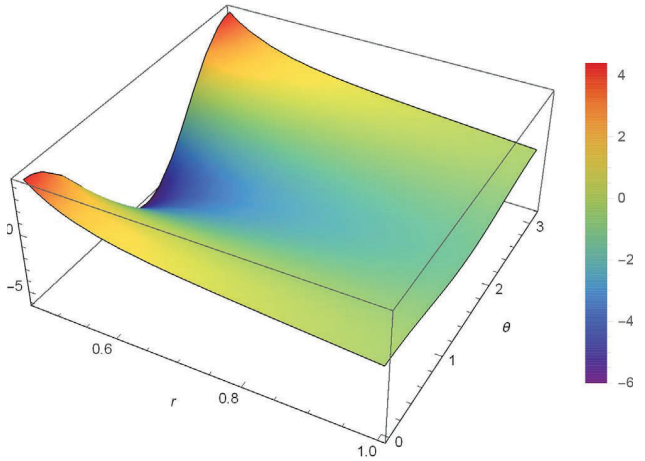

Fig. 5. Distribution of the stress $\sigma_{\theta\theta}$.

$$\boldsymbol{\Sigma} = P\begin{pmatrix} 1 & 0 & 0 \\ 0 & 1 & 0 \\ 0 & 0 & -2 \end{pmatrix} \tag{40}$$

The macroscopic strain tensor writes

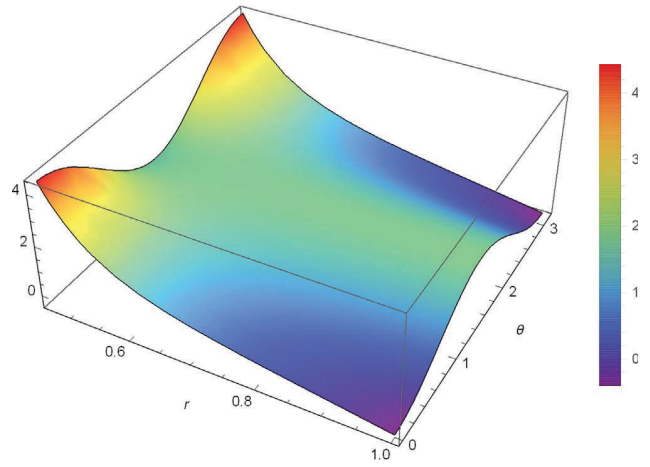

Fig. 6. Distribution of the stress $\sigma_{\phi\phi}$.

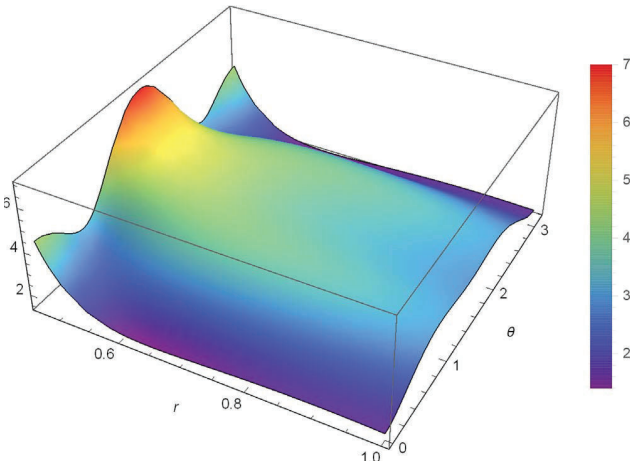

Fig. 7. The von Mises stress distribution σ_{eq}.

$$\Xi = P\begin{pmatrix} \frac{1}{2\mu} & 0 & 0 \\ 0 & \frac{1}{2\mu} & 0 \\ 0 & 0 & -\frac{1}{\mu} \end{pmatrix} \tag{41}$$

Notice that the effective stress and strain are deviatoric ($tr(\Sigma) = tr(\Xi) = 0$).

4. Yield point of the hollow sphere

The experimental tests show that deformable solids and structures subjected to external loads exhibit an elastic behavior when the stress states remain within an elastic domain Υ, which is defined by a differentiable and convex yield function $\mathcal{H}$ of the stress tensor $\boldsymbol{\sigma}$:

$$\Upsilon = \{\boldsymbol{\sigma};\ \mathcal{H}(\boldsymbol{\sigma}) \leq 0\} \tag{42}$$

In the case where the stress state lies on the threshold curve $\mathcal{H}(\boldsymbol{\sigma}) = 0$, the material yields and develops irreversible plastic deformation. The stress states for which $\mathcal{H}(\boldsymbol{\sigma}) > 0$ are not supported by the structure.

For isotropic materials, the most commonly used criterion is the one of von Mises model [37]. The later is expressed in the following form:

$$\mathcal{H}(\boldsymbol{\sigma}) = \sigma_{eq} - \sigma_0 \leq 0 \tag{43}$$

where $\sigma_{eq} = \sqrt{\frac{3}{2}}||\boldsymbol{s}|| = \left(\frac{3}{2}s_{ij}s_{ij}\right)^{1/2}$ is von Mises equivalent stress, $\boldsymbol{s} = dev(\boldsymbol{\sigma})$ and σ_0 is the yield limit of the material under uniaxial tension test.

For the hollow sphere under consideration, the closed form expression of von Mises equivalent stress reads:

$$\begin{aligned}
&\sigma_{eq}\left(r,\theta\right) \\
&= \left|P\right|\left|\frac{1}{2}\left[\frac{3}{2}\frac{\mu^2}{r^{10}}(72\sin^2(2\theta)((7+2\nu)r^7A_2 + r^5B_2 + 2(1+\nu)r^2C_2 - 4D_2)^2\right. \\
&+ 4(3\cos(2\theta)+1)^2((4\nu+7)r^7A_2 + r^5B_2 + 4(\nu-2)r^2C_2 + 6D_2)^2 \\
&+ (2(8\nu-7)r^7A_2 - 2r^5B_2 + 2(8\nu-7)r^2C_2 \\
&+ 3\cos(2\theta)(14r^7A_2 + 2r^5B_2 - 6r^2C_2 + 7D_2) + 3D_2)^2 \\
&+ (4(7-2\nu)r^7A_2 + 4r^5B_2 - 2r^2(4\nu C_2 + C_2) \\
&\left.+ 3\cos(2\theta)(8\nu r^7A_2 + 2(4\nu-5)r^2C_2 + 5D_2) + 9D_2)^2)\right]^{1/2}
\end{aligned} \tag{44}$$

where A_2, B_2, C_2 and D_2 are given by the relations (30,31,32,33).

Figs. 7–9 depict von Mises equivalent stress distribution σ_e, the contour plot and the variation of σ_{eq} on the outer and inner boundaries

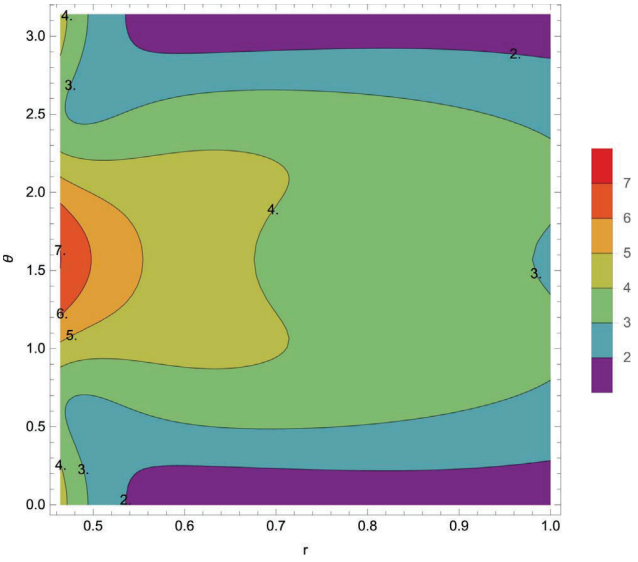

Fig. 8. Contour plot of σ_{eq}.

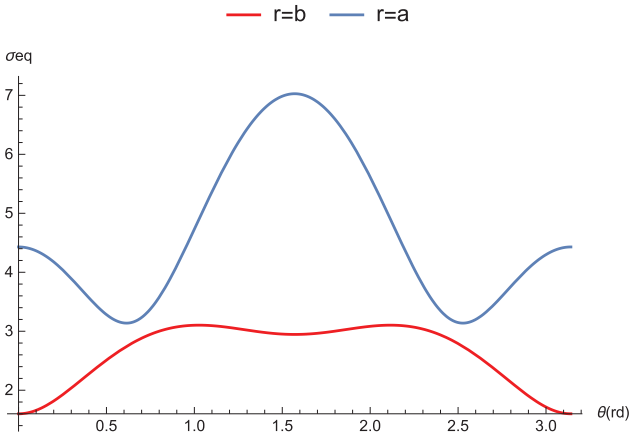

Fig. 9. Variation of σ_{eq}/μ with respect to θ on the boundaries $r = a$ and $r = b = 1m$.

respectively for $b = 1m$, $f = 0.1$, $|P| = 1MPa$, $E = 2.1\ 10^5 MPa$ and $\nu = 0.3$. They show that von Mises stress σ_e is symmetric with respect to the plane $\theta = \pi/2$.

Moreover, it can be proved that the most heavily loaded point,

where σ_e reaches its maximum value, is located on the inner surface $r = a$ at the pole $\theta = \pi/2$. Therefore, if the load parameter $|P|$ increases gradually, the yield condition $\sigma_{eq} - \sigma_0 = 0$ is firstly reached at yield point with coordinates $(r = a, \theta = \pi/2)$, unlike the hollow sphere under hydrostatic pressure for which incipient irreversible plastic strains appear along the total inner surface of the spherical shell.

5. Conclusion

In this paper, the analytical solution of the axisymmetric loaded hollow sphere within the framework of the small strain elasticity has been derived. The load is defined by a free traction boundary on the inner radius and an axisymmetric and pure deviatoric surface forces exerted onto the exterior surface. The method of solution is based on Boussinesq-Neuber-Papkovitch potentials and the stress and displacement fields are given in terms of the spherical harmonics. For the practical use in limit analysis and shakedown analysis of ductile voided media, the effective properties of the stresses and strains have been provided. Also, for a matrix obeying to von Mises criterion, it has been found that incipient plastic deformations develop on the internal radius $r = a$ and at the pole $\theta = \pi/2$.

References

[1] J. Paik, A. Thayamballi, G. Kim, The strength characteristics of aluminum honeycomb sandwich panels, Thin Wall Struct 35 (1999) 205–231.
[2] J. Kim, S. Lee, K. Shin, Manufacturing and structural safety evaluation of a composite train carbody, Compos Struct 78 (2007) 468–476.
[3] E. Knox, M. Cowling, I. Winkle, Adhesively bonded steel corrugated core sandwich construction for marine applications, Mar Struct 11 (1998) 185–204.
[4] P.V. Naik, S. Kerkhofs, J.A. Martens, PDMS mixed matrix membranes containing hollow silicalite sphere for ethanol/water separation by pervaporation, J Membr Sci 502 (2016) 4856.
[5] Z.Q. Sun, C. Lu, J.M. Fan, Porous silica ceramics with closed-cell structure prepared by inactive hollow spheres for heat insulation, J Alloy Comp 662 (2016) 157–164.
[6] Z.G. Wang, G. Cheng, Y.L. Liu, Novel coreshell Cerium(IV)-immobilized magnetic polymeric microspheres for selective enrichment and rapid separation of phosphopeptides, J Colloid Interface Sci 417 (2014) 217–226.
[7] H. He, W. Cai, Z. Dai, Fabrication of porous Ag hollow sphere arrays based on coated template-plasma bombardment, Nanotechnology 24 (46) (2013) 465302.
[8] Y. Li, N. Ren, Y. Wang, Synthesis and properties of polyacrylamide/hollow coal gangue spheres superabsorbent composites, J Appl Polym Sci 130 (3) (2013) 2184–2187.
[9] A.L. Gurson, Continuum theory of ductile rupture by void nucleation and growth – part I: yield criteria and flow rules for porous ductile media, J Eng Mater Technol 99 (1977) 2–15.
[10] L. Dormieux, D. Kondo, F.G. Ulm, Microporomechanics, Wiley, 2006.
[11] M. Leonard, N. Murphy, A. Karac, A. Ivankovic, A numerical investigation of spherical void growth in an elastic-plastic continuum, Comput Mater Sci 64 (2012) 38–40.
[12] J.B. Leblond, Mécanique de la rupture fragile et ductile, Hermes Science Publications, 2003.
[13] L. Sheng, G. de Saxcé, D. Kondo, A stress-based variational model for ductile porous materials, Int J Plast 55 (2014) 133–151.
[14] L. Sheng, Y. Jia, A. Oueslati, G. de Saxcé, D. Kondo, A bipotential-based limit analysis and homogenization of ductile porous materials with non-associated DruckerPrager matrix, J Mech Phys Solid 77 (2015) 1–25.
[15] W. Shen, A. Oueslati, G. de Saxcé, Macroscopic criterion for ductile porous materials based on a statically admissible microscopic stress field, Int J Plast 70 (2015) 60–76.
[16] J. Zhang, W.Q. Shen, A. Oueslati, G. de Saxcé, Shakedown of porous materials, Int J Plast 95 (2017) 123–141.
[17] J. Zhang, W.Q. Shen, A. Oueslati, G. de Saxcé, A macroscopic criterion of shakedown limit for ductile porous materials subjected to general cyclic loadings, Mech Mater 115 (2017) 76–87.
[18] K.B. Carlisle, M. Koopman, K.K. Chawla, R. Kulkarni, G.M. Gladysz, M. Lewis, Microstructure and compressive properties of carbon microballoons, J Mater Sci 41 (2006) 3987–3997.
[19] M. Koopman, G. Gouadec, K. Carlisle, K.K. Chawla, G. Gladysz, Compression testing of hollow microspheres (microballoons) to obtain mechanical properties, Scr Mater 50 (2004) 593–596.
[20] R. Shorter, J.D. Smith, V.A. Coveney, J.C.B. James, Axial compression of hollow elastic spheres, J Mech Mater Struct 5 (5) (2010) 693706.
[21] N.K. Gupta, G.L.E. Prasad, S.K. Gupta, Axial compression of metallic spherical shells between rigid plates, Thin-Walled Struct 34 (1999) 21–41.
[22] N.K. Gupta, Venkatesh, Experimental and numerical studies of dynamic axial compression of thin walled spherical shells, Int J Impact Eng 30 (2004) 1225–1240.
[23] W.S. Sanders, L.J. Gibson, Mechanics of hollow sphere foams, Mater Sci Eng, A 347 (2003) 70–85.
[24] Z.Y. Gao, T.X. Yu, H. Zhao, Mechanical behavior of metallic hollow sphere materials: experimental study, J Aero Eng 21 (4) (2008) 206–216.
[25] D. Karagiozova, T.X. Yu, Z.Y. Gao, Stress-strain relationship for metal hollow sphere materials as a function of their relative density, J Appl Mech- Trans ASME 74 (5) (2007) 898–907.
[26] X.L. Dong, Z.Y. Gao, T. Yu, Dynamic crushing of thin-walled spheres: an experimental study, Int J Impact Eng 35 (2008) 717–726.
[27] P. Li, N. Petrinic, C.R. Siviour, Finite element modelling of the mechanism of deformation and failure in metallic thin walled hollow spheres under dynamic compression, Mech Mater 54 (2012) 43–54.
[28] X.X. Wei, Z.M. Wang, J. Xiong, The analytical solutions for the stress distributions within elastic hollow spheres under the diametrical point loads, Arch Appl Mech 85 (2015) 817–830.
[29] X. Chen, C. Li, X.X. Wei, Stress analysis of a hollow sphere compressed between two flat platens, Int J Mech Sci 118 (2016) 67–76.
[30] R.D. Gregory, T.I. Milac, F.Y.M. Wan, The axisymmetric deformation of a thin, or moderately thick, elastic spherical cap, Stud Appl Math 100 (1998) 67–94.
[31] R.D. Gregory, I. Thomas, Y.M. Frederic, A thick hollow sphere compressed by equal and opposite concentrated axial loads: an asymptotic solution, SIAM J Appl Math 59 (3) (1999) 1080–1097.
[32] Y.H. Pao, A.N. Ceranoglu, Determination of transient response of a thick-walled spherical shell by the ray theory, J Appl Mech ASME 45 (1) (1978) 114–122.
[33] R.W. Soutas-Little, Elasticity, Dover, 1973.
[34] L. Solomon, Elasticité linéaire, Masson, 1968.
[35] Wolfram. Mathematica. http://www.wolfram.com.
[36] A. Constantinescu, A.M. Korsunsky, Elasticity with Mathematica, Cambridge University Press, 2007.
[37] R. von Mises, Mechanik der festen Korper im plastisch-deformablen Zustand, Nachr Kgl Ges Wiss Gottingen, Math Phys Klasse (1913) 582–592.